6

LUNAR ROCKS

G. Jeffrey Taylor, Paul Warren, Graham Ryder, John Delano, Carlé Pieters, and Gary Lofgren

INTRODUCTION: A GUIDE TO LUNAR ROCKS

Lunar Rocks

The Moon, like the Earth, is made of rocks. To learn about the Moon and its history, one has to learn something about lunar rocks—what they are made of, how they are studied and classified, and how our experiences in interpreting rocks on the Earth have been applied to rocks on the Moon.

The lunar samples have provided our only direct information about the Moon's minerals, chemical composition, and age. Lunar rocks have also provided information about the Moon's origin, the evolution of its crust, and the timing of critical events such as volcanism and meteorite bombardment.

The Moon is not a uniform, homogeneous planet. It consists of different rocks, formed in different ways at different times. Some of the Moon's rocks are familiar. The *basalt* lava flows that cover the dark maria formed in the same way as many of the lava flows on Earth—by melting deep in the planet, followed by ascent of molten rock to the surface and eruption through fractures and vents. Other lunar rocks are less familiar; the numerous lunar *breccias* are made up of fragments of older rocks that have been shattered, crushed, and melted by meteoroid impacts, either during an ancient episode of intense meteoroid bombardment that ended about 3.8 b.y. ago or by the rarer impacts of more recent times.

Within any group of rocks (e.g., basaltic lavas), the rocks are not identical. There are differences in mineral composition, in mineral shapes and sizes, and in each rock's chemical composition. These differences have been studied in detail because they are the clues to a rock's origin, history, and relations to other rocks. The immense database for lunar rocks, collected from the Apollo and Luna missions and from lunar meteorites, has made it possible to raise our understanding of some aspects of the origin, evolution, and history of the Moon to a level unmatched for any other planet—maybe even the Earth.

The information obtained from lunar samples can also be applied to larger areas of the Moon, including regions never visited by astronauts or robot sample return vehicles. Natural X-ray and γ-ray signals mapped from orbit by the Apollo command modules provide chemical data from areas on the Moon that were never sampled (Chapter 10). In addition, Earth-based telescopes have been used—and are still being used—to measure the spectral characteristics of the light reflected from the Moon's surface. By making similar spectral measurements in the laboratory on well-studied lunar samples, it is possible to better interpret the spectral data obtained for other lunar regions. The lunar samples provide the "ground truth" for extending our remote mapping to little-known areas of the Moon.

Unfortunately, the many differences among lunar rocks also promote complex classifications, each with many subdivisions that have been developed (sometimes too enthusiastically) by lunar scientists. In some cases, terrestrial rock names have been successfully applied to their lunar equivalents. In others, new terms have had to be coined. These subdivisions, and their technical definitions, are

important, but can be baffling to the nongeologist and even daunting to Earth-oriented geologists. This introduction provides a brief background for the detailed material in subsequent sections.

Classification of Lunar Rocks

The rocks of the Moon fall into four distinct groups: (1) *basaltic volcanic* rocks, including *lava flows* and *pyroclastic* (volcanic ash) rocks; (2) *pristine* rocks from the lunar highlands (i.e., those highland rocks, shattered by impact or not, that have original lunar compositions uncontaminated by impact mixing); (3) complex *polymict breccias,* formed by impacts that shatter, mix, and recompact the lunar surface, and *impact melts* formed by melting of older lunar rocks during meteoroid impacts; and (4) the *lunar soil,* which is the fragmental (<1 cm) unconsolidated debris within the *lunar regolith* that covers the lunar surface. Because of the unique character of the lunar regolith and its importance on the Moon, it is discussed separately in Chapter 7. This chapter discusses only solid, consolidated rocks from the Moon.

All of these rocks were originally *igneous,* that is, they formed by cooling of molten material (*magma*) to form rocks made up of interlocking minerals and sometimes glass. Most of these rocks consist of a few minerals: pyroxenes, olivine, plagioclase feldspar, ilmenite, and silica minerals (tridymite or cristobalite). For detailed information on lunar minerals, see Chapter 5.

Melting and subsequent cooling of the Moon occurred at different places and different times. Early melting occurred soon after the Moon formed and produced the light-colored, Al-rich rocks now exposed in the lunar highlands. Later episodes of internal melting and volcanic eruptions produced the dark-colored lava flows that cover the mare basins.

Some of the samples returned from the Moon are *pristine,* that is, they have not been significantly changed by the effects of meteoroid impacts. However, most lunar rocks have been altered by meteoroid impacts; they have been shattered, crushed, melted, and mixed. Such rocks (breccias and impact melts) are formed by energetic recycling of older rocks and might not correspond to any single igneous rock within the lunar crust. Some of the "recycled" impact-melt rocks can be hard to distinguish from pristine rocks; these distinctions are often controversial among lunar scientists who study them.

Mare basaltic lavas and related volcanic rocks (see sections 6.1 and 6.2). The mare basaltic lavas formed by processes that are both familiar and long-studied on the Earth. In some ways they are the simplest and best understood of lunar rocks. They were formed by melting of the solid interior of the Moon, probably at depths of 100-400 km, followed by the buoyant rise of molten rock to the lunar surface and its eruption.

Two types of volcanic rocks have been erupted at the lunar surface:

1. *Lava flows:* Lunar lava flows apparently erupted from fissures in the lunar surface. Because lunar basalts contain more Fe and less Si and Al than terrestrial basalts, the lavas were quite fluid and formed thin, widespread flows. The lavas cooled at different rates, dependent on the thickness of individual flows, to produce a variety of mineral textures. Many lava flows accumulated in thick stacks that partly filled many of the mare basins.

2. *Pyroclastic deposits (volcanic ash):* Gases contained within rising magmas can be explosively released when the magmas reach the surface of a planet. As lavas pour from a fissure vent, gases may be released to drive a fountain of molten droplets. On the Moon, these *lava fountains* associated with eruptions of basalt formed small glassy beads. Deposits of these beads are widely dispersed around lunar volcanic vents because of low gravity and eruption into a vacuum. Such *pyroclastic deposits* are similar to the volcanic ash deposited around lava fountains on Earth. Two striking examples of lunar pyroclastic rocks are the *orange soils* (although they really are not soils, but rather volcanic deposits) from the Apollo 17 landing site and the *green glass* from the Apollo 15 landing site. Orbital photographs of the lunar surface reveal *dark-mantle deposits,* which may also be of pyroclastic origin, surrounding apparent volcanic vents (section 4.2.1).

Pristine highland rocks (see section 6.3). Among the wide variety of rock types collected from the lunar highlands are at least a few that probably represent material from the original lunar crust that formed between 4.6 and 4.3 b.y. ago. The chemical compositions of these rocks indicate that, during this interval, extensive melting occurred in the outermost part of the Moon. According to several models, the Moon was covered by a *"magma ocean":* a layer of molten silicate perhaps hundreds of kilometers deep (section 2.4).

The question of a lunar magma ocean is fundamental to lunar history. If such an ocean cooled and crystallized, the physical separation of crystals (the floating of lower-density plagioclase feldspar) produced the original lunar crust.

After crustal formation, the long history of intense meteoroid bombardment has masked most of the actual unaltered (*pristine*) lunar crust. Samples of nonbasaltic (e.g., highland) pristine rocks are rare. The few such samples that are believed to be pristine have been subjected to extensive study because of

the clues they provide to understanding the origin and early history of the Moon. This work has been enlivened by the difficulty in distinguishing between genuine pristine highland rocks and similar rocks produced in large meteoroid impacts.

Classification for pristine highland rocks is roughly parallel to that for similar terrestrial rocks. Pristine highland rocks are divided into several groups:

1. *Ferroan anorthosite:* These rocks are light-colored, rich in Ca and Al, and are composed mostly of plagioclase feldspar. Minor minerals include pyroxene and olivine, which are richer in Fe than those of most Mg-rich crustal rocks (see below); hence the adjective "ferroan" is applied to these anorthosites. These anorthosites may be the pro-ducts of flotation of plagioclase in a magma ocean.

2. *Mg-rich rocks:* This second group of rocks is more varied, including some plagioclase-rich rocks, but many rocks with more pyroxene and olivine and correspondingly smaller amounts of plagioclase. Within the Mg-rich group are several rock types distinguished by their major minerals: *Gabbros* and *norites* are composed of pyroxene and plagioclase, *troctolites* contain mostly olivine and plagioclase, and *dunites* are nearly pure olivine rocks. If a magma ocean did indeed form on the Moon, the Mg-rich rocks probably formed after it had largely solidified.

3. *KREEP rocks:* In contrast to most other lunar rocks, the KREEP rocks are highly enriched in potassium (K), rare earth elements (REE), and phosphorus (P). The few known pristine KREEP rocks are basaltic lavas. They are apparently older than most of the basaltic lavas that fill mare basins. KREEP rocks appear to be most abundant around the Imbrium Basin. Because of its unique chemical character, KREEP is recognized in many breccia samples (see below); only a small amount is needed to produce a distinctive chemical signature.

Breccias (see sections 6.3 and 6.4). Nothing better demonstrates the intensity of meteoroid bombardment of the lunar surface throughout its history than the fact that most rock samples returned by the Apollo missions are *breccias* (consolidated fragmental rocks), which were formed during meteoroid impacts. Breccias are complex rocks composed of discrete rock, mineral, or glass fragments (*clasts*) set in *a matrix* (the fine-grained material between the larger rock and crystal fragments; matrix can be made up of similar fragments that are just smaller, or it may be made of a completely different rock type). The individual clasts may represent a wide range of components of different composition and age, including lunar bedrock, pieces of older breccias, and clots of impact-melted rock (textures of the melt rocks can range from glassy to completely crystalline).

Such complex rocks have bred complex classification schemes, but two fundamental types can be distinguished: *monomict breccias* and *polymict breccias.*

Monomict breccias contain only a single rock type, which has been broken into myriad deformed and crushed clasts. Monomict breccias are, in fact, simply highly crushed samples of a single lunar bedrock type. They have not been mixed with other rock types and may preserve some clasts with their original textural character. For that reason, they have been included with the pristine highland rocks in section 6.3.

Polymict breccias, discussed in section 6.4, are the most common of lunar breccias. As the name implies, they contain a variety of different materials, derived from several types of bedrock, earlier generations of breccias, and impact melts. Their classification is correspondingly complicated, but several general types can be distinguished on the basis of the nature of the fragments and especially the matrix. The breccia types described in section 6.4 are:

1. *Fragmental breccias:* These rocks are composed of fragments of rocks, often including earlier-formed breccias, in most cases just barely stuck together. The matrix consists of finer-grained fragments of the same material.

2. *Glassy melt breccias:* These breccias consist of a similar variety of fragments (clasts), enclosed in a matrix of impact-melt glass. The glassy matrix has not crystallized, implying rapid cooling of the rocks. As the number of fragments decreases, glassy melt breccias grade into fragment-poor *impact glasses,* although no dividing line has been established between the two rock types.

3. *Crystalline melt breccias:* These rocks are similar to the glassy melt breccias, but the melt matrix cooled more slowly. As a result, the originally molten matrix has solidified to form a crystalline igneous rock that often resembles a lava. The ratio of clasts to matrix varies widely.

4. *Clast-poor impact melts:* Crystalline melt breccias sometimes have so few clasts that they may have textures similar to a lava, and can be referred to as clast-poor impact melts. In many cases it is difficult to distinguish between these melt breccias and pristine lunar igneous rocks. A lot of research and discussion between lunar geologists has been directed, not always successfully, to making distinctions between clast-poor impact melts and lavas. Relatively high concentrations of rare elements thought to be introduced by meteoroid contamination (e.g., Ir, Au, Os; see section 8.6) are often used as a criterion of impact-melt origin.

5. Granulitic (metamorphic) breccias: Granulitic breccias were formed during the alteration and recrystallization of other breccias that have been subjected to high temperatures (~1000°C) since they were formed. Under these conditions the original textures have been obliterated during recrystallization and replaced by an even-grained *granulitic* texture. A completely recrystallized rock that retains none of its original texture is *a granulite.*

6. Dimict (two-component) breccias: Two-component breccias may have been produced in the shattered rocks injected by and mixed with impact melt below an impact crater. Similar rocks have formed this way on Earth, where the impact-melt component is called *pseudotachylite.*

7. *Regolith breccias:* Breccias that preserve distinctive regolith features, such as small glass spheres and vesicular regolith glasses (*agglutinates*), are classified as regolith breccias. These breccias are simply regolith that has just barely been turned into a rock.

These lunar rock classifications are discussed below in approximately the order of their definition above.

6.1. MARE BASALTIC LAVAS AND VOLCANIC GLASSES

Volcanism is a fundamental planetary process. Even though lava flows and pyroclastic deposits form less than 1% of the lunar crust, they provide information about the Moon's internal constitution and its thermal history. Mare basalt lavas were produced inside the Moon by *partial melting* of the lunar mantle. If this melting process involved chemical equilibrium between the melted and unmelted portions, then the lavas will preserve clues to the chemical and mineral compositions of the regions that underwent partial melting. They will also contain information about the pressures (and therefore the depths) at which melting occurred. Furthermore, the ages of lunar volcanic rocks tell when they were erupted; by age-dating different lavas, it is possible to determine how the rate and depth of melting changed with time, revealing details of the Moon's thermal history.

Lunar volcanic rocks and their landforms may also contain important potential resources. The volcanic plains that form the maria are rich in Fe, and many are rich in Ti, most of which is in the mineral ilmenite ($FeTiO_3$). This mineral can provide TiO_2, Fe, and 0 by chemical reduction, the TiO_2 useful as a refractory, the Fe for materials fabrication, and the O for life support and rocket propellants. In addition, because the older lunar rocks are pervasively shattered by meteoroid bombardment, virtually the only areas of near-surface intact bedrock on the Moon are in the younger lunar maria, which might be an important consideration for building large structures. Lava tubes, which are the hollow underground channels where lava once flowed, might even be used as shelters from solar and galactic radiation (Hörz, 1985a).

6.1.1. Chemical Composition, Classification, and Properties of Mare Basalts

Like terrestrial basalts, lunar basalts are low in silica (<54% SiO_2). Most other lunar rocks, however, are also low in silica. This contrasts with Earth, where the crust contains abundant high-silica granitic rocks. The range of compositions among lunar basalts is great, and allows for recognition of a wide variety of lunar mare basalt types. Representative chemical compositions for mare basalts are listed in Tables A6.1 (major elements) and A6.2 (trace elements).

One of the most fundamental features of the Moon is its division into two chemically distinct terrains: the mare basalts and the more abundant highland regions. Mare basalts contain greater concentrations of FeO and TiO_2 and have higher CaO/Al_20_3 ratios than do rocks from the highland areas, a situation that reflects the lower proportion of Al-rich plagioclase feldspar in the basalts. Fragments of older mare basalts, which have been found in rocks from the highlands, demonstrate that mare-type volcanism actually began before the final flooding of the visible maria (e.g., *Ryder and Taylor,* 1976; *Taylor et al.,* 1983; *Schultz and Spudis,* 1983).

One of the most striking chemical characteristics of mare basalts is their large variation in TiO_2 contents. This variation has allowed recognition of three major groups of different mare basalts: *high-Ti* (>9 wt.% TiO_2), *low-Ti* (1.5-9 wt.% TiO_2), and *very-low-Ti* (<1.5 wt.% TiO_2). Although these groups have been defined from analysis of returned samples, remotely-sensed spectral data that cover unsampled areas of the Moon suggest that there is in fact a continuous gradation from very-low- to high-Ti mare basalts (*Pieters,* 1978).

Other chemical parameters can be used to subdivide these three groups, as shown in Fig. 6.1, which is a three-axis plot of TiO_2, Al_20_3, and K_2O. Some low-Ti basalts are richer in Al_20_3 than others; these have been designated *aluminous low-Ti* mare basalts. Apollo 11 high-Ti mare basalts have been subdivided into high-K (>0.3 wt.% K_20) and low-K (<0.1 wt.% K_20). A group of aluminous mare basalts from the Apollo 14 site are, for the Moon, exception-ally rich in K_20, averaging 0.9 wt.%; these have been designated *very-high-K,* or *VHK,* mare basalts (*Shervais et al.,* 1985b). Detailed reviews of mare

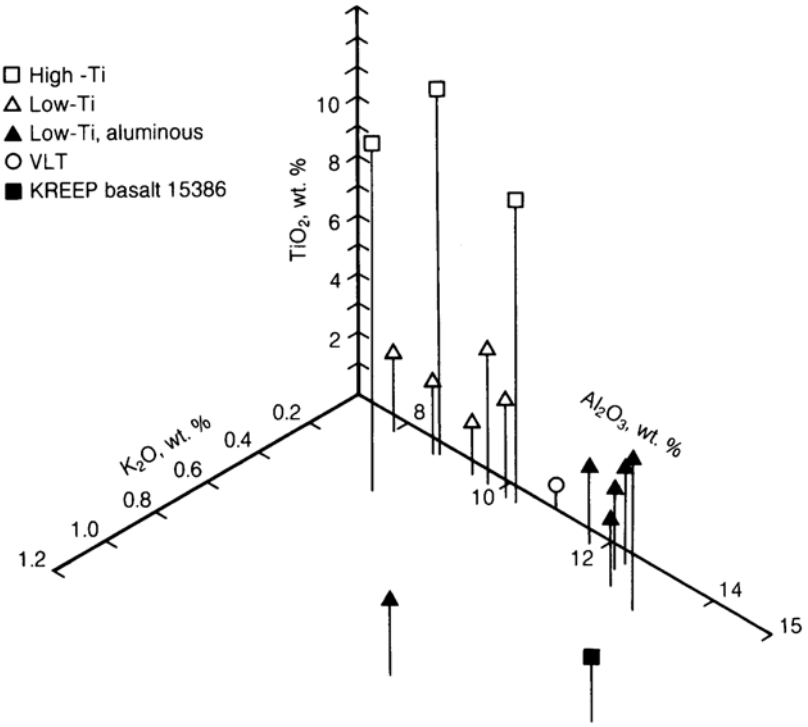

Fig. 6.1. K_2O-TiO_2-Al_2O_3 plot for chemical compositions of representative lunar mare basalt types. The plot shows the separation of lunar basalts into chemically distinct groups, especially on the basis of TiO_2 content. Data are from Table A6.1.

basalt chemical compositions are given by *Papike et al.* (1976), *Papike and Vaniman* (1978), and *BVSP* (1981).

High-Ti mare basalts. Basalts collected from the Apollo 11 and 17 sites are mainly high-Ti mare basalts. Rare high-Ti mare basalt fragments are also found in the regolith at the Apollo 16 highland site; they were probably thrown to that site by impacts on distant mare basalt surfaces, perhaps on Mare Nectaris (*Delano,* 1975). The Apollo 11 high-Ti basalts have been subdivided into two main groups, low-K and high-K (Fig. 6.1). The Apollo 17 high-Ti basalts include one group that is much like Apollo 11 low-K basalts, as well as another very-high-Ti group, which is more abundant, that contains even more TiO_2 and more of the opaque mineral ilmenite (Table 6.1).

Even within these groups, the compositions of high-Ti basalts vary significantly from sample to sample. Explanations for these differences are complicated by the fact that virtually all mare basalt samples were collected as loose blocks in the regolith, and no identifiable lava flows were sampled directly on the lunar surface (although sampling at the Apollo 15 site came within a few meters of lava bedrock). Nevertheless, studies of terrestrial lava flows suggest that the observed variations from sample to sample reflect variation both within and between individual lava flows.

These variations are thought to result from the crystallization and separation of early-forming minerals. Analyses of numerous samples of high-Ti basalts show that TiO_2 decreases and Al_2O_3 increases as MgO decreases (Figs. 6.2a,b). This variation is consistent with the crystallization of Fe-Ti oxide minerals, such as ilmenite and armalcolite (both Ti-rich), and of olivine (Mg-rich), followed by their separation (e.g., by sinking) from the remaining liquid magma. This early crystallization could have taken place as the erupted lavas cooled while flowing across the lunar surface or sitting in lava ponds. The early-crystallizing minerals contain little or no Al_2O_3, and this component therefore becomes enriched in the remaining liquid as crystallization proceeds. Removal of roughly equal amounts of ilmenite and olivine drives the chemical trends (referred to as *fractionation trends*) toward lower TiO_2 and MgO contents (Fig. 6.2a). By contrast, the Apollo 11 high-K basalts have little chemical variation, but they still lie along similar fractionation trends.

The contents of trace chemical elements (*trace elements*) in high-Ti mare basalts are listed in Table A6.2. The relative abundances of rare earth elements (*REE;* Fig. 6.3) are of particular interest. Because these elements are chemically similar and dilute enough in the magma to have relatively "ideal" and well-determined behavior, their contents give

TABLE 6.1. Modal mineral abundances (vol.%, normalized to 100%) of the major minerals in lunar mare basalts (from *BVSP*, 1981).

	Rock Type	Opaques*	Pyroxene	Olivine	Plagioclase
Apollo 17	very-high-Ti	24.4	47.7	4.6	23.4
Apollo 11	high-K	20.6	57.5	0.1	21.7
Apollo 17	low-K	15.1	51.6	—	33.3
Apollo 11	low-K	14.6	50.9	2.3	32.2
Apollo 12	ilmenite	9.3	61.1	3.6	25.9
Apollo 12	pigeonite	9.1	68.4	1.4	21.1
Apollo 12	olivine	7.1	53.5	20.2	19.2
Luna 16		7.1	51.5	0.1	41.2
Apollo 15	olivine	5.5	63.3	7.0	24.1
Apollo 15	pigeonite	3.7	62.5	—	33.8
Apollo 14	aluminous (14053)	3.2	53.8	—	43.0
Luna 24	very-low-Ti	1.8	48.6	10.4	39.1
Apollo 17	very-low-Ti	1.0	61.7	5.4	31.9

* Opaques are minerals that do not transmit light in thin section (e.g., armalcolite, ilmenite, spinel, troilite).

clues to the processes of melting, crystallization, and crystal separation from a melt. In the high-Ti basalts, the REE have pronounced bow-shaped patterns (Fig. 6.3). The relative REE abundances (when normalized to abundances in chondritic meteorites, a common standard; see section 8.4) increase from La to Sm, then decrease from Gd to Lu. The high-K basalts contain greater abundances of REE because these elements tend to concentrate along with K, Rb, and some other elements.

All of the high-Ti mare basalts have low Eu contents (negative *Eu anomalies*) relative to the other REE (see section 2.4.4). The explanation for negative Eu anomalies is that Eu behaves differently from the other REE because a significant amount of it occurs as the divalent ion Eu^{2+}, as well as the trivalent ion Eu^{3+}, in contrast to the other REE, which are only trivalent. This difference causes Eu to concentrate in Ca feldspar, $CaAl_2Si_2O_8$, by substitution for Ca^{2+}. Negative Eu anomalies appear to be a fundamental characteristic of the basalt source regions in the lunar mantle. This condition suggests that there was a Moonwide earlier stage of feldspar removal from the chemical system that produced the source regions, and that the separated feldspar took much of the Eu with it. One possibility, widely accepted, is that plagioclase crystallization and flotation occurred during a magma ocean episode early in the Moon's history, when the outer Moon may have contained a layer of melt tens or hundreds of kilometers thick (section 2.4.3). However, other explanations for the Eu anomaly, involving less extreme conditions, have been proposed (e.g., *Walker,* 1983).

Low-Ti mare basalts. A wide variety of low-Ti mare basalts were collected at the Apollo 12, Apollo 15, and Luna 16 landing sites on various maria, as well as at the Apollo 14 landing site. The Apollo 12 and 15 varieties each consist of two main basalt types, *olivine basalts* and *pigeonite* (low-Ca pyroxene) *basalts.* In general, the olivine basalts have more MgO and less CaO, Al_2O_3, and TiO_2 than do the pigeonite basalts at the same site.

Like the high-Ti mare basalts, none of these low-Ti basalts crystallize plagioclase feldspar early as they cool. Both types show clear evidence for the early separation of olivine or pigeonite, but not of ilmenite. The resulting trends of chemical composition show increasing TiO_2 and Al_2O_3 with decreasing MgO (Figs. 6.2c,d). In addition to these basalts, some of the low-Ti basalts collected at the Apollo 12 site are noticeably richer in ilmenite than the others; these have been designated *ilmenite basalts.* The REE abundances in low-Ti basalts (Fig. 6.4) are, in general, lower than in the high-Ti basalts, although both groups have the same bow-shaped pattern and both have negative Eu anomalies. Concentrations of other *incompatible elements* (i.e., those elements that tend to stay in the liquid rather than in the early crystallizing minerals) such as Sr and U are also lower in the low-Ti basalts than in the high-Ti basalts (Table A6.2).

Aluminous low-Ti mare basalts. Some groups of low-Ti basalts contain more Al_2O_3 than do those from the Apollo 12 and 15 sites (Fig. 6.1); these have been called *aluminous.* Three major categories of aluminous mare basalts can be distinguished on the basis of their location and chemistry: those from the

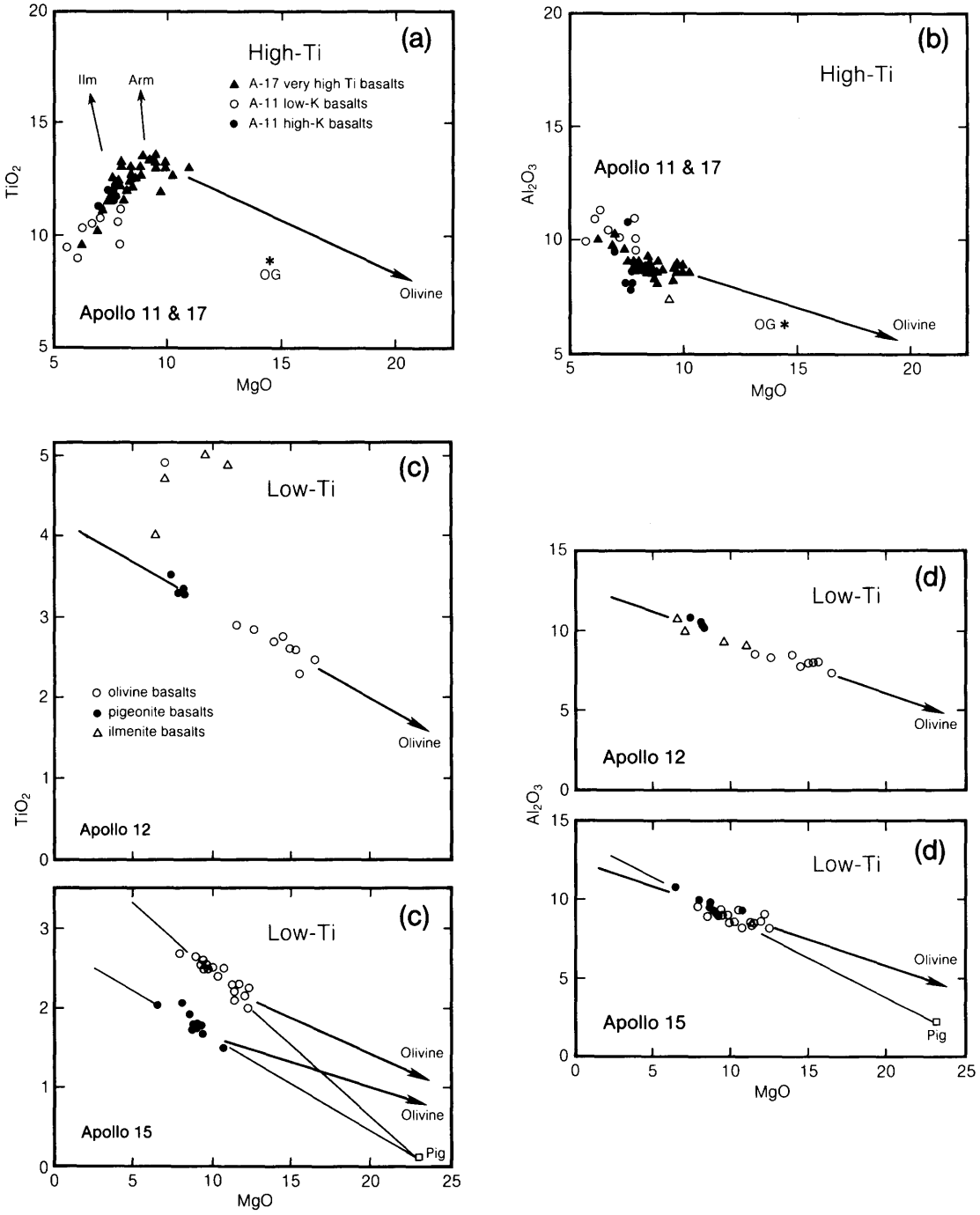

Fig. 6.2. Chemical variation diagrams showing MgO-TiO_2 and MgO-Al_2O_3 relations for high-Ti **(a,b)** and low-Ti **(c,d)** lunar mare basalts (*Papike et al.,* 1976). Actual basalt compositions are represented by circles, dots, and triangles. "OG" in panels **(a)** and **(b)** shows the composition of Apollo 17 orange glass. Arrows point toward the compositions of specific minerals that crystallize from the basaltic magmas (Ilm = ilmenite, Arm = armalcolite, Pig = the low-Ca pyroxene *pigeonite*). If these minerals or combinations of them are removed, the composition of the remaining liquid will be driven in an opposite direction, producing the trend of plotted points.

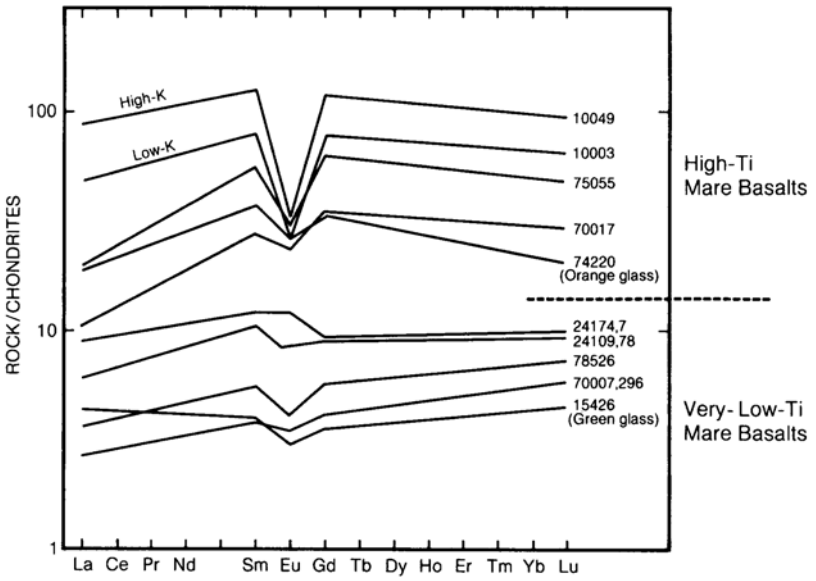

Fig. 6.3. Plot of rare earth element (REE) contents in high-Ti and very-low-Ti (VLT) mare basalts (data from Table A6.2 and from *BVSP,* 1981). REE contents are normalized to the contents in chondritic meteorites. The high-Ti basalts have higher REE concentrations in a convex-upward ("bow-shaped") pattern interrupted by a large to small negative Eu anomaly. The VLT basalts have a flatter pattern in which small negative Eu anomalies may or may not be present.

Luna 16 site, some from the Apollo 14 site (mostly from one breccia sample, 14321), and others from the Apollo 14 site that are enriched in K_2O. The Luna 16 mare basalts contain the most TiO_2 of any of the aluminous low-Ti basalts, averaging about 5 wt.%. They also have distinctive REE patterns (Fig. 6.5) that are characterized by much greater abundances of the light REE (La through Sm) than the heavier REE. The Luna 16 basalts do, however, display the same typical bow-shaped pattern, with a negative Eu anomaly, that is characteristic of other mare basalts.

A rich variety of aluminous mare basalts was collected from the Apollo 14 site. Several fragments of aluminous basalt, contained in a single breccia sample (14321), actually represent a suite of related rocks from several distinct lava flows. They have relatively uniform major-element compositions (Table A6.1), but this uniformity is coupled with an eightfold variation in the abundances of REE and other incompatible elements (Table A6.2; Fig. 6.5). None of these basalts has the typical bow-shaped REE pattern that characterizes the mare basalts described above, although all have negative Eu anomalies. The highest REE group, designated Group 1 by *Dickinson et al.* (1985), has a REE pattern lower than but similar to that of the unusual *KREEP basalts* (Fig. 6.5), a highland rock type that is rich in incompatible elements (see section 6.3.2). Some Apollo 14 mare basalts have higher REE contents than do the Group 1 rocks, but they have much flatter REE patterns (*Shervais et al.,* 1985a). The lowest REE group (Group 5) in breccia 14321 has an REE pattern characterized by a continuous rise from La to Lu; a negative Eu anomaly is still present. Groups 2, 3, and 4 have REE distributions that fall between the extremes of Groups 1 and 5.

A few mare basalt fragments in other Apollo 14 highland breccias, samples 14304 and 14305, contain exceptionally high quantities of K_2O (0.6-1.4%) for mare basalts (*Shervais et al.,* 1985b) and are designated *very-high-K,* or *VHK,* mare basalts. These basalts are high in K_2O for basalt samples from the Moon; they are also high in comparison to terrestrial ocean-floor basalts, with ~0.1-0.3% K_2O, but much lower than many types of terrestrial continental basalts that commonly have K_2O contents of ~2% and may have more than 4% K_2O (this difference between Earth and Moon reflects the depletion of the entire Moon in K relative to Earth). The VHK basalts have major-element compositions much like the Apollo 14 aluminous mare basalts, except for the enrichment in K_2O. Their REE contents, however, are not significantly greater than those of Apollo 14 aluminous basalts, and the REE enrichment that might normally accompany the K_2O enrichment is not observed. Consequently, the VHK magmas could not have been derived from basalts like those in sample 14321 by any simple process involving mixing of Group 5 basalts with KREEP. Their unusual characteristics may have been produced by more complex processes involving assimilation of lunar high-silica ("granitic") materials (see section 6.3.5 for descriptions of granitic materials, and *Shervais et al.,* 1985b or *Shih et al.,* 1986, for assimilation models).

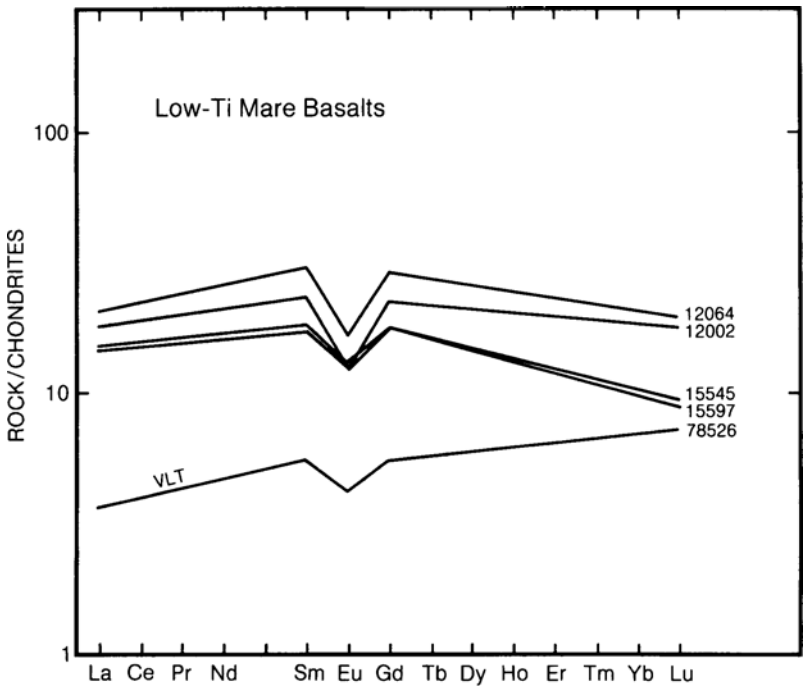

Fig. 6.4. Plot of REE contents in low-Ti mare basalts. These basalts have convex-upward ("bow-shaped") patterns with small negative Eu anomalies. One very-low-Ti mare basalt (VLT) is shown for comparison (data from Table A6.2).

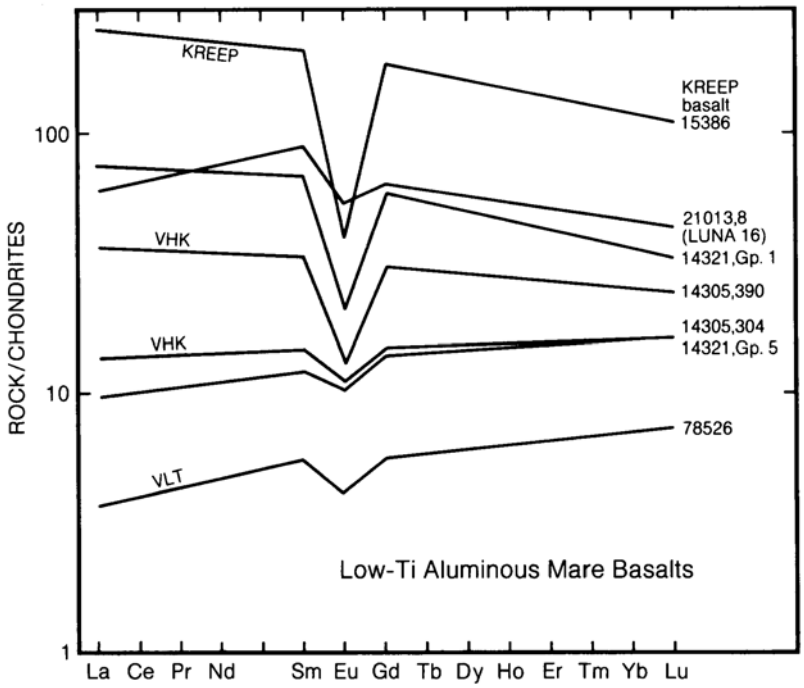

Fig. 6.5. Plot of REE contents in low-Ti, aluminous mare basalts. The REE patterns vary from slightly depleted in the light REE (left side of diagram) to slightly enriched. Curves labeled "VHK" indicate very-high-K basalts that occur as fragments within sample 14305. Data for very-low-Ti (VLT) and KREEP basalts are shown for comparison (data from Table A6.2 and from *Shervais et al.,* 1985b).

Very-low-Ti (VLT) mare basalts. VLT mare basalt's were first discovered as tiny fragments in the Apollo 17 drill core (*Vaniman and Papike,* 1977c). The basalt particles collected by Luna 24 from Mare Crisium were also VLT mare basalt's. Besides containing lower amounts of TiO_2 (<1.5%) than other mare basalt's, VLT basalt's are distinctive in having low abundances of REE and other incompatible elements; they also have REE patterns that are not bow-shaped. Instead, the REE contents (Fig. 6.3) rise continuously from La to Lu, although Luna 24 VLT basalt's have rather flat patterns among the heavy REE (Gd to Lu). All but one fragment of the Luna 24 basalt's have small negative Eu anomalies. A similar basaltic composition, the Apollo 15 green-glass pyroclastic deposits (section 6.1.7), has comparable chemical characteristics.

Comparison with other planetary basalt's. The chemistry of lunar mare basalt's differs in many ways from that of terrestrial basalt's. In general, Ti and Cr concentrations and Fe/Mg ratios are considerably higher in lunar basalt's, and Al, Na, and K concentrations are lower.

Lunar mare basalt's are also depleted in volatile elements (K, Na, Rb, Pb, C, H, etc.) compared to terrestrial basalt's. This condition is illustrated by the low K/U ratios of lunar basalt's (Fig. 6.6). The K/U ratio is especially useful for recognizing volatilization events; K and U behave similarly during melting and crystallization of silicate magmas, but K is volatile (vaporizes at low temperatures) and U is refractory (vaporizes at high temperatures). Therefore, the K/ U ratio will not be much altered by normal melting and crystallization, but it will be sensitive to any high-temperature volatilization events.

Except for some rare meteorites (*eucrites* or *basaltic achondrites*), lunar mare basalt's (and lunar highland rocks as well) have lower K/U ratios than all other planetary samples, including the unusual basaltic *SNC* meteorites, which may have come from Mars (e.g., *McSween,* 1985). One might argue that the low K/U ratios in lunar basalt's reflect an enrichment in U instead of a depletion in K. However, there is ample additional evidence for the general depletion of volatile elements in the Moon—the totally water-free nature of lunar basalt's, as well as the extremely low abundances of other volatile elements such as Bi, Cd, and Ti (*Wolf et al.,* 1979). Curiously, S, though usually volatile in its terrestrial behavior, occurs in greater abundance in lunar mare basalt's than in terrestrial basalt's.

Lunar basalt's are also depleted in *siderophile* elements, elements that tend to concentrate in metallic iron (Ni, Co, Au, Ir, etc.). This depletion has been discussed and debated in much detail, because it has great bearing on how the Moon formed and on whether or not the Moon has a metallic core (e.g., *Newsom,* 1986). An example of this depletion is the relationship between Mo (a siderophile element) and Nd (a rare earth element; Fig. 6.7). Both elements are refractory, so differences in their abundances are not caused by volatilization of one of them. Furthermore,

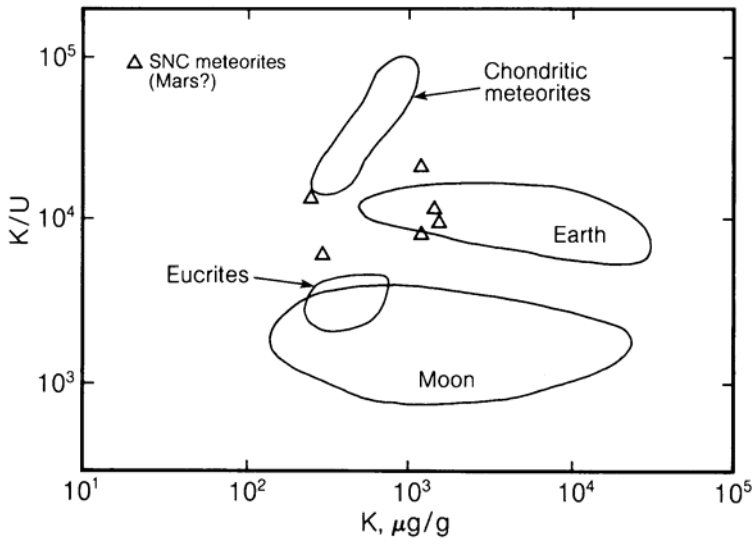

Fig. 6.6. Plot of potassium/uranium (K/U) vs. K for various analyzed solar system materials (after *Taylor,* 1982). The uniformly low K/U ratios of lunar samples demonstrate the Moon's general depletion of volatile elements and sets it clearly aside from most other solar system objects.

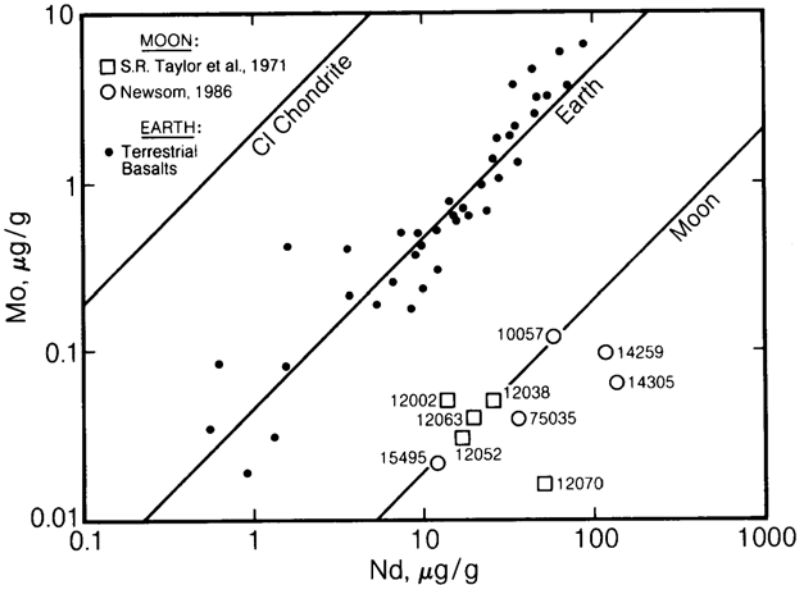

Fig. 6.7. Plot of Mo (a siderophile element) vs. Nd (a lithophile element) in terrestrial basalts (filled circles) and lunar basalts (open symbols with sample numbers). The data show that lunar basalts (and hence the lunar mantle, from which they were derived) are depleted in siderophile elements compared to terrestrial basalts and Earth's mantle *(Newsom,* 1986).

in systems where no metallic iron is present, Mo behaves geochemically very much like Nd, so the observed depletion cannot be due to any process that occurs in a melt that is free of metallic iron. Consequently, the depletion of Mo (Fig. 6.7) has been interpreted (*Newsom,* 1986) as an indication that all lunar basalts (and the lunar mantle that melted to form them) contain uniformly lower siderophile element abundances than do terrestrial basalts and the mantle of the Earth. Extensive analyses of lunar rocks have shown that the greater the tendency of an element to concentrate in metallic iron, the more depleted it is in lunar rocks (*Newsom,* 1986).

Oxygen partial pressures (fugacities) during crystallization. Even a cursory look at lunar basalts shows that they formed under substantially more reducing conditions (lower oxygen partial pressures) than did terrestrial basalts. Lunar basalts invariably contain metallic iron, which occurs naturally on Earth under only the most extraordinary circumstances. However, there is no real contradiction between the widespread presence of metallic iron and the generally low abundances of the siderophile elements (such as Ni) that should associate with metallic iron. Most of the metallic iron in lunar basalts has been formed from the reduction of FeO during the crystallization of the basalts (see section 5.4.2), long after the siderophiles were removed from the mantle materials that melted to produce the basalts. Further evidence of reduction is the fact that there is virtually no Fe_2O_3 in lunar lavas.

Intrinsic oxygen *fugacities* (effective partial pressures in terms of thermodynamic chemical potential) of mare basalts (Figs. 6.8 and 5.17) are about a million times lower than those in terrestrial basalts at any given temperature. The reduced character of lunar lavas causes some elements, such as Eu and Cr, to have lower valence states and thus to have different chemical behavior on the Moon than they do in terrestrial rocks.

Viscosity. The low viscosity of lunar lavas is suggested by the way they spread out in thin, extensive flows on the lunar surface. This low viscosity has been confirmed by measurements of the viscosity of a synthetic liquid with the composition of Apollo 11 high-Ti basalt (*Murase and McBirney,* 1970). The measured viscosity ranges from 4.5 p at 1495°C to 10p at 1395°C when measured in air. Measurements in an Ar atmosphere yielded similar results. These viscosities are approximately that of heavy motor oil at room temperature. Terrestrial lavas are typically 10 times more viscous (Fig. 6.9). Section 5.2 discusses some of the implications of this viscosity difference for potentially effective concentration of heavy crystals by settling in lunar mare magmas.

6.1.2. Mineralogy of Mare Basalts

The minerals that make up a basaltic rock and their relative amounts are largely dependent on the chemical composition of the lava from which the

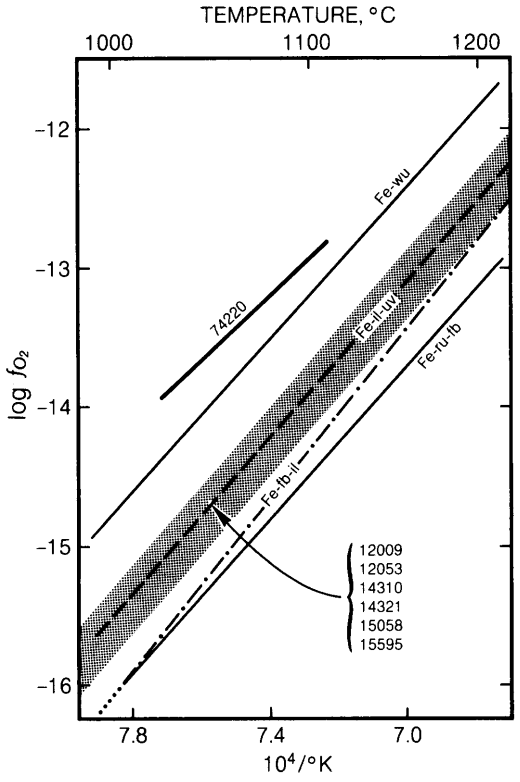

Fig. 6.8. Plot of fO_2 (oxygen fugacity; a measure of effective oxygen chemical potential roughly related to oxygen availability) vs. temperature in equilibrium with lunar mineral assemblages and lunar igneous rocks (sample numbers). Note that sample 74220 *is* the Apollo 17 orange glass (Table A6.1). Measured oxygen fugacities in lunar igneous rocks fall in the shaded area. Labeled lines are mineral equilibrium "buffer" curves for the Fe-FeO-TiO_2 system: Fe = iron metal; il = ilmenite; uv = ulvöspinel; wu = wüstite; fb = ferropseudobrookite; ru = rutile. Adapted from *Taylor* (1982). In contrast, terrestrial basalts would plot just above this diagram (see Fig. 5.17).

rock crystallized. Lavas that contain substantial amounts of TiO_2, for example, will crystallize more ilmenite and other Fe-Ti oxide minerals than will lavas that are low in TiO_2.

The mineralogy of a basaltic rock is also affected by how fast the lava cooled. In cases of extremely rapid cooling, as experienced by the particles ejected in lava fountains, no minerals form at all; the resulting rock is all quenched glass. At the other extreme, very slow cooling will allow separation of crystallizing minerals from lava, allowing the remaining liquids to develop a significant range of chemical compositions.

Lunar mare basalts are composed chiefly of four major minerals: pyroxene, plagioclase, olivine, and metal oxides (ilmenite, armalcolite, and spinel). Mare basalts also contain minor amounts of minerals that form near the end of crystallization. These late-stage minerals include silica minerals (cristobalite or tridymite), potassium feldspar, zircon and other Zr-bearing silicates, phosphate minerals (apatite and whitlockite), metallic iron, and iron sulfide (troilite). These minerals are described in detail in Chapter 5. Varying amounts of late-stage glass may also be preserved in mare basalts.

Abundances of the four major mineral types in mare basalts have been normalized to 100% in Table 6.1; the amounts of other minerals rarely exceed 5%. The abundance of metal-oxide minerals varies directly with TiO_2 content, because high TiO_2

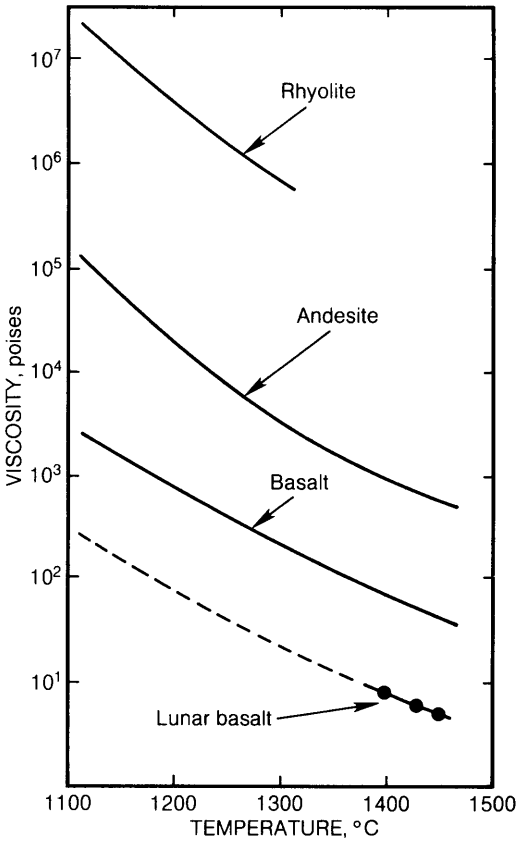

Fig. 6.9. Plot of measured viscosity as a function of temperature for lunar high-Ti mare magma, compared to terrestrial magmas (from *Murase and McBirney,* 1970). Lunar basaltic magmas are only about one-tenth as viscous as terrestrial basaltic magmas.

contents result in the formation of Ti-rich oxide minerals such as ilmenite (see also Fig.5.18). Apollo 17 very-high-Ti basalts have the most oxide minerals (largely ilmenite), followed by other high-Ti basalts, low-Ti basalts, and very-low-Ti basalts. Because Al occurs chiefly in plagioclase feldspar, the aluminous mare basalts (14053 and Luna 16 in Table 6.1) have the highest plagioclase-to-pyroxene ratios. A more detailed comparison between major-element composition and mineral abundances is given by *BVSP* (1981, p. 254).

The chemical compositions of the individual minerals reflect both the bulk composition and the cooling rate of the lava in which they formed. These relations are shown most dramatically by the pyroxenes. Individual pyroxene crystals in mare basalts are *compositionally zoned* (i.e., the composition, especially the amounts of Fe, Mg, and Ca, varies significantly) from their centers to their edges, and there are also substantial variations from one pyroxene crystal to another (Fig. 5.3). The chemical variations are not confined to the major elements (Fe, Mg, Ca) alone, but also involve minor elements such as Ti, Al, and Cr. Detailed discussions of pyroxene composition and how it is affected by lava composition, cooling rate, oxidation-reduction conditions, and temperature are given by *Bence and Papike* (1973), *Papike et al.* (1976), and *BVSP* (1981). Extensive chemical zonation is also found in other minerals. In fact, most mineral grains in mare basalts are not entirely uniform in composition, except very small ones and the silica minerals (e.g., cristobalite).

Mineral compositions can also be affected by the sequence in which different minerals crystallize from the cooling lava. This sequence is not the same in all lavas. It depends on the bulk chemical composition of the lava, on the cooling rate, and on the extent to which the first-formed minerals are removed (*fractionated*) from the lava.

6.1.3. Textures of Mare Basalts

The *texture* of a rock is defined by the sizes and shapes of the minerals that compose it and by the mutual geometric relationships between them. Texture is important because it contributes to a rock's physical properties, such as strength. In volcanic rocks, the observed textures reflect the crystallization history, including the cooling rate, and they also provide clues to the amount of crystallization that took place before the lava was erupted.

The texture of a volcanic rock is determined chiefly by the composition, initial temperature, and cooling rate of the lava from which it crystallized. Geologists have given names to many different textures that occur in terrestrial basalts. Applying these names to lunar mare basalts is complicated by the fact that plagioclase feldspar, which plays an important role in naming a texture, is more abundant in terrestrial basalts than in lunar ones. Nevertheless, geologists have managed to find appropriate textural terms for virtually all lunar basalts. Some of the most important textures are described below and shown in Figs. 6.10 to 6.13. A guide to textural terms appears as Table 1.3.3.1 in *BVSP* (1981).

High-Ti mare basalts. Most Apollo 11 high-K basalts have *intersertal* textures, in which pyroxene and ilmenite crystals form an open fretwork around plagioclase and glass. Other high-K basalts have *ophitic* textures, characterized by pyroxene crystals enclosed by plagioclase. *Grove and Beaty* (1980) prefer to call these two textures *"anti-intersertal"* and *"anti-ophitic"* to distinguish them from the normal intersertal and ophitic textures in terrestrial rocks, where plagioclase forms the fretwork or is enclosed within pyroxene. Some high-K basalts are *vitrophyric;* these contain a glassy matrix (*groundmass*) in which relatively large crystals are embedded. Examples of some textures appear in Fig. 6.10; for details, see *Beaty and Albee* (1978), *Beaty et al.* (1979), *Grove and Beaty* (1980), *Papike et al.* (1974), *Longhi et al.* (1974), and *Warner et al.* (1978b).

Low-K, high-Ti mare basalts have *ophitic* to *subophitic* textures (Fig. 6.10). This variability in texture results primarily from the variability in pyroxene size. Where pyroxene partially encloses the plagioclase, the texture is called *subophitic;* where pyroxene is coarser and fully encloses individual plagioclase crystals, it is called *ophitic*.

The sizes and shapes of individual crystals are also important in defining the textures of mare basalts, and certain crystal sizes and shapes tend to be associated with certain textures. Pyroxene crystals tend to be *euhedral* (i.e., regularly shaped and well faceted) in the more slowly cooled rocks, which commonly have coarsely granular or *ophitic* textures. Large, early-formed crystals (*phenocrysts*) of olivine occur only in the finer-grained *intergranular* basalts, in which the smaller crystals form a network resembling *intersertal* textures but lacking glass. In the coarser ophitic basalts, olivine crystals are smaller (or lacking) and are often mantled by later-crystallizing pyroxene.

Ilmenite in mare basalts forms elongate, bladed grains in the finer-grained subophitic rocks, grading to more equant, *anhedral* grains (lacking crystal faces) in the coarse ophitic samples. Many high-Ti basalts collected at the Apollo 17 site have *porphyritic* or *microporphyritic* textures, in which large crystals of olivine and armalcolite occur in finer-grained matrices. The olivine crystals are often *mantled* (rimmed by another crystal in crystallogra-

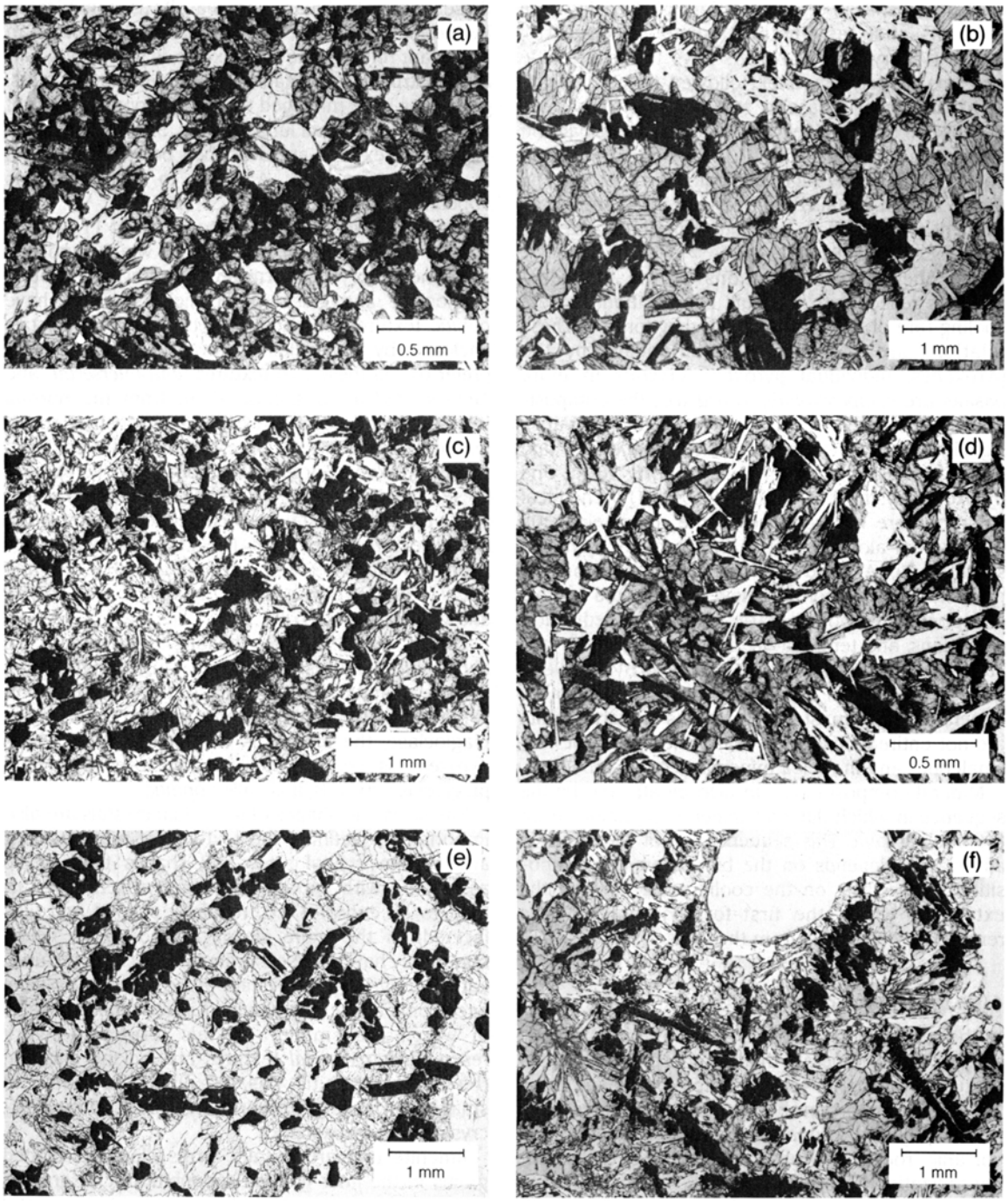

Fig. 6.10. Photomicrographs of high-Ti mare basalts showing the wide range of textures developed during crystallization. The major minerals are pyroxene and olivine (light gray), plagioclase (white), ilmenite (black). **(a)** Sample 10017,20, displaying an anti-ophitic texture; **(b)** sample 10044,55, displaying a subophitic texture; **(c)** sample 10003,40, displaying an intergranular texture; **(d)** sample 10062,44, displaying an ophitic to intergranular texture; **(e)** sample 70035,19, displaying a subophitic texture; **(f)** sample 71035,28, displaying a microporphyritic texture with a coarsely radiate matrix.

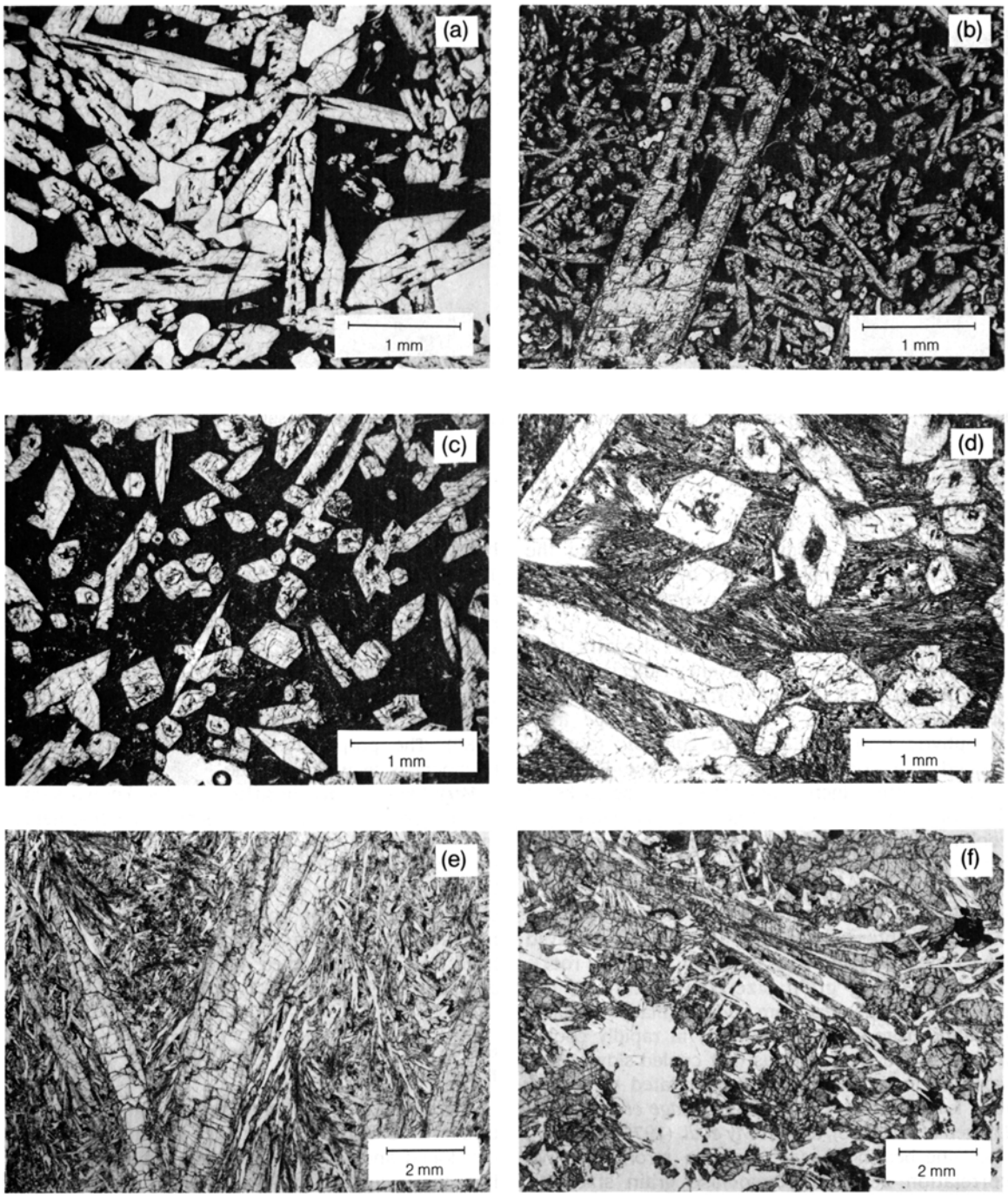

Fig. 6.11. Photomicrographs of low-Ti pigeonite basalts showing a range of textures from completely crystalline (*gabbroic*) to largely glassy (*vitrophyric*). **(a)** Sample 15486,22, porphyritic with an aphanitic groundmass; **(b)** sample 15597,17, microporphyritic with occasional large phenocrysts in an aphanitic matrix; **(c)** sample 15595,37, microporphyritic texture with a fine radiate matrix; **(d)** sample 15596,16, porphyritic with medium radiate matrix; **(e)** sample 15476,32, porphyritic with coarse radiate to intergranular matrix; **(f)** sample 15058,126, subophitic texture; **(g)** sample 15076,12, subophitic texture; **(h)** sample 15085,19, subophitic texture with distinctly coarse plagioclase.

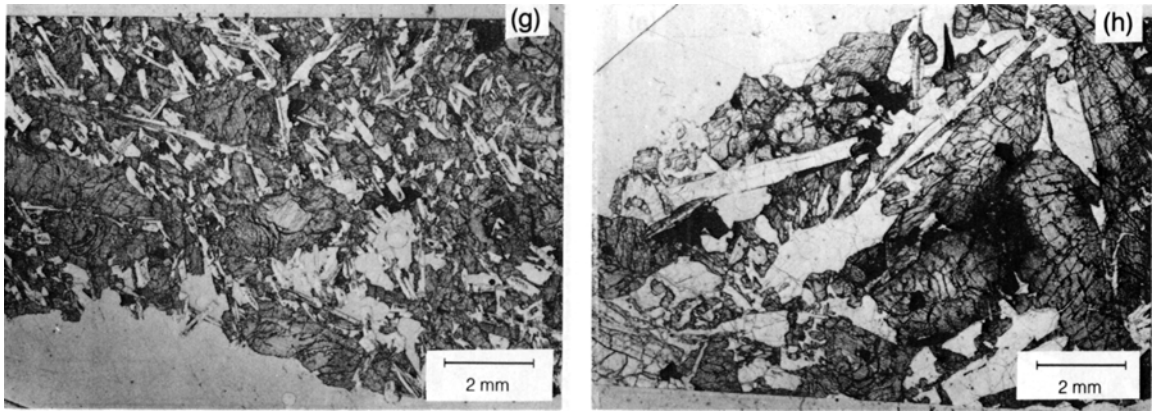

Fig. 6.11. (continued) **(g)** Sample 15076,12, subophitic texture; **(h)** sample 15085,19, subophitic texture with distinctly coarse plagioclase.

phically matched orientation) by augite, and the armalcolite is generally mantled by ilmenite. A few Apollo 17 samples have very coarse-grained subophitic textures.

Low-Ti mare basalts. Low-Ti basalts that contain pigeonite (low-Ca pyroxene), especially those from the Apollo 15 site, show an extraordinary range of textures. In these rocks, textures range from vitrophyric (mostly glassy) to *gabbroic* (coarse-grained and completely crystalline; see Fig. 6.11). Olivine becomes increasingly rare in these rocks as the grain size increases, indicating that with slow cooling olivine reacts with the liquid to produce pyroxene. The finer-grained rocks in this series are *porphyritic,* containing large, early-formed crystals (*phenocrysts*) in a finer, later-formed *groundmass.* Most of the phenocrysts are pigeonite, but embayed olivine phenocrysts occur in the most glassy rocks. With increasing grain size, the texture of the groundmass changes from *radiate* (bladed crystals radiating from common centers) in rapidly cooled rocks to subophitic in lavas that cooled slowly. This variation in groundmass texture, related to cooling rate, is discussed in detail in *Baldridge et al.* (1979), *Lofgren et al.* (1975), and *Dowty et al.* (1973, 1974a).

Olivine-bearing basalts have a strong positive correlation between plagioclase grain size and normative olivine content (*Walker et al.,* 1976). (The *normative* olivine content is calculated from the chemical analysis; the *modal* olivine content is measured from the sample with a microscope.) This relation suggests that the different samples formed by crystal settling inside a single, relatively thick flow. Observed textures range from vitrophyric to gabbroic; representative textures are shown in Fig. 6.12. Textures of ilmenite basalts range from fine-grained and porphyritic to coarse-grained (Fig. 6.12); this range of textures is also consistent with derivation within a single lava flow.

Most aluminous low-Ti mare basalts have subophitic to ophitic textures, though a few are vitrophyric (*Shervais et al.,* 1985a,b; *Dickinson et al.,* 1985). The porphyritic varieties have plagioclase phenocrysts, as well as olivine.

Very-low-Ti mare basalts. All the known samples of very-low-Ti mare basalts are small fragments found in soils, and determination of textures is therefore more difficult than would be the case for larger samples. The observed textures are generally subophitic to microporphyritic (Fig. 6.13), but fragments with both vitrophyric and ophitic textures have also been observed. For details, see *Vaniman and Papike* (1977c) and *G. J. Taylor et al.* (1978).

6.1.4. Crystallization Experiments on Mare Basalts

A great deal of effort has been spent in trying to understand how the textures of mare basalts developed and what the textures can tell us about how the lavas formed. In addition to studies of the rocks themselves, dynamic crystallization experiments have been performed on small samples with the compositions of lunar basalts. These samples are first completely melted and then cooled from their *liquidus* (completely molten) temperatures at various rates. These experiments have shown that the development of textures in basaltic rocks is con-

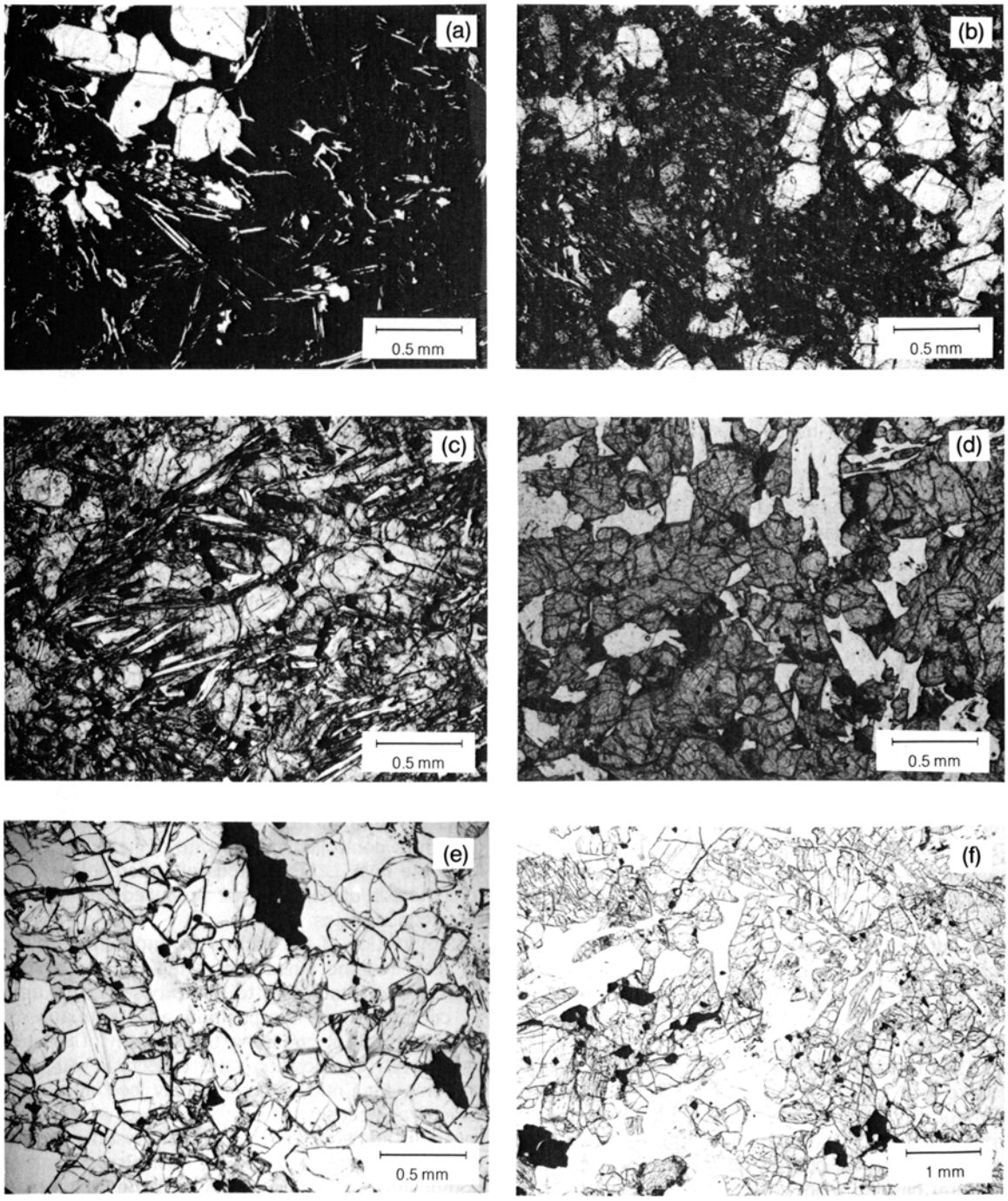

Fig. 6.12. Photomicrographs of low-Ti olivine **(a,c,f)** and ilmenite **(b,d,e)** basalts. **(a)** Sample 12009,11, porphyritic texture with coarse equant and fine dendritic phenocrysts and an aphanitic matrix; **(b)** sample 12022,110, microporphyritic with fine radiate matrix; (c) sample 12004,55, subophitic texture; **(d)** sample 12056,7, subophitic texture; **(e)** sample 12005,12, cumulate texture; **(f)** sample 12035,24, ophitic, gabbroic texture.

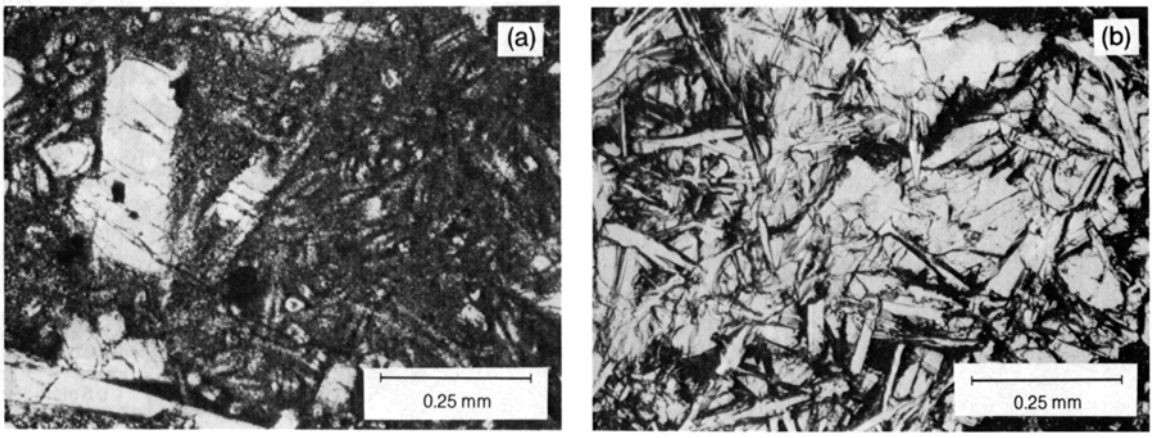

Fig. 6.13. Photomicrographs of very-low-Ti mare basalts. **(a)** Sample 70007,325L1, displaying a microporphyritic texture; **(b)** subophitic texture in sample 70009,295L1.

trolled by nucleation and growth rates of crystals, cooling rates of lavas, compositions of the liquids, and the amount of fluid flow within the lavas (*Lofgren,* 1980, 1983).

Dynamic crystallization experiments have also shown that the nature of the melt when cooling begins can have a dramatic effect on the resulting textures (*Donaldson et al.,* 1975; *Bianco and Taylor,* 1977; *Lofgren*, 1977, 1983; *Lofgren et al.,* 1978). *A* key factor is the existence of nuclei in the melt, on which crystals can then form and grow. Such nuclei may be either tiny crystalline fragments or specks of debris completely unlike the crystals that form around them. In general, if crystal nucleation occurs more easily for any reason (e.g., because nuclei are already present as a result of incomplete melting), the resulting product will be more completely crystallized. The final grain size will depend more on the number of nuclei per unit volume than on the growth rate of individual crystals. The effect of melt history (e.g., number of nuclei, cooling rate) on texture is most dramatic at cooling rates less than 10°C/hr.

The uncertain effects of nucleation on texture make it difficult to relate the large array of textures produced in experiments to the textures observed in natural rocks. To make direct comparisons, one must have some idea of the number of nuclei in a natural basaltic melt at the onset of cooling. There is virtually no observational information on this matter and none at all for lunar rocks. However, as we accumulate more information about the precooling nucleation condition of the melt, we will ultimately be able to interpret not only the crystallization history of a basalt lava but also the history of the magma prior to eruption.

The cooling rate is determined by the initial temperature, the thickness of the lava flow, and the rate of heat loss from it. This rate controls the time available for nucleation to occur and provides the driving force for crystal growth once nuclei are present. The influence of cooling rate on texture is greatest when the melt is free of nuclei at the start of cooling. In the absence of nuclei, nucleation in the cooling melt can be delayed to create a high degree of *supercooling* (cooling below the normal freezing point), and the shapes and compositions of the resulting crystals are more profoundly affected (*Lofgren,* 1980). Once nuclei are present, growth proceeds immediately upon cooling; the rate of growth is controlled by the rate of heat extraction from the lava. Large degrees of supercooling (tens to hundreds of degrees) are produced only at very rapid cooling rates.

Composition of the melt is an important variable to keep in mind when comparing textures among basalts and attempting to relate observed textures to cooling rates. Composition affects texture in several ways. For one thing, the viscosity of the melt varies with composition (and especially with SiO_2 content), and nucleation generally becomes more difficult as viscosity increases, as it does in high-SiO_2 rocks. In addition, the intervals of crystallization of different minerals in a cooling melt also depend on composition and affect the resulting textures in complex ways. For example, if a melt of a certain composition is characterized by a significant temperature interval in which the liquidus phase (the first mineral that forms as the lava cools) crystallizes alone before a second mineral appears, the crystals of the first mineral tend to grow larger, producing a greater tendency for a porphyritic texture during

cooling (*Lofgren,* 1974). However, this porphyritic texture will form only if the density of nuclei in the melt is low (i.e., the crystallization is restricted to a few spots). Porphyritic textures do not form during the cooling of basalts that are saturated (or nearly so) with two or more minerals at the liquidus (*Walker et al.,* 1978; *Lofgren,* 1980). In these cases, both minerals crystallize together. Porphyritic textures in such lavas, when observed, indicate that the large crystals are inherited from earlier crystallization at depth.

The effects of magmatic flow in bodies of molten lava usually appear as textures containing large or small aligned crystals (*trachytic* or *pilotaxitic* textures). Flow can also suspend larger crystals that might otherwise settle to the bottom of the melt body. This effect is restricted to relatively thin flows. Crystal settling only becomes a factor in the development of textures in mare basalt flows thicker than about 10 m. By mixing different portions of the melt together, flow can also promote *heterogeneous nucleation,* in which crystal growth does not begin spontaneously but starts around a foreign object.

For details of dynamic crystallization experiments and their interpretation, see the following papers: high-Ti basalts: *Usselman et al.* (1975), *Usselman and Lofgren* (1976), *Grove and Beaty* (1980); low-Ti pigeonite basalts: *Lofgren et al.* (1974), *Grove and Bence* (1977), *Grove and Raudsepp* (1978), *Lofgren et al.* (1975), *Walker et al.* (1977); low-Ti olivine basalts: *Donaldson et al.* (1975), *Walker et al.* (1976), *Bianco and Taylor* (1977); very-low-Ti basalts: *Grove* (1978), *Grove and Bence* (1979).

6.1.5. Cooling Rates of Mare Basalts

The rates at which mare basalt lavas have cooled after eruption have been estimated by two methods. One method is by the dynamic crystallization experiments discussed above (section 6.1.4), in which artificial samples with compositions like mare basalts are melted and then cooled from their melting temperatures at known rates; the resulting textures are compared with those observed in lunar basalts. These comparisons involve qualitative matching of textures as well as quantitative assessments based on such parameters as crystal size. The other method is theoretical, in which mineral compositions and kinetic parameters such as diffusion coefficients are combined to calculate the rate at which a basalt cooled (e.g., *Onorato et al.,* 1978). These two methods are complementary, and they give the same results to well within an order of magnitude.

These studies indicate that most mare basalts cooled at rates ranging from about 0.1°C to 30°C/hr. This range can be produced by cooling in lava flows only a few meters thick. *Brett* (1975a), using petrographic and geologic data, estimated that most mare basalts formed in flows thinner than 8 m, and his conclusions are consistent with photogeologic observations of lunar lava flows. For example, the flows in the walls of Hadley Rille at the Apollo 15 landing site (*Howard et al.,* 1972) average less than 10 m thick (*Schaber et al.,* 1976), although some individual flows appear to be 10-20 m thick. The heights of flow fronts photographed in Mare Imbrium are generally less than 15 m, although they range from 1 to 96 m (*Gifford and El-Baz,* 1981). Thicker flows, or ponding of flows in depressions to form lava lakes, will result in much slower cooling rates and may produce basalt textures very different from any yet observed.

6.1.6. Vesicles and Nature of the Gas Phase

Many mare basalts contain numerous frozen gas bubbles, now empty, called *vesicles* (Fig. 6.14), which almost certainly formed when gases dissolved in the melt came out of solution in response to decreasing pressures associated with eruption. Rapid cooling of the lavas has preserved these bubbles. However, none of the gas remains, and its original nature is still a matter for speculation.

On Earth, vesicles are formed by outgassing of H_2O and CO_2, the dominant volcanic gases of terrestrial lavas. However, because there is no water in lunar rocks, CO_2 was likely to be more important than H_2O. Because of the chemically reducing conditions

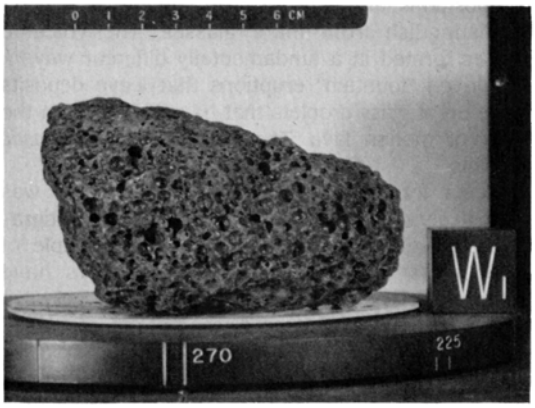

Fig. 6.14. Specimen of low-Ti, vesicular mare basalt 15016 collected from the Apollo 15 site at Hadley Rille. The specimen is about 10 cm long; the cube marked "W_1" is 2 cm on each edge. The numerous large cavities (*vesicles*) are frozen gas bubbles, now empty. In similar terrestrial rocks, the main gas phase in such bubbles would be H_2O, but on the Moon it was probably CO_2.

in lunar rocks, a significant amount of CO was probably present along with CO_2. Other gases may also have been present. For example, sulfur contents are high in lunar pyroclastic deposits (see section 6.1.7 below), suggesting that sulfur species may be another component of lunar volcanic gases.

These speculations are supported by analyses of mare basalts, which contain from 3 to 80 µg/g carbon (*Gibson,* 1977, and Table A8.6). When the basalts are analyzed by acid hydrolysis, both CO and CO_2 are released; the CO/CO_2 ratio ranges from 1/2 to 1/4. These gases appear to have been produced during the crystallization of the lavas, possibly by the reaction of carbon or carbides in the magma with FeO, to produce metallic iron (which is observed in mare basalts) and CO and CO_2. Sulfur contents are much higher in lunar basalts (up to 0.3 wt.%) than in terrestrial basalts (less than 0.15 wt.%), but the nature of the sulfur-bearing gases present during crystallization is still speculative (see sections 8.5, 8.7, and 8.8 for a more quantitative discussion of carbon and sulfur).

6.1.7. Lunar Pyroclastic Deposits

Glass droplets and fragments are a common component in the lunar soil; they have a broad range in both composition and texture. Lunar glasses have been produced by two very different processes, meteoroid impacts (impact melting) and volcanic eruptions. Glasses formed by impact melting are discussed in section 6.4.3; such glasses can generally be recognized by their heterogeneous textures and compositions, although they are sometimes difficult to distinguish from mare glasses. The volcanic glasses formed in a fundamentally different way, in gas-driven "fountain" eruptions that leave deposits made up of glass droplets that have chilled from the spray of molten lava. These are called *pyroclastic* deposits.

Except for Apollo 17 orange glass, which was most likely collected in place, no field or stratigraphic evidence exists to show that any sample of lunar glass is volcanic, but investigators have developed other criteria for distinguishing between these two types of glasses. These criteria, discussed in detail by *Delano* (1986), are the following:

1. Absence or presence of schlieren and exotic inclusions: Volcanic liquids are unlikely to become contaminated with large quantities of chemically and mineralogically exotic material. The result is a fairly uniform glass. In contrast, glasses of impact origin are commonly heterogeneous; they contain streaks of fine-grained debris, called *schlieren,* together with inclusions with compositions different from that of the glass.

2. *Homogeneity of composition:* Individual pieces of volcanic glass, which are samples of hot, magmatic reservoirs, should be chemically uniform, at least for the nonvolatile elements. Impact glasses have cooled rapidly, and have not remained as liquids long enough for diffusion to homogenize them. Consequently, individual pieces of impact glass tend to be chemically heterogeneous.

3. *Clustering of chemical compositions:* Volcanic glasses are quenched samples of a magma reservoir that was probably chemically uniform over substantial distances. As a result, the droplets produced by the eruption of lava from this reservoir will tend to be chemically uniform as well. Tight compositional clustering is therefore a frequently observed aspect among the volcanic glasses. In magma bodies and lava flows, crystal/liquid fractionation can also produce tight chemical trends within the resulting suite of volcanic glasses. In contrast, impact glasses are produced by the instantaneous fusion of multi-component, chemically heterogeneous targets; as a result, their compositions tend to define chemically diffuse clusters.

4. *Volatile element enrichments:* The best-known examples of lunar volcanic glasses, the Apollo 15 green glass and Apollo 17 orange glass, are highly enriched in volatile elements compared to most lunar samples (*Butler and Meyer,* 1976). This characteristic was apparently related to the presence of a transient gas phase that accompanied the eruption and not to implantation from the solar wind while these glasses resided on the lunar surface (see section 8.8 for details on the solar-wind component of lunar rocks).

5. *Ferromagnetic resonance intensity:* As described in sections 5.4.3 and 7.3.1, the ferromagnetic intensity is a measurement of the amount of small particles of single-domain iron in a glass sample. These particles are a common component of impact glasses and they apparently form by the reduction of small amounts of divalent iron (Fe^{2+}) during impact melting. Clearly volcanic glasses, particularly the Apollo 15 green glass and Apollo 17 orange glass, have been found to possess lower ferromagnetic resonance intensities and thus less single-domain iron than impact glasses (*Stone et al.,* 1982).

6. *High Mg/Al ratios:* Areas of pyroclastic deposits on the Moon whose chemistry has been measured from orbital instruments (see section 6.2) are known to have higher Mg/Al ratios than do mare regoliths (e.g., *Schonfeld and Bielefeld,* 1978). Samples of volcanic glasses have high Mg/Al ratios between 1.7 and 3.3; impact glasses have ratios similar to sampled regoliths, i.e., <1.5.

Chemical compositions and varieties of volcanic glasses. Twenty-five distinct varieties of

volcanic glasses have been identified from the Apollo landing sites (*Delano,* 1986). Their major-element compositions are given in Table A6.3. In some cases, different glasses can be related to each other as a series produced by fractional crystallization and differentiation of a single parent magma. In these cases, the most magnesian members of the suite define the composition of the parent magma. *Delano* (1986) discusses aspects of each variety in detail.

Volcanic glasses span a large range in TiO_2 contents, from 0.26 to 16.4 wt.%. However, most identified volcanic glasses are either very-low-Ti (<1.5 wt.% TiO_2) or high-Ti (>8 wt.% TiO_2), and only 3 of the 25 types fall in the range of most low-Ti basalts (2-5 wt.% TiO_2). The chief chemical distinction between volcanic glasses and mare basalts is the greater concentration of compatible elements (elements such as Mg and Ni that fit into olivine, pyroxene, and other common minerals of the lavas) in the glasses (Figs. 6.15 and 6.16). This relation suggests that the magmas that erupted to produce volcanic glasses underwent less crystallization (and removal of crystals) during their ascent to the lunar surface than did the magmas that gave rise to the mare basalt lavas.

Abundances of trace elements in most types of volcanic glasses have not been measured. Exceptions are the Apollo 15 green and yellow/brown glasses and Apollo 17 orange glass, for which there are extensive datasets (Tables A6.5, A6.6, and A6.7).

Apollo 17 orange glass has the same bow-shaped REE pattern that is characteristic of high-Ti mare basalts (Fig. 6.3), but it also has distinct enrichments in volatile elements, such as F, CI, Zn, and Pb (see below). There are several chemically distinct groups of Apollo 15 green glass, all intermingled in a fragile clod composed of numerous glass spheres (sample 15426). The information in Table A6.6, therefore, is a grand average of all the Apollo 15 green glass groups, because the analyses were done on this green glass clod. The REE pattern (Figs. 6.3 and 6.17) is characterized by a negative slope from La to Sm and a positive slope from Gd to Lu, with a negative Eu anomaly. Like the Apollo 17 orange glass, Apollo 15 green glass is enriched in volatile elements. Trace element data are also listed for Apollo 15 yellow/brown volcanic glasses (Table A6.7). This glass type is much rarer than the green glass and it has not been studied in detail.

Textures and cooling rates. Lunar pyroclastic deposits are not composed entirely of glass droplets. Many of the spheres, which were erupted as droplets of molten lava, are now substantially crystalline. Subunits within the orange "glass" deposit from the rim of Shorty Crater at the Apollo 17 site, for example, are composed largely of black droplets because of the presence of very-fine-grained crystals of ilmenite, olivine, spinel, and metallic iron in the spheres. Many Apollo 15 green "glass" spheres also contain small crystals of olivine.

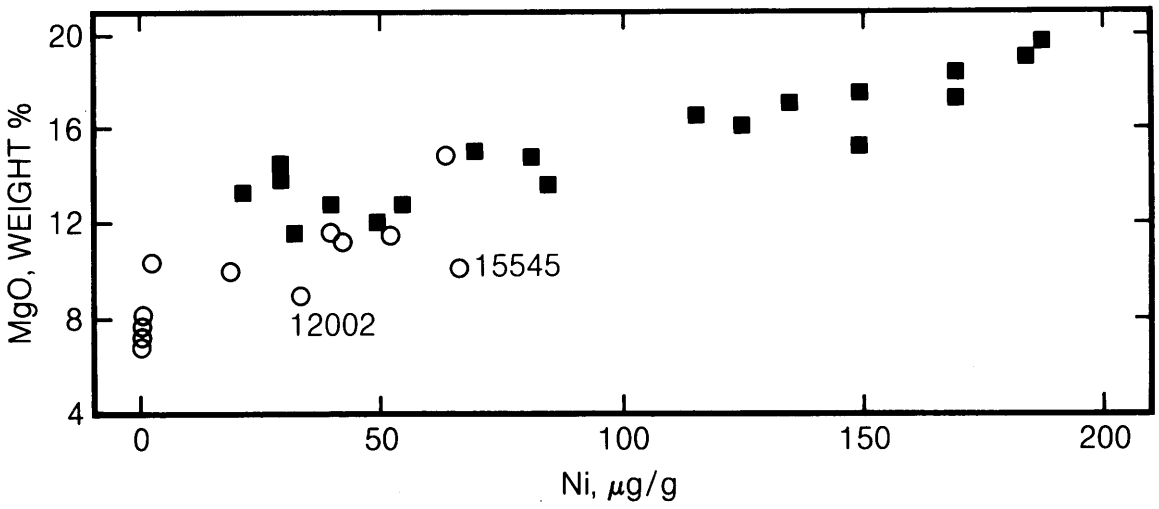

Fig. 6.15. Plot of Ni and MgO abundances in mare basalts (open circles) and in pristine lunar glasses (solid squares). The two elements are positively correlated with each other, and glasses tend to be richer in both Ni and Mg. Samples 12002 and 15545 (olivine basalts) are relatively Ni-rich for their MgO contents, relative to other basalts.

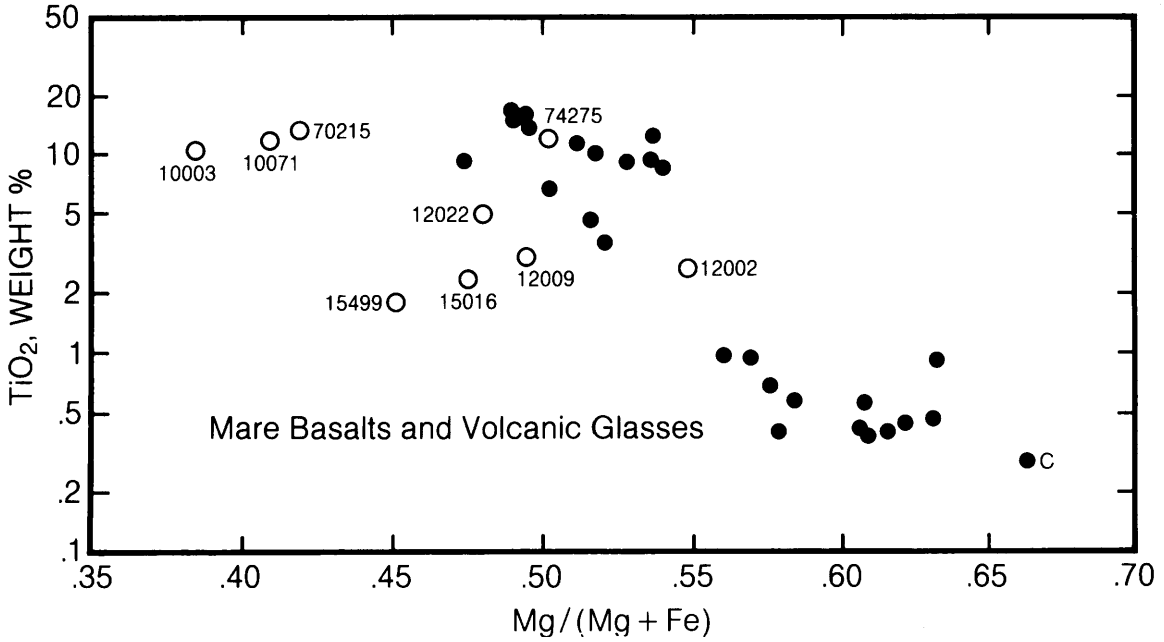

Fig. 6.16. Plot of TiO_2 against Mg/(Mg + Fe) mole ratios in mare basalts (numbered open symbols) and in pristine lunar glasses (solid circles). Each symbol represents a distinct magma type. For any given abundance of Ti, the pristine glasses commonly have higher Mg/(Mg + Fe) ratios than do the basalts. If the pristine glasses correspond to the initial compositions of comparable basalts, then the basalt lavas must have lost Mg (probably by the removal of olivine). The pristine glass labeled "C" in the lower right corner of this figure is the Apollo 15 green glass with the highest Mg/(Fe + Mg) ratio (*Delano,* 1979).

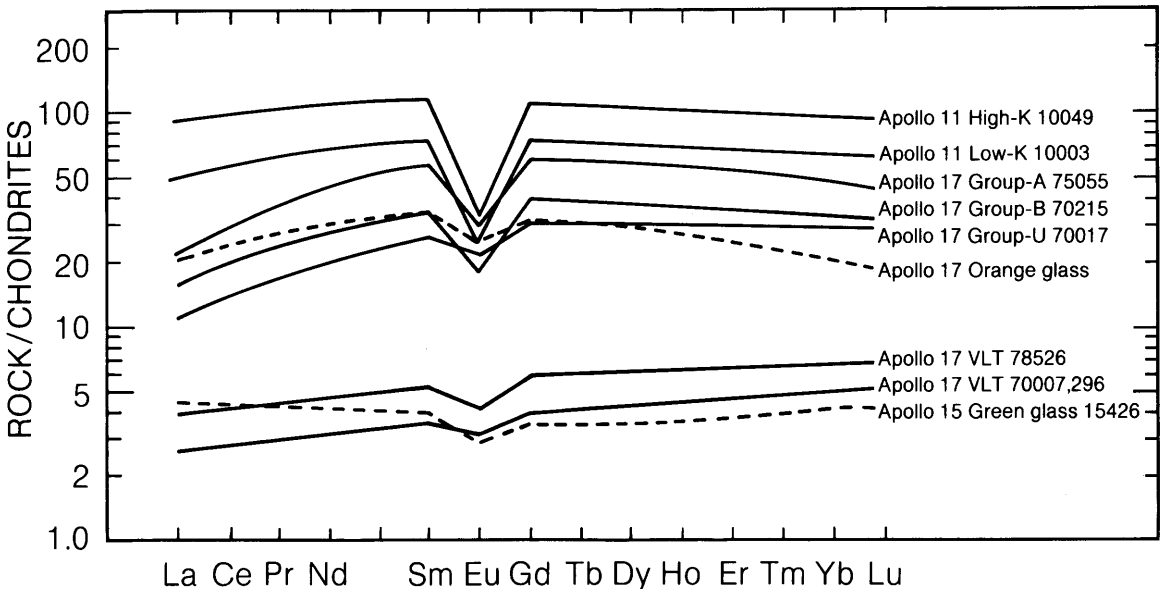

Fig. 6.17. REE contents, normalized to chondritic meteorites, in a range of mare basalts and related glasses. The Apollo 17 orange glass appears to be related to the high-Ti basalts plotted in the upper part of the diagram; it has the same REE contents, "bow-shaped" pattern, and negative Eu anomaly. Such similarities, however, do not prove a relationship. This figure is modified from *BSVP* (1981).

Experiments have shown that melt droplets with the composition of orange glass must cool faster than 10-60°C/sec to prevent crystallization (*Uhlmann et al.,* 1974). Similar droplets of noncrystalline green glass must have cooled even faster. Those spheres that contain crystallites obviously cooled more slowly.

Calculations of radiative cooling using a modified version of the Stefan-Boltzmann formula (*Arndt et al.,* 1979, 1984) indicate that the volcanic spheres containing crystallites must have cooled 10-1000 times more slowly than would isolated spheres erupted into the lunar vacuum. This result suggests that the spheres actually cooled in a hot, transient atmosphere of volcanic gas that accompanied the eruptions. The shapes of glass spheres (*McKay et al.,* 1973; *Heiken and McKay,* 1977; *Clanton et al.,* 1978) also indicate that the droplets were colliding repeatedly in a turbulent stream of gas. The spheres may have remained suspended in this gas for as long as 10 minutes (*Arndt et al.,* 1984), which is a long time compared to the ballistic flight-time of about 1 minute in the absence of a gas phase (*McGetchin and Head,* 1973).

Volatile elements associated with pyroclastic deposits. The most striking feature of the Apollo 15 and 17 pyroclastic deposits is their enrichment in volatile elements such as F, Cl, Zn, and Pb, when compared with other lunar materials (Table A6.8). These elements undoubtedly existed in the gas phase associated with the pyroclastic eruptions. The volatile elements tend to be concentrated on the surfaces of individual glass spheres. Other pyroclastic deposits on the Moon may show the same features, but our sampling of them is too limited to be sure.

The surface coatings of volatile elements on droplets of orange glass and green glass have been studied extensively; references are listed in Table A6.8. Key observations are listed below.

1. At least some of the elements listed in Table A6.8 were transported as fluorides, chlorides, or sulfides (*Wasson et al.,* 1976).

2. The elements Au, Sb, and Ge occur on the surfaces of both Apollo 15 green glass and Apollo 17 orange glass particles in the same ratios that are found in CI-type chondritic meteorites (*Morgan and Wandless,* 1984; *Delano,* 1980).

3. The volatile deposits on Apollo 17 orange glass particles possess an isotopic uranium/lead ratio, $^{238}U/^{204}Pb$, of <29 (*Tera and Wasserburg,* 1976), which is much lower than that found in both mare basalts and nonmare rocks. The Pb in the interior of green glass spheres is isotopically distinct from that on the surfaces, however (*Tatsumoto et al.,* 1987).

4. The U-Pb model age of the surface-correlated component on the Apollo 15 green glass and Apollo 17 orange glass is about 4.6 b.y. (*Tera and Wasserburg,* 1976; *Meyer et al.,* 1975). This result contrasts with the model ages determined for most nonmare lunar rocks, 4.3 b.y.

5. The formation ages measured for Apollo 15 pyroclastic fragments (~3.3 b.y.) and Apollo 17 pyroclastic fragments (3.75 b.y.) are nearly identical with the times of local mare volcanism at both sites. However, no crystalline equivalents (i.e., basalts) with the chemical compositions of these glasses have been identified.

6. Trapped noble gases occur in the Apollo 15 green glasses. Trapped Ne has an isotopic composition similar to that of solar Ne (*Barraclough and Marti,* 1985). However, this Ne was not implanted by the solar wind, because it is uniformly distributed through the green glass particles and not concentrated at grain surfaces.

6.1.8. Experimental Petrology and Phase Relations

The melting and crystallization relationships in synthetic melts of mare basalt composition have been extensively studied in the laboratory. Some dynamic crystallization experiments and their use in interpreting the textures in mare lavas are described in section 6.1.4. This section summarizes static (or near-equilibrium) experiments, which are used to interpret the temperatures at which different minerals crystallize rather than the textures that they form. Some experiments are carried out at low pressure (~1 bar), and the results bear on our understanding of basalt crystallization in lava flows erupted at the lunar surface. Other experiments are carried out at high pressures, ~5-25 kbar, appropriate to depths of 100 to 500 km (on the Moon, 1 kbar = a depth of 18 km). These are the depths at which formation and early crystallization of lunar magmas occurred. Reviews of experimental studies of mare basalts are given by *Kesson and Lindsley* (1976) and by *BVSP* (1981, their Tables 3.4.1 and 3.4.2).

Phase relations at low pressure. Low-pressure experiments attempt to duplicate the conditions in a continually cooling basaltic lava erupted at the lunar surface. Pressure is kept constant, the temperature is allowed to drop until crystallization occurs, and the temperatures at which different minerals appear are noted. The low-pressure equilibrium crystallization behavior of representative mare basalts is illustrated by the data in Tables 6.2, 6.3, and 6.4. The temperature at which each molten basalt begins to crystallize, called the *liquidus temperature,* ranges from 1150° C to almost 1400° C.

TABLE 6.2. Low-pressure (0-1 bar) equilibrium experimental results on high-Ti mare basalts.

Sample	Rock Type	Reference	Temp(°C)	Phases Present*
10072	high-Ti	*Walker et al.* (1975)	1195	liq
			1159	liq + Ol + armal + ilm
			1149	liq + Ol + ilm
			1145	liq + Ol + loCapx + ilm
			1140	liq + loCapx + ilm
			1130	liq + loCapx + hiCapx + ilm
			1122	liq + loCapx + hiCapx + ilm + plag
10020	low-K	*O'Hara et al.* (1974)	1170	liq
			1160	liq + Ol + sp
			1153	liq + Ol + sp
			1151	liq + Ol + sp + ilm
			1145	liq + Ol + sp + ilm + px + plag
			1133	liq + sp + ilm + pig + aug + plag
			1108	liq + sp + ilm + pig + aug + plag
71569	very-high-Ti	*Walker et al.* (1975)	1192	liq
			1156	liq + Ol + armal + sp
			1146	liq + Ol + armal + sp
			1142	liq + Ol + hiCapx + armal + ilm
			1138	liq + Ol + hiCapx + ilm + plag
			1137	liq + hiCapx + loCapx + ilm + plag
			1127	liq + hiCapx + loCapx + ilm + plag
			1119	liq + hiCapx + loCapx + ilm + plag
74220	orange glass	*Walker et al.* (1975)	1398	liq
			1302	liq + Ol
			1251	liq + Ol
			1195	liq + Ol + sp
			1159	liq + Ol + ilm + sp
			1149	liq + Ol + ilm + sp
			1145	liq + Ol + ilm
			1140	liq + Ol + ilm + sp
			1130	liq + Ol + pig + ilm

* "Phase" designates either mineral, liquid, or glass. In this table, liq = liquid; Ol= olivine; armal = armalcolite; ilm = ilmenite; sp = spinel; loCapx = low-Ca pyroxene; hiCapx = high-Ca pyroxene; pig = pigeonite; aug = augite; plag = plagioclase.

The basalts richest in FeO tend to have the lowest liquidus temperatures. The temperatures at which lavas of mare basalt composition become totally solid upon cooling (the *solidus temperatures*) have not been determined directly. Nevertheless, the lowest temperature listed for each basalt is probably close to the solidus temperature. The data imply that if solid mare basalts were heated they would begin to melt around 1050° C. This melting temperature is about 100° C higher than those of terrestrial basalts, chiefly because of the lack of H_2O in lunar basalts.

Phase relations at high pressures. Laboratory experiments at high pressures (5-25 kbar) are intended to examine a different problem, the formation of basaltic melts by partial melting of the lunar mantle at depths of perhaps 100-500 km. Such partial melting rarely consumes more than a few percent of the original mantle rock in producing the basaltic melt, so that, until it moves, the newly-formed magma remains in chemical equilibrium with the minerals that make up the unmelted *residue* of the mantle. By experimentally applying high pressures and temperatures to solid basalts and their molten equivalents, it is possible to estimate (1) the pressure (and hence the depth) at which the magma formed and (2) the nature of the minerals in the original mantle with which the melt was in equilibrium.

In these experiments it is assumed that during melting at least two of the original mantle minerals remain in equilibrium with the newly-formed basaltic melt. Therefore, the depth of origin can be

TABLE 6.3. Low-pressure (0-1 bar) equilibrium experimental results on low-Ti mare basalts.

Sample	Rock Type	Reference	Temp(°C)	Phases Present*
12002	olivine	*Walker et al.* (1976)	1350	liq
			1328	liq + Ol
			1266	liq + Ol
			1232	liq + Ol + sp
			1201	liq + Ol + sp
			1176	liq + Ol + sp + px
			1164	liq + Ol + sp + px
			1150	liq + Ol + sp + px
15065	pigeonite	*Walker et al.* (1977)	1273	liq + Ol
			1249	liq + Ol
			1225	liq + Ol + sp + px
			1205	liq + Ol + sp + px
			1172	liq + Ol + sp + px
			1148	liq + sp + px + plag
			1129	liq + sp + px + plag
			1125	liq + Ol + sp + px + plag
			1101	liq + sp + px + plag
14072	aluminous	*Walker et al.* (1972)	1285	liq
			1262	liq + Ol
			1212	liq + Ol
			1190	liq + Ol + sp
			1175	liq + Ol + sp + pig + plag
			1170	liq + Ol + sp + pig + plag
			1140	liq + Ol + sp + pig + aug

* "Phase" designates either mineral, liquid, or glass. In this table, liq = liquid; Ol = olivine; sp = spinel; px = pyroxene; pig = pigeonite; aug = augite; plag = plagioclase.

TABLE 6.4. Low-pressure (0-1 bar) equilibrium experimental results on very-low-Ti mare basalts.

	Rock Type	Reference	Temp(°C)	Phases Present*
Luna 24	average	*Grove and Vaniman* (1978)	1192	liq
			1189	liq
			1182	liq + plag
			1155	liq + plag + Ol + px
			1143	liq + plag + Ol + px
			1071	liq + plag + Ol + px
Apollo 15	green glass	*Grove and Vaniman* (1978)	1408	liq
			1392	liq + Ol
			1359	liq + Ol
			1221	liq + Ol
			1192	liq + Ol + px
			1163	liq + Ol + px
			1155	liq + Ol + px + plag
			1143	liq + Ol + px + plag
Apollo 14	VLT glass	*Chen et al.* (1982)	1390	liq
			1365	liq + Ol
			1210	liq + Ol
			1150	liq + Ol + px + plag

* "Phase" designates either mineral, liquid, or glass. In this table, liq = liquid; Ol = olivine; px = pyroxene; plag = plagioclase.

TABLE 6.5. High-pressure equilibrium experimental results on basaltic compositions thought to represent primary magmatic compositions.

	Basalt Type	Pressure*	Depth, km†	Phases‡	Olivine Fo§	Ref.¶
Apollo 15	red (high-Ti) glass	24	480	Ol, opx	75	a
Apollo 17	orange glass	20	400	Ol, opx	81	b
Apollo 14	VLT glass	19	380	Ol, pig	79	c
Apollo 17	VLT glass	18	360	Ol, pig	79	c
Apollo 15	green glass	15	300	Ol, opx	84	d, e
12002	low-Ti olivine	12.5	250	Ol, pig	78	f
74275	high-Ti	11	220	Ol, pig, aug	75	b
12009	olivine	7.5	150	Ol, pig	75	g
70215	high-Ti	6.5	130	Ol, aug	76	h

* Pressure (kbar) at which melt becomes saturated with two or more phases; errors are typically ±2 kbar.
† Depths calculated from multiple-saturation pressures assuming a pressure gradient of 1 kbar/20 km; errors are typically ±40 km.
‡ Phases present at multiply-saturated liquidus: Ol = olivine; pig = pigeonite; opx = orthopyroxene; aug = augite.
§ Fo = liquidus olivine forsterite [Mg/(Mg + Fe)] content at the multiple-saturation pressure.
¶ (a) *Delano* (1980); (b) *Green et al.* (1975); (c) *Chen et al.* (1982); (d) *Stolper* (1974); (e) *Green and Ringwood* (1973); (f) *Walker et al.* (1976); (g) *Green et al.* (1971); (h) *Longhi et al.* (1974).

estimated by determining the pressure at which a given basalt melt first becomes *multiply saturated* (i.e., in equilibrium with two or more minerals). If the extent of original partial melting is so great that only one mantle mineral remains in the residue, then no unique pressure or depth can be determined.

In principle, these experiments involve keeping the temperature constant and increasing the pressure on a sample of basaltic melt until minerals form. For example, in some basalts olivine is the liquidus phase (i.e., as the magma cools, olivine crystallizes first and then coexists stably with the remaining magma), and olivine remains the only liquidus phase at pressures of one atmosphere up to several kilobars. At a higher pressure, olivine may be joined by pyroxene on the liquidus, i.e., the two minerals then coexist stably with the magma. This pressure is taken to be the pressure at which the basaltic magma was derived by partial melting. The compositions of the pyroxene and olivines formed are taken to represent those of the pyroxene and olivine present in the lunar mantle when the basaltic melt was first formed.

Such estimates of the depth of origin are also dependent on the extent to which the basaltic melt changed in composition as it migrated toward the surface. For the depth estimate to be accurate, the melt composition ought not to have changed at all. Such unchanged magmas are called *primary magmas*. In practice, formation and separation of crystals (*fractional crystallization*) will usually occur as the magma moves from the source region to the surface; this effect will cause the estimated depth of origin to be less than the real depth. Problems in interpreting experimental data and in recognizing primary magma compositions are discussed at length by *BVSP* (1981) and succinctly by *Delano* (1980).

The pressures and depths estimated for the origin of several proposed primary magmas are listed in Table 6.5, along with the minerals with which they are saturated and the composition of the olivine present. The magma types are listed in order of decreasing inferred depth of origin. The data suggest vaguely that the basalts formed at greater depths have originated from rocks containing more Mg in the residual olivine. This trend could imply that variations in the Mg/Fe ratio with depth existed in the Moon during the time these mare basalts formed. However, the trend is weak, and more data are needed to test its validity.

6.1.9. Ages of Mare Basalts

Formation ages of numerous samples of mare basalts and related pyroclastic deposits have been determined by radioactive-isotope age-dating methods. (For summaries, see BVSP, 1981, their Table 7.3.1; *Ryder and Spudis,* 1980; and *Taylor,* 1982, his Table 6.6). Ages have also been estimated photo-geologically using the abundances of craters and the state of preservation of individual craters on mare surfaces. In these studies, images of the Apollo and Luna landing sites, where the ages are known, are used as calibration points. (For a summary, see *Schultz and Spudis,* 1983). Photogeologic ages are not as precise as radiometric ones, but they provide coverage of large areas of the Moon.

The high-Ti basalts from the Apollo 11 and Apollo 17 sites are relatively old, generally more than 3.5 b.y. The low-K, high-Ti basalts from the Apollo 11 site range in age from 3.55 to 3.86 b.y.; Apollo 11 high-K, high-Ti basalts appear generally younger, about 3.55 b.y. The Apollo 17 high-Ti basalts, though of similar age (3.59-3.79 b.y.), seem to have erupted over a shorter span of time than did those at the Apollo 11 site. However, the Apollo 17 orange glass is slightly younger (3.48 b.y.) than the crystalline Apollo 17 basalts.

It is not certain, however, that all high-Ti basalts are old. Photogeologic data indicate that some high-Ti basalts may have erupted onto the lunar surface as recently as about 1 b.y. ago; an area east of the crater Lichtenberg is one example of such relatively recent volcanism (see *Schultz and Spudis,* 1983).

Low-Ti mare basalt samples are generally younger; they range in age from 3.08 to 3.37 b.y. Those from the Apollo 12 site are slightly younger (3.08 to 3.29 b.y.) than those from the Apollo 15 site (3.21 to 3.37 b.y.). The ages of the Apollo 15 olivine and pigeonite basalts are not distinguishable from each other. The Apollo 15 green glass formed at about the same time as the Apollo 15 basalts (3.3 b.y. ago).

The aluminous, low-Ti mare basalts are the oldest mare basalts that have been dated directly. Clasts of these basalts in Apollo 14 breccias range in age from 3.9 to 4.2 b.y. (*Taylor et al.,* 1983). Photogeologic observations of the distribution of dark-halo craters, which have probably excavated mare basalt layers from beneath the ejecta of lunar basins, support the inference of widespread mare-type volcanism prior to 3.9 b.y. (*Schultz and Spudis,* 1983). However, fragments of aluminous mare basalts from other sites are not so ancient; an Apollo 12 fragment is 3.1 b.y. old, and one from the Luna 16 site is 3.4 b.y. old.

The ages of very-low-Ti basalts are uncertain because of the small number of samples, but they seem to span a considerable interval. One fragment of very-low-Ti mare basalt from the Luna 24 site has been dated; its age is 3.3 b.y. Very-low-Ti basalts found in Apollo 17 soils have not yet been dated directly, but those found as fragments in breccia 72235 must be older than the melt-rich matrix of the breccia, which crystallized 4.01 b.y. ago.

Measurements of isotopic compositions of basalts also give information about an earlier time when the source regions for the mare basalts were formed in the lunar mantle. These data suggest that the mare basalt source regions had formed by 4.4 b.y. ago. This age probably represents the end of the initial lunar differentiation during which the crust, mantle, and core formed (section 2.4).

6.2. EXTENDED MAPPING OF MARE LAVAS AND PYROCLASTIC DEPOSITS BY REMOTE SPECTRAL OBSERVATIONS

6.2.1. Techniques

A major limitation to understanding the nature and history of lunar mare volcanism is that the detailed data on compositions, formation ages, and properties of mare lavas are limited to the samples returned from only nine spots on the Moon. However, it has proved possible to extend this information to other areas of the Moon by making remote observations of the sites from which known samples have been returned and then making comparable observations of unsampled regions.

Imagery and photogeologic observations have already helped establish the nature and approximate ages of large areas of exposed mare lavas. An equally important and more specialized role is being played by remote spectral observations in the visible and infrared wavelengths, which can provide detailed information on the mineralogy and chemical composition of lunar basalts. By combining orbital information from the Apollo missions, Earth-based telescopic observations, and laboratory studies of returned samples, it has become possible to draw important conclusions about the chemistry, mineral composition, and origin of the lavas and glassy deposits that cover large areas of the Moon.

Earth-based spectral observations of the Moon are limited to the visible and near-infrared part of the electromagnetic spectrum. A lower wavelength limit of 0.3 μm is fixed by the absorption of shorter wavelengths by ozone in the Earth's atmosphere. The upper limit is set by thermal infrared radiation, which becomes significant beyond about 2.5 μm. Most reflectance data for mare regions were obtained in the late 1970s using visible and near-infrared spectrometers (0.3 to 1.1 μm). More recent measurements, made with more advanced sensors, have extended the spectral observations to 2.5 μm (see *Pieters,* 1978; *BVSP* 1981). These spectral observations have been supplemented by other remote measurements such as the γ-ray spectrometry done by the Apollo 15 and 16 missions, and by the critically important ground truth provided by Apollo and Luna samples.

The major silicate minerals in lunar basalts (pyroxene, plagioclase, and olivine) have characteristic absorption bands in the near-infrared spectral region. These individual absorption features do not combine in a simple linear fashion to produce a reflectance spectrum of basalt, because each mineral has a different overall opacity. Although the strength of an absorption band is dependent on the abundance of the absorbing species, detailed analytical

models of reflectance from soil particles are needed to determine the abundance of each component from raw spectral data (e.g., *Mustard and Pieters,* 1987).

The spectral character of lunar basalts tends to be dominated by the two strong absorption bands of Ca-rich clinopyroxene near 0.97–1.0 μm. This condition occurs in both laboratory samples of basalt powders (Fig. 6.18) and in telescopic spectra of young mare craters that have exposed fresh basalt bedrock (Fig. 6.19). Plagioclase influences the basalt spectrum (e.g., for rock 12063; Fig. 6.18) by producing a superimposed and weaker absorption band near 1.3 μm. These diagnostic features of mare basalt spectra are more subdued in spectra of older lunar soils that have few fresh fragments of basaltic bedrock.

Glasses of basaltic composition have spectra that are fundamentally different from those of crystalline basalts, chiefly because the specific absorption peaks produced by crystals of silicate minerals are absent. Reflectance spectra of three pyroclastic glass samples are shown in Fig. 6.20. For these glasses, the combined abundance of FeO and TiO_2 strongly affects the amount of absorption in the ultraviolet and blue portions of the spectrum (*Bell et al.,* 1976). Although both contain abundant FeO, the TiO_2-rich orange glass (74220) is much more absorbing than the TiO_2-poor green glass (15401). The weak bands near 1.0 and 1.8 μm are caused by Fe^{+2} in the slightly ordered atomic structure of glass. The black glass beads of sample 74001 are crystallized equivalents of the orange glass 74220. They consist of abundant thin plates of ilmenite in an orange glass groundmass and produce a reflectance spectrum dominated by the spectral character of ilmenite (*Adams et al.,* 1974).

6.2.2. Regional Distribution of Mare Basalts and Pyroclastic Glasses

Distribution of mare basalt types. Few dark mare basalts are seen on the lunar farside. An unknown, but possibly larger volume was erupted prior to the end of the intense meteorite bombardment of the Moon about 3.9 b.y. ago, and much of this is probably buried by ejecta from the large impacts that formed the mare basins. However, most of the visible maria occur on the nearside of the Moon. This concentration of maria on the nearside makes it possible to carry out Earth-based telescopic observations of the maria and to obtain important compositional information about mare basalts by measuring and analyzing their reflectance spectra. Actually, these observations measure the spectra of lunar soils that have developed on the mare lava flows.

The results of this spectral mapping are presented in detail in section 10.4. The maria exhibit great variety on a regional scale across the Moon. Stratigraphy derived from photogeological studies implies that a considerable heterogeneity also exists in the vertical dimension (see section 10.4). Of the basalts mapped on the lunar nearside, only about

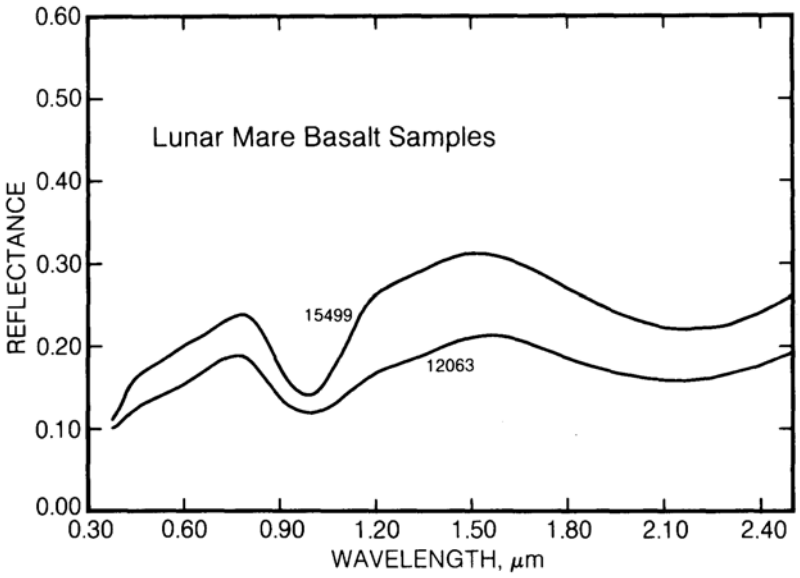

Fig. 6.18. Reflectance spectra in the visible and near-infrared, plotted as a function of wave-length for lunar mare basalt samples 12063 and 15499. The strong absorption band at 0.9-1.0 μm is diagnostic for pyroxenes in general and indicates the presence of Ca-pyroxene in this sample.

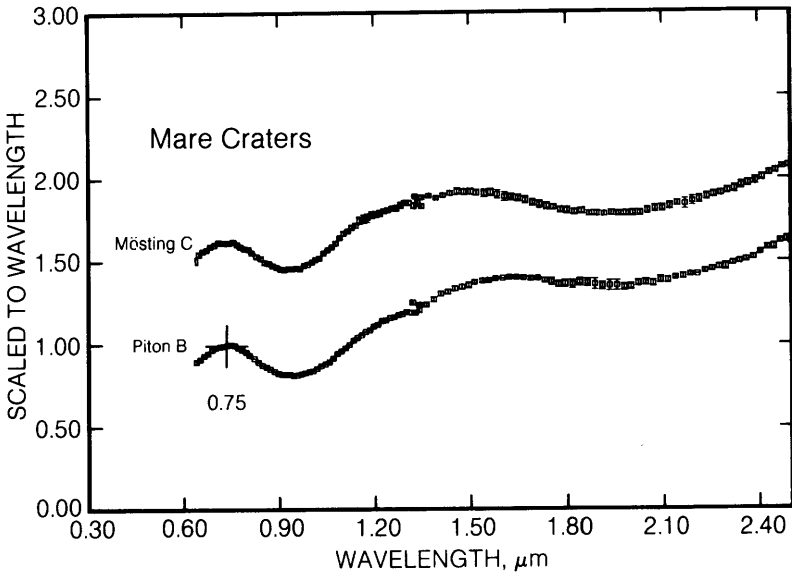

Fig. 6.19. Scaled visible and near-infrared reflectance spectra of lunar mare craters (Piton B, Mösting C) obtained with Earth-based telescopes. These spectra have been scaled to unity at 0.75 μm and offset vertically. The strong absorption at 0.9-1.0 μm indicates that Ca-pyroxene is abundant in the mare material excavated by these two young craters.

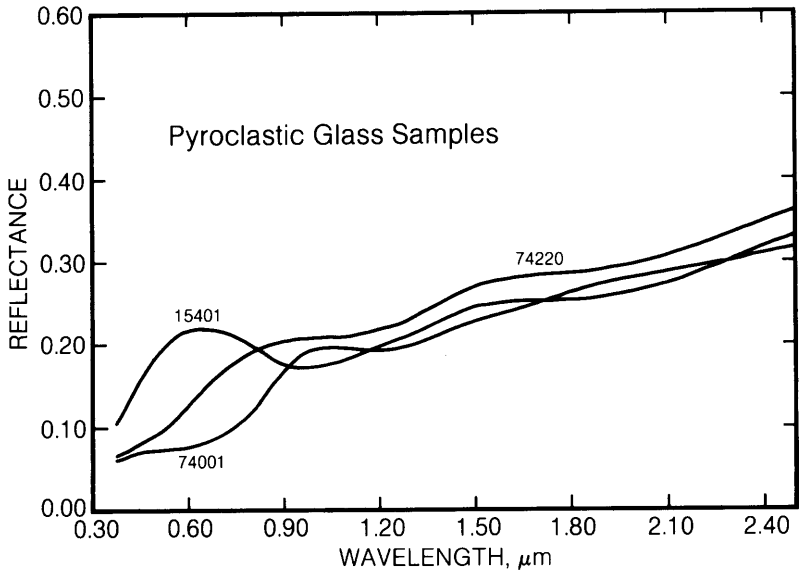

Fig. 6.20. Visible and near-infrared reflectance spectra of lunar volcanic glass samples 74220 (Apollo 17 orange glass), 74001 (Apollo 17 "black glass," the crystallized equivalent of orange glass), and 15401 (Apollo 15 green glass). The Ti-rich orange glass and black glass have greater absorption in the ultraviolet and blue regions of the spectrum (left side of graph, 0.3-0.4 μm).

one-third of them have compositions similar to the basalts sampled by Apollo and Luna missions. Our knowledge of mare volcanism is clearly incomplete.

Distribution of pyroclastic deposits. Remote-sensing data indicate that deposits of volcanic glasses (like those described in section 6.1.7) are fairly abundant on the Moon. Figure 6.21 shows the distribution of one type of possible pyroclastic unit, the dark-mantle deposits (see section 4.2), including the one sampled in the form of orange and black glass by the Apollo 17 mission. Such pyroclastic deposits often occur on the edges of the maria and overlap onto the adjacent highland regions (see Fig. 10.10). As their name implies, these deposits have low albedos (they are poor reflectors of visible light) and so appear dark.

Other types of pyroclastic deposits may exist, however, and *Gaddis et al.* (1985) have shown that not all pyroclastic deposits are necessarily dark. They observed that thick dark mantle deposits exhibit low

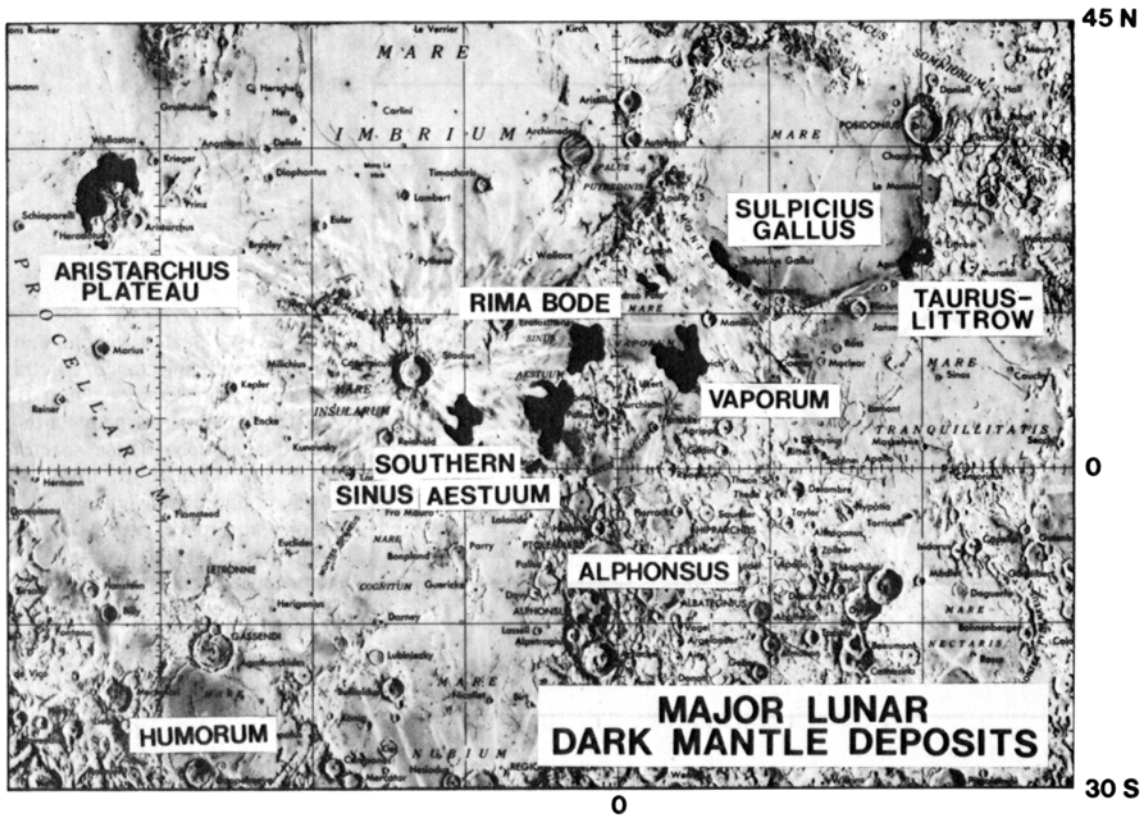

Fig. 6.21. Lunar map showing the distribution of major dark-mantle deposits (black) on the nearside northern hemisphere of the Moon (after *Head,* 1976a). These deposits are thought to be pyroclastic units ejected as a mixture of gas and lava droplets from volcanic vents.

intensities on depolarized 3.8-cm radar maps, indicating the absence of surface scatterers (such as boulders) in the 1 to 50 cm range. *Gaddis et al.* (1985) suggest that numerous other areas, with the same low radar scattering intensities, are likely to contain pyroclastic deposits. Some of these other pyroclastic units may be as large as the observed dark mantle deposits. If the dark mantle deposits and similar units are indeed pyroclastic, then they should be composed of relatively homogeneous glasses with concentrations of volatile elements on their surfaces, similar to Apollo 15 green glass and the Apollo 17 orange glass.

6.3 HIGHLAND PRISTINE ROCKS: IGNEOUS ROCKS AND MONOMICT BRECCIAS

The lunar crust onto which the mare basalts flowed, between about 4.0 and 3.1 b.y. ago, had itself formed within a few hundred million years of the origin of the Moon and the solar system (4.6 b.y. ago). As this crust formed, it suffered frequent large impacts as the violent process of planetary accretion drew to a close. This heavy bombardment continued for ~500 to 600 m.y. after the crust formed. Many researchers contend that the end of this period was marked by a *terminal cataclysm* that accounts for most of the impact brecciation in the lunar crust.

These frequent and severe impacts transformed the upper few kilometers of the solid crust into a layer of fragmental and chaotically mixed impact debris, often referred to as *megaregolith.* In this manner, rocks of the upper crust were shattered, broken, and mixed down to submillimeter scales. The crustal rocks were also heated at the same time because a significant portion of the impact energy was converted into heat. As a result, virtually all of the highland rock samples collected by the Apollo missions are mixtures of diverse pulverized or shock-melted fragments of many different older rocks. These hybrid fragmental rocks, called *polymict breccias,* are the subject of the following section (section 6.4). In contrast, the present section de-scribes rocks that, although shattered and deformed, have not been mixed together with other rocks. These *monomict breccias* are not hybrid mixtures.

A lunar monomict breccia is a rock that, although brecciated in texture and shattered into fragments, still represents a single original rock type. It has survived the meteoritic bombardment with no contamination, mixing, or other significant alteration of its original chemical composition. Because monomict breccias represent a single rock type rather than a mixture, they provide important clues to the makeup of the lunar crust.

Even rarer than monomict breccias are purely igneous highland rocks. These are crystalline rocks that have solidified from an original melt; they are not only monomict but also not brecciated. Together, monomict breccias and igneous rocks are often termed *pristine* highland rocks, using "pristine" in a chemical sense. They are rare among the lunar samples, but they are important because they are preserved components of the primary lunar crust. Among the Apollo samples, pristine highland rocks range in size from tiny clasts of less than 1 mg mass (i.e., only observable by chance in a thin section) to the fifth largest highland rock in the collection, the Apollo 16 ferroan anorthosite 60015 (5574 g, including a thin partial coating of impact glass).

In analyzing and interpreting a highland sample, it is essential to know whether it is a pristine rock (igneous rock or monomict breccia) or a polymict breccia. This distinction is especially important when interpreting chemical data. The bulk chemical composition of a polymict breccia represents an average of many older rocks that have been mixed together, but it does not correspond to any primary lunar rock type. If not recognized as mixtures, analyses of polymict breccias can convey a misleading impression that there is only a limited compositional diversity among highland rocks. Only by physically separating polymict breccias into their pristine components (or by doing equivalent mathematical separations on the resulting data) can we properly assess the compositional and genetic diversity of the highland crust.

How can pristine rocks be distinguished from polymict rocks? Sometimes the difference is obvious from microscopic examination of a thin section. A pristine rock may have a uniform coarse-grained, crystalline igneous texture throughout. In contrast, a polymict rock might be an obvious blend of fragments of different rocks.

Microscopic examinations may not always be adequate, however. Even pristine highland rocks are generally severely brecciated, obscuring their original textures. Some polymict rocks, formed by the cooling of impact-generated melts, have textures virtually indistiguishable from pristine igneous basaltic lavas. Electron microprobe analyses, which can determine the compositions of small areas of a crystal, can be made on the different minerals to determine whether or not a particular breccia is monomict. In pristine rocks, the minerals tend to have a narrow range of compositions that reflects their formation together near chemical equilibrium. In contrast, polymict breccias tend to have minerals from different sources that have different compositions. This general distinction must be applied with caution, for pristine rocks from shallow levels in the crust can also have varied mineral compositions caused by disequilibrium in crystal growth.

Because textural and mineralogical data may be ambiguous, the most commonly used method for distinguishing between pristine and polymict rocks involves chemical analyses. The *siderophile* (i.e., geochemically associated with Fe metal) trace elements are especially useful discriminators. Compared with typical CI carbonaceous chondrite meteorites, pristine lunar igneous rocks are generally depleted in siderophile elements such as Au, Ge, Ir, Os, and Re, by factors of roughly 10,000 (section 8.6). Because large meteoroid impacts are primarily responsible for producing polymict breccias out of pristine rocks, the small amounts of meteoroid mixed into the resulting polymict breccia produce enhanced concentrations of siderophile elements. In general, a sample with a concentration of one of these siderophile elements >0.0003 times the concentration in CI carbonaceous chondrites is considered to be a polymict rock (*Warren and Wasson,* 1977); samples with less than this amount are considered pristine. This boundary is not an absolute discriminator; some monomict rocks have concentrations well above this limit (*Warren et al.,* 1987). However, a concentration below this value is usually a reliable indication that a sample is pristine. Other trace-element data may also assist in distinguishing pristine from polymict rocks.

In summary, there is no simple method for deciding whether a given lunar rock is pristine or polymict. In a few cases, all the available evidence is ambiguous, and the nature of the sample remains uncertain. For example, one entire category of possible pristine igneous rocks, the Apollo 15 KREEP basalts, may instead be coarse-grained impact-melt rocks (*Taylor,* 1982), simply because it is difficult to distinguish a pristine igneous texture from a relatively coarse-grained impact melt. In another example, the Apollo 14 sample 14310 has a texture (*lames,* 1973) comparable to typical Apollo 15 KREEP basalts, and 14310 was therefore once presumed to be igneous (e.g., *Apollo Soil Survey,* 1971). The subsequent discovery of a clast of fine-grained polymict breccia in one thin section of 14310 (*Carlson and Walton,* 1978) eventually proved that 14310 is a polymict rock. Even before this conclusive

evidence was found, however, most petrologists had already concluded that 14310 is an impact-melt breccia, on the basis of its textural heterogeneity, high contents of meteoritic siderophile elements (*Baedecker et al.,* 1972; *Morgan et al.,* 1972a,b), and high plagioclase content, which is greater than expected for rocks formed by partial melting in the lunar interior (e.g., *Green et al.,* 1972).

6.3.1. Classification of Pristine Igneous Highland Rocks

Most petrologists distinguish three major classes of pristine igneous lunar highland rocks: KREEP rocks, ferroan anorthosites, and Mg-rich rocks. KREEP rocks have been found as small basaltic fragments in Apollo 15 and Apollo 17 breccia samples. The ferroan anorthosites and Mg-rich rocks are rarely found as plutonic (coarsely crystalline) rocks; most occur as monomict breccias. Volumetrically, KREEP rocks are far less important than ferroan anorthosites and Mg-rich rocks.

The KREEP rocks are named for their characteristically high contents of incompatible elements, especially K, rare earth elements (REE), and P, which always occur in virtually the same pattern of element:element ratios (see sections 2.4.4 and 8.4.2). In practice, because of their generally fine-grained crystalline textures, KREEP rocks are also considered to be basalts, crystallized on or just below the lunar surface.

A few other lunar rocks also show similar enrichments of the same elements, but do not show the same basaltic textures. One example is a quartz- and feldspar-rich lunar "granite" (*Warren et al.,* 1983b). The exact relationship between these coarse-grained KREEPy (or KREEP-like) rocks and the more common, fine-grained KREEP basalts remains a matter of debate and speculation.

A common synonym for KREEP rocks is "Fra Mauro basalt," because the highland rocks returned by the Apollo 14 mission, which landed on the Fra Mauro Formation, are almost exclusively KREEPy breccias or impact melts with major-element compositions (e.g., low silica) that approximate the compositions of basalts.

The other two types of common monomict highland rocks, *ferroan anorthosites* and *Mg-rich rocks,* are (or have been) derived from large igneous bodies rich in plagioclase feldspar. Earlier workers (e.g., *Kell et al.,* 1972) tended to combine them on the basis of mineral composition, with plagioclase-rich polymict rocks into a single category "ANT" (for Anorthosite-Norite-Troctolite rocks). However, evidence of a pristine character is now considered a more important criterion for classification than mineralogy, and the pristine rocks in the earlier ANT series have been divided into two subgroups of roughly equal size. The ferroan anorthosite subgroup is chemically distinct from other highland rocks, as can be seen on plots of Mg/(Mg + Fe) against Na/(Na + Ca) (Fig. 6.22). Within typical large igneous bodies, which probably solidify with fractional crystallization and crystal separation, the Mg/ (Mg + Fe) ratio tends to vary inversely with the Na/ (Na + Ca) ratio. Typical ferroan anorthosites, however, do not show such a trend (Fig. 6.22).

The other subgroup, the Mg-rich rocks, contains less plagioclase and more Mg-rich minerals like olivine and pyroxene. Chemically, this group is distinguished from the ferroan anorthosites by showing the expected inverse variation between the Mg/(Mg + Fe) and Na/(Na + Ca) ratios that would be produced by crystal separation during cooling and crystallization.

These two groups of rocks are probably genetically distinct; chemically, they show no overlap on plots such as Mg/(Mg + Fe) vs. Na/(Na + Ca). Further-more, the ferroan anorthosites tend to have much higher plagioclase contents (generally >95 vol.%) than Mg-rich rocks (generally 40-80 vol.%).

Other pristine lunar highland rock types include high silica granites and alkali (Na-rich) anorthosites. These rocks may have been produced by extreme chemical differentiation from an Mg-rich rock, from a KREEP rock, or from both. Many petrologists also make a distinction, first proposed by *James and Flohr* (1983), between the Mg-rich rocks that contain abundant high-Ca pyroxene (*Mg-gabbronorites*) and the majority of Mg-rich rocks, which have little or no high-Ca pyroxene.

Another lunar rock type, "very-high-alumina basalt" or "highland basalt," was first believed to be an important monomict highland rock that occurred chiefly as lava flows. However, most petrologists soon agreed that "VHA basalt" was not a truly igneous rock type. Most, if not all, VHA basalts are actually polymict impact-melt rocks that formed as mixtures of other "pristine" rock types such as anorthosites, KREEP basalts, etc. (*Dowry et al.,* 1974c).

The naming and classification of lunar highland rocks can be confusing, even for petrologists. The nomenclature is largely based on mineralogy, the essence of which can be summarized on a diagram (Fig. 6.23) showing the relative abundances of the major mineral constituents: feldspar, pyroxene, and either olivine or a silica mineral. Magnesian olivine and a silica mineral cannot occur together in equilibrium (they react to form pyroxene), so each rock type can be represented in either the feldspar-pyroxene-olivine or the feldspar-pyroxene-silica

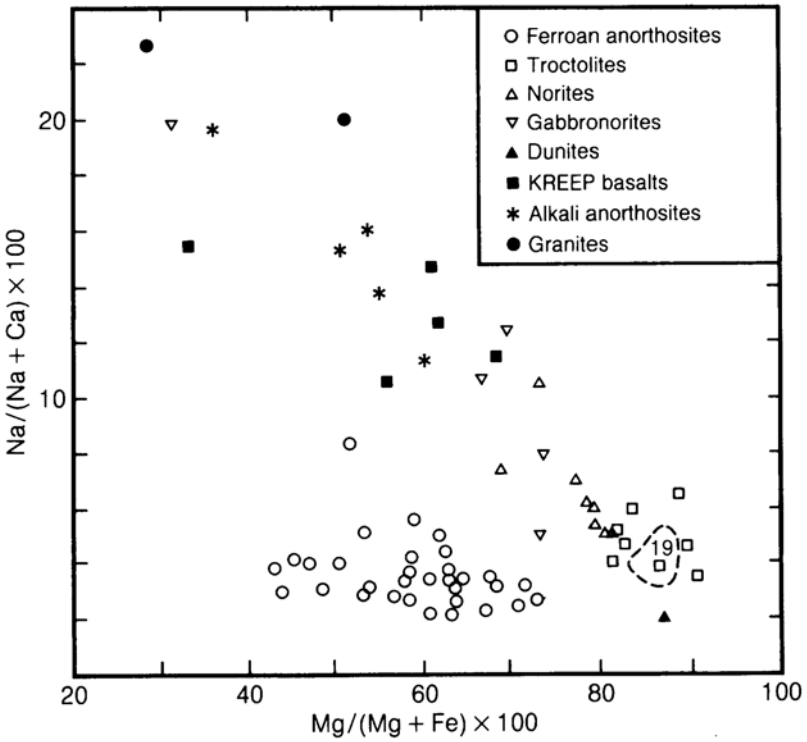

Fig. 6.22. Bulk-rock Na/ (Na + Ca) vs. Mg/(Mg + Fe), mole ratios, for a variety of pristine highland igneous rocks (after *Warren,* 1986). Dashed field (lower right) encompasses 19 troctolites. The ferroan anorthosites (lower center) have distinctive, low Mg/(Mg + Fe), low Na/(Na + Ca) compositions.

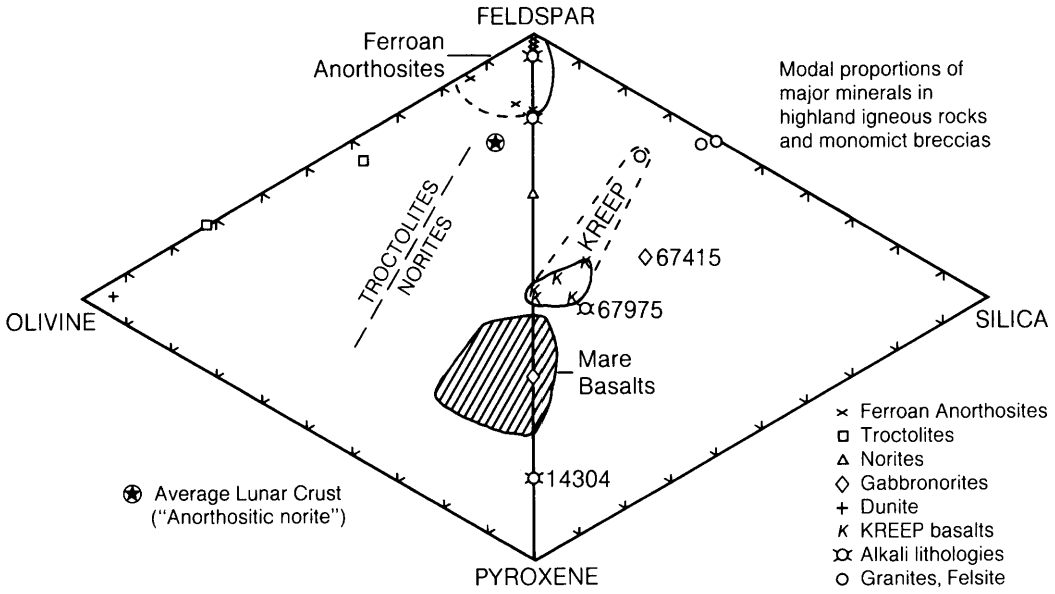

Fig. 6.23. Modal (volume) proportions of the four major minerals in highland pristine igneous rocks and monomict breccias (Tables 6.6, 6.7, 6.8, and 6.10). Gabbronorites include the sodic ferrogabbro 67415; alkali lithologies include two alkali anorthosites (with abundant feldspar), alkali norite 14304, and alkali granite 67975. The general area of mare basalt composition (*BVSP,*1981) is shown for comparison (ruled area). The KREEP basalts have higher amounts of feldspar and silica minerals. The boundary between norite and troctolite is defined by the line representing a 1:1 olivine-to-pyroxene ratio (*Stöffler et al.,* 1980).

system. This diagram is also a good indication of the major mineral components that could be obtained for processing if the rocks shown were disaggregated. Other important variations are described in the text and in the tables.

6.3.2. KREEP Rocks

Even though KREEP is known to be a major chemical component of the upper lunar crust at the Apollo 12 and 14 landing sites, actual fragments of pristine KREEP rocks have only rarely been recognized in samples from any mission other than Apollo 15. Igneous-textured KREEP rocks are mainly basalts; the KREEPy granite and quartz monzodiorite types are much less common (Fig. 6.23; section 6.3.5).

The precise locations of KREEP bedrock are not known. The Apennine Bench Formation, exposed about 70 km west of the Apollo 15 landing site, is thought to extend under the younger plains of mare basalts near the landing site itself and to be the source of the Apollo 15 KREEP basalts (*Spudis and Ryder,* 1985). The two largest samples of KREEP rocks are the Apollo 15 basalt samples 15382 and 15386 (3.2 and 7.5 g, respectively). Pristine KREEP rocks from other Apollo sites include a series of basalt clasts in Apollo 17 breccia *72275* (*Ryder et al.,* 1977; *Salpas et al.,* 1987) and a single tiny clast, not definitely pristine, of basalt in Apollo 16 breccia 67749 (*Ryder and Norman,* 1980). A thoroughly brecciated olivine norite clast from the Apollo 14 breccia 14318 may be related to KREEP, but this clast is neither definitely monomict, nor of typical Apollo 14 KREEP composition (*Warren et al.,* 1986).

Figure 6.24 illustrates several examples of textures in igneous, unbrecciated KREEP rocks. Most igneous KREEP rocks are basalts; they are generally subophitic to intersertal in texture (see section 6.1.3 for

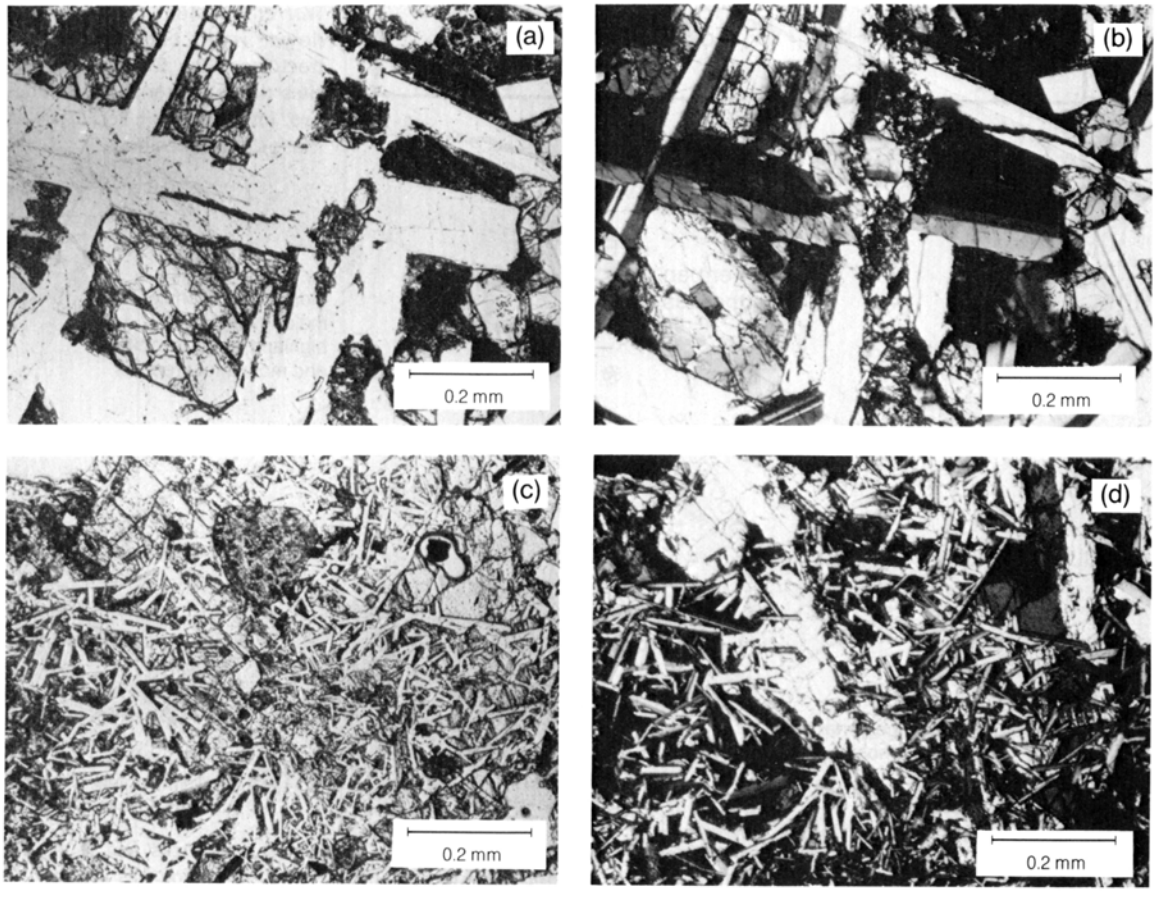

Fig. 6.24. Photomicrographs of small fragments of KREEP basalts collected from the Apollo 15 core sample 15007. Image **(a)** shows subophitic texture in plane-polarized light and **(b)** shows the same texture in cross-polarized light; **(c)** shows intersertal texture in plane-polarized light and **(d)** shows the same texture in cross-polarized light.

TABLE 6.6. Modal mineral composition (in vol.%) of some monomict KREEP rocks.

	14303c	A15KF*	15382	15386	15405c	72275 c
Plagioclase	33	41	43	43	35	40
Olivine	tr	—	—	—	—	tr
Orthopyroxene	—	P	9	P	—	P
Pigeonite	—	P	32	P	18	P
High-Ca pyroxene	11	P	P	P	18	P
Total pyroxene	-11	35	-41	43	-36	40
Ilmenite	1	—	P	3	1.6	P
FeNi metal	tr	tr	tr	tr	0.2	tr
Troilite (FeS)	tr	tr	tr	tr	tr	tr
Total opaque minerals	-1	3	6†	-3	-2	—
Quartz	23	—		—	11	—
Cristobalite	—	4	P	8	—	P
Total SiO_2 minerals	-23	-4	—	-8	-11	—
Zircon	tr	—	—	—	0.6	tr
K-feldspar	32	—	—	tr	15	tr
Apatite	tr	—	tr	—	—	—
Whitlockite	—	—	tr	tr	0.8	tr
Glassy mesostasis	—	17	8	P	—	20

* A15KF indicates the "typical" mode reported for six small fragments (coarse soil particles) of Apollo 15 KREEP basalt (*Powell et al.*, 1973).

† Total opaque phases reported for 15382 include minor Cr,Fe-spinel, armalcolite, baddeleyite, tranquillityite, and zirconolite.

Abbreviations: P = present,"tr"= trace.

Additional references: "granite" 14303c, *Warren et al.* (1983b); basalt 15382, *Dowty et al.* (1976), *Hollister and Crawford* (1974); basalt 15386, *Steele et al.* (1972), *Simonds et al.* (1975), *Takeda et al.* (1984); quartz-monzodiorite 15405c, *G. J. Taylor et al.* (1980); basalt 72275c, *Ryder et al.* (1977).

a discussion of textural terms). Some coarser varieties have porphyritic textures. In these rocks, the phenocrysts are usually euhedral or subhedral prismatic crystals of orthopyroxene (containing almost no Ca), with smaller, lathlike (sometimes skeletal) plagioclase, normally intergrown with low-Ca pyroxene (pigeonite) rims. These textures indicate an origin as volcanic lavas (*Ryder,* 1987). However, several KREEP rocks have coarser, more equigranular textures that imply slower cooling and suggest an intrusive origin.

The higher-silica KREEPy rocks, quartz monzodiorite and granite, which occur as clasts in Apollo 15 breccia 15405, are themselves brecciated, but their original textures appear to have been "coarse basaltic, with plagioclase laths" (*Ryder,* 1976, 1985). Unlike typical KREEP basalts, these clasts contain intergrowths of silica and K-feldspar. These clasts also have unusually high incompatible element contents, even by KREEP standards. Another KREEP-like granite clast, from the Apollo 14 breccia 14303, is a thoroughly brecciated sample of a coarse, equigranular rock with abundant intergrowths of silica and K-feldspar (*Warren et al.,* 1983b).

Table 6.6 illustrates the range in modal composition (mineral abundances by volume percent) among pristine KREEP rocks. Olivine is uniformly rare. Among the KREEP basalts, pyroxenes show a characteristically wide range in composition from the earliest-formed orthopyroxenes with Mg/ (Mg + Fe) = 0.8 and essentially no Ca, to the later low-Ca, lower-Mg (pigeonite) and high-Ca (augite) varieties (Fig. 6.25). However, pyroxenes in the small clast in sample 67749 do not include any of the orthopyroxene, or even the low-Ca, high-Mg pigeonite, found in all other KREEP basalts (*Ryder and Norman,* 1980). Plagioclase feldspar in KREEP basalts (e.g., 15382) typically has normal zonation, from 95% Ca-feldspar (anorthite) in the crystal center to 80% or less at the edges (see section 5.1.2 and *Dowty et al.,* 1976). There is also strong enrichment in K (the orthoclase component), as Ca (the anorthite component) decreases in the plagioclase; this is illustrated in Fig. 6.26 for the 72275 clasts (*Ryder et al.,* 1977).

In many respects, the chemical compositions of igneous KREEP basalts (Table A6.9; Figs. 6.27 and 6.28) are remarkably uniform. The diagram in Fig. 6.27 is based on melting and crystallization

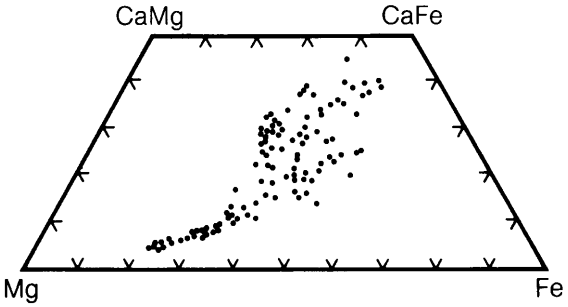

Fig. 6.25. Compositions (Mg:Fe:Ca atomic proportions) of zoned pyroxene crystals from Apollo 17 KREEP basalt 72275c. The first crystals to form were high-Mg orthopyroxenes (lower left). Formation of these crystals changed the composition of the remaining liquid, causing Fe- and Ca-rich rims (center and upper right) to form on the original Mg-rich cores. Data from *Ryder et al.* (1977).

experiments using actual lunar basalt compositions (*Walker et al.,* 1973a,b), and incorporating the five major oxides in the highland crust (Al_2O_3, CaO, FeO, MgO, and SiO_2). The experimental results define stability fields for the three most abundant minerals in the highland crust: plagioclase feldspar, low-Ca pyroxene, and olivine. The compositions of KREEP basalts tend to cluster near the curve that represents melts that are saturated with (and therefore crystallizing) both plagioclase and low-Ca pyroxene. In particular, the KREEP compositions cluster near the high-temperature (low-SiO_2) end of the curve, where melts are cosaturated with plagioclase, low-Ca pyroxene, and olivine.

Although the KREEP rocks show relatively constant ratios between individual incompatible elements (Fig. 6.28), they have a considerable range in total incompatible element enrichments. As a result,

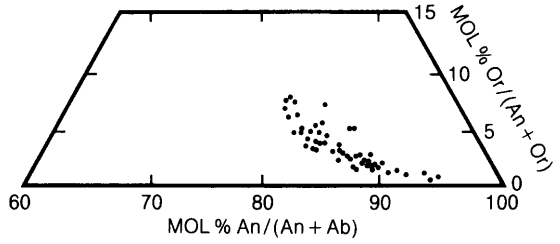

Fig. 6.26. Compositions of zoned plagioclase crystals from Apollo 17 KREEP basalt 72275c, showing molecular proportions of Ca-feldspar (An), Na-feldspar (Ab), and K-feldspar (Or). The earlier-formed crystals are Ca-rich (high An). As the An content decreased in the later-formed crystals (and in the rims on earlier-formed crystals), the Or content also increased. Data from *Ryder et al.* (1977).

the KREEP rocks can be divided into subgroups on the basis of their incompatible element contents. Potassium (K) is a convenient discriminator and is used to distinguish "low-K," "medium-K," and "high-K" KREEP types. Typical low-K KREEP is divided from medium-K KREEP at K_2O = 0.35 wt.% (corresponding to La = 46μg/g, Lu = 2.1 μg/g, etc.). Medium-K KREEP is divided from high-K KREEP at K_2O = 0.7 wt.% (or La = 93 μg/g, Lu = 4.2 μg/g, etc.).

With the exception of the quartz monzodiorite clast in sample 15405, all known pristine KREEP rocks are medium-K KREEP; samples of low-K KREEP and volcanic high-K KREEP have been found only as polymict breccias. There is, in fact, even considerable doubt as to whether significant volumes of pristine igneous low-K KREEP ever existed, because this composition could easily result from impact-induced mixing of medium-K or high-K KREEP with typical nonKREEPy highland rocks. An average composition for high-K KREEP polymict breccias is included in Table A6.9.

Table A6.10 lists the ratios of incompatible elements used to define the characteristics of KREEP rocks. These incompatible element ratios are nearly constant among rocks with a wide range of overall incompatible-element enrichments. Despite their high incompatible-element contents (which would normally be produced by a high degree of igneous fractionation, in which the Mg/Fe ratio should decrease) typical KREEP rocks have moderately high Mg/(Mg + Fe) ratios (Fig. 6.29).

Radioactive age dating of KREEP basalts indicates that they formed at about 3.8-4.0 b.y. ago, either just before the oldest mare basaltic lavas or perhaps contemporaneously with them. Ages determined for Apollo 15 igneous KREEP basalt 15382 range from 3.82 b.y. (Rb-Sr system; *Papanastassiou and Wasserburg,* 1976), to 3.90-3.91 b.y. (^{40}Ar-^{39}Ar system; *Stettler et al.,* 1973; *Turner et al.,* 1973). A similar basalt, 15386, yielded a Rb-Sr age of 3.86 ± .04 b.y. (*Nyquist,* 1977) and a Sm-Nd age of 3.85 ± .08 b.y. (*Carlson and Lugmair,* 1979). Initial $^{87}Sr/^{86}Sr$ ratios (a measure related to the evolution of the melted mantle source) reported for these rocks are 0.700241 and 0.70038 ± 10, respectively. Another probable igneous Apollo 15 KREEP basalt, 15434,73, yielded a similar Rb-Sr age of 3.83 ± .04 b.y., but an initial $^{87}Sr/^{86}Sr$ ratio of 0.70070 ± 10 (*Nyquist,* 1977). The Apollo 17 KREEP basalt 72275 yielded a Rb-Sr age of 3.93 ± .04 b.y. and an initial $^{87}Sr/^{86}Sr$ ratio of 0.69957 ± 14 (*Compston et al.,* 1975). Model ages calculated for the source regions that produced the monomict Apollo 15 KREEP basalts are typically 4.2-4.4 b.y. (*Nyquist,* 1977; *Carlson and Lugmair,* 1979); however, *Nyquist* (1977) calculated a model age of 4.00-4.06 b.y. for the source of KREEP basalt 72275.

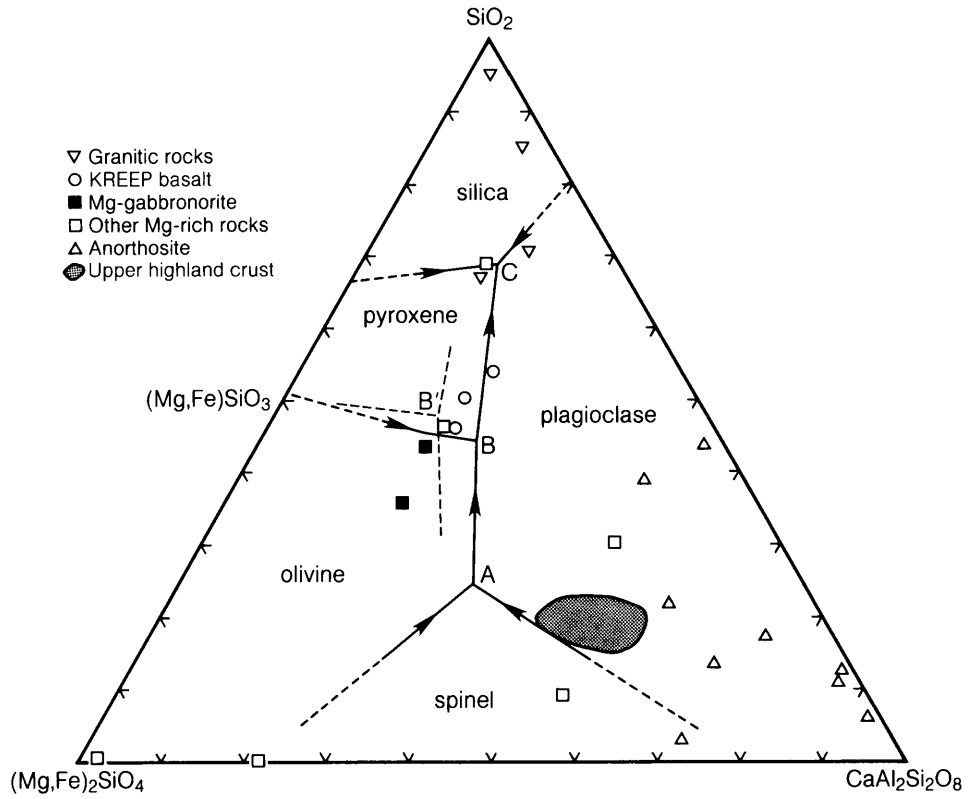

Fig. 6.27. Three-component (ternary) diagram for the system $(Mg,Fe)_2SiO_4$-$CaAl_2Si_2O_8$-SiO_2, representing olivine—Ca-feldspar—silica, based on crystallization experiments by *Walker et al.* (1973a,b). The triangular plot is divided into several regions; melt compositions within each region will crystallize out the indicated mineral upon cooling. For the natural lunar compositions used to infer the boundary locations, the Mg/(Mg + Fe) ratio varies from 0.51 (at point C), to 0.64 (at point B), to 0.76 (at point A). The diagram is "pseudo" ternary because spinel is actually an oxide mineral, not a mixture of $(Mg,Fe)_2SiO_4$ and $CaAl_2Si_2O_8$. The light-dashed curves show the equivalent crystallization-field boundaries determined by *Stolper* (1977) for similar but more FeO-rich compositions; the Mg/(Mg + Fe) ratio at point B' is 0.385. *Longhi and Pan* (1986) provide further data on shifts of these boundary curves as a function of bulk composition. Any Na in Ca-feldspar of anorthosites pulls these points (triangles) toward the SiO_2 apex because the diagram ignores the Na but not its associated SiO_2. Compositions of monomict highland rocks (Tables A6.9, A6.11, A6.12, and A6.13) are shown. Also shown for comparison (shaded field) is a range of compositions for typical highland regolith samples, including three lunar meteorites (all regolith breccias), the Luna 20 soil, and average Apollo 16 soil (*Warren and Kallemeyn,* 1987). The average composition of the upper highland crust presumably plots within this field.

Age measurements on other KREEP-related rocks are less clear cut. The quartz monzodiorite clast in sample 15405 has been the subject of numerous isotopic studies. Unfortunately, it has been heavily shocked and the impact effects have severely disturbed the isotopic systems used for age dating. In one study, *Nyquist et al.* (1977) attempted to correct for Rb loss during shock by assuming an original Rb ratio similar to that of typical Apollo 15 KREEP; they concluded that the Rb-Sr age of the quartz monzodiorite is about 4.1 b.y., with an initial $^{87}Sr/^{86}Sr$ ratio of 0.699. *Compston et al.* (1984b) used a high-resolution ion microprobe to obtain data for the U, Th, and Pb isotopes contained in four zircon grains from the quartz monzodiorite. Their results suggest that these zircons originally crystallized 4.365 ± .030 b.y. ago. *Compston et al.* (1984a) also obtained similar results for the 14303 granite clast; its zircon apparently crystallized 4.33-4.40 b.y. ago. Evidently the volcanic KREEP basaltic lavas tend to be younger than the coarser-grained, higher-silica KREEP-rich rocks.

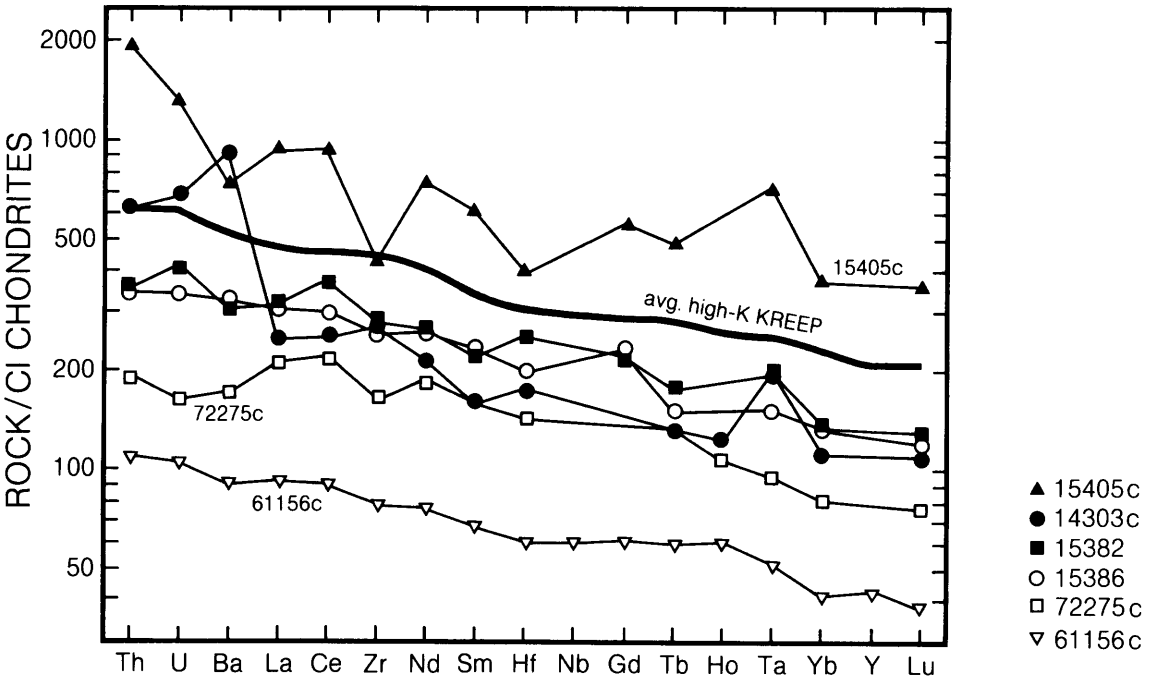

Fig. 6.28. Contents of various *incompatible elements* (i.e., elements not taken up by the common minerals in a crystallizing basalt) in KREEP-rich samples and related rocks. A lower-case "c" after the sample number indicates that a clast from within the sample was separated and analyzed. Higher incompatible-element contents correspond to higher KREEP content. The heavy line labeled "average high-K KREEP" represents polymict breccias of that composition. Sample 61156 is a VHA (very-high-alumina) "basalt" that is actually a type of polymict melt breccia. This sample is shown for comparison with the pristine KREEP rocks. Data for relatively coarse-grained rocks (samples 15405, 14303, and 15382) are plotted as solid symbols; these samples may be especially subject to errors caused by small sample sizes (e.g., major changes in Zr and Hf contents resulting from chance distribution of the mineral zircon). Data are from Table A6.9, normalized to element abundances in CI carbonaceous chondrites (*Anders and Ebihara,* 1982).

The fact that KREEP rocks tend to occur as volcanic lavas makes it difficult to use the Apollo data to estimate their overall abundance in the lunar crust. By assuming that (1) the lunar surface rocks are representative of the entire thickness of lunar crust and (2) most pristine KREEP occurs in the low-K form, *Taylor* (1975) produced a model lunar crust with 20 wt.% KREEP. However, if most of the KREEP rocks are broad, thin lava flows on the lunar surface, then the crust as a whole may be considerably less KREEP-rich than the outer surface. *Warren and Wasson* (1979a) estimate that, assuming that most monomict KREEP is of the "high-K" variety, KREEP rocks constitute only about 2 wt.% of the crust.

Recent analyses of meteorites from the Moon that have been collected in Antarctica (e.g., *Warren and Kallemeyn,* 1987) also suggest that the lunar crust as a whole is relatively poor in KREEP except for the small region near the center of the Moon's nearside that includes the Apollo and Luna sampling sites. This region covers 4.7% of the lunar surface. In other words, the post-Apollo lunar meteorite data also favor a reduction from earlier estimates of the overall crustal inventory of KREEP.

6.3.3. Ferroan Anorthosites

The single most common type of pristine highland rock is *ferroan anorthosite* (Fig. 6.23). It is distinguished from all other highland rocks by the peculiar combination of low-Na plagioclase feldspar with low-Mg pyroxene, with or without olivine. The majority of monomict rock types identified from the Apollo 16 site, the only sampled location in a typical highland region, are ferroan anorthosites. Among the lunar meteorites found since 1979 in Antarctica, the majority of pristine rock types identified as clasts

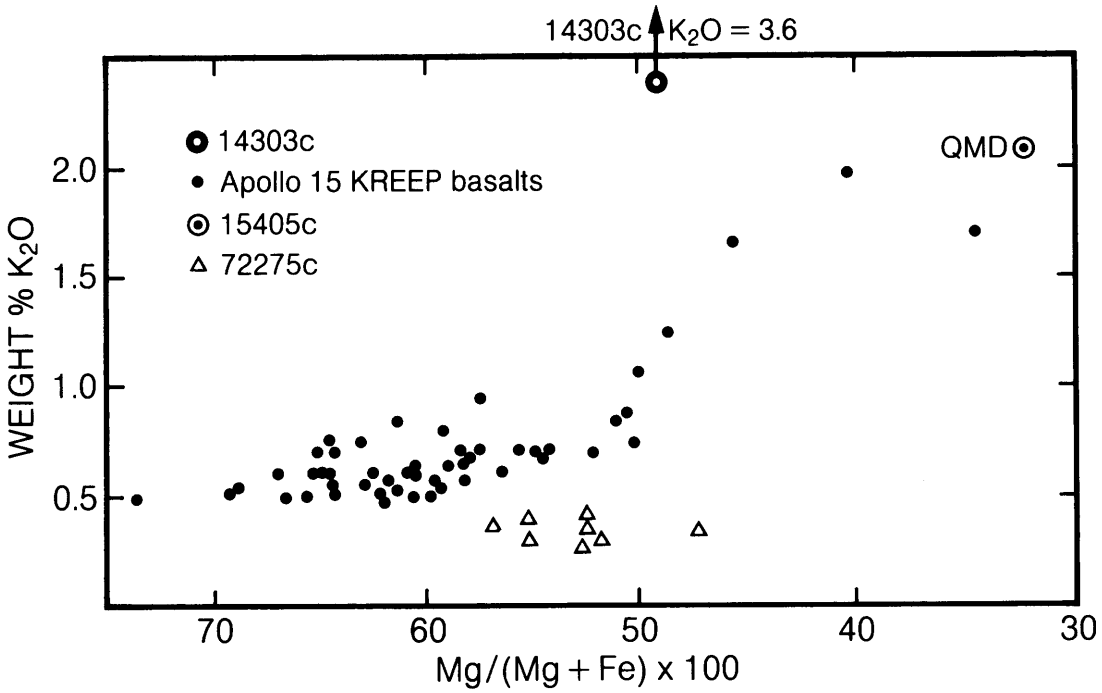

Fig. 6.29. Plot of mole Mg/(Mg + Fe) ratios against K_2O for pristine KREEP rocks. This plot illustrates a paradoxical characteristic of KREEP rocks: the combination of high Mg/(Mg + Fe) ratios (normally found in early-crystallized materials), with high K_2O contents (normally found in late-crystallized materials). Data are from *Irving* (1977), except for 14303c (a KREEP-like granite clast), which is from *Warren et al.* (1983b). These data have been obtained mainly from defocused-beam electron microprobe analyses, which are less reliable than most other types of major-element analyses of rocks. Note: QMD = quartz monzodiorite.

have similar ferroan (Fe-rich, Na-poor) mineral compositions. If the available Apollo pristine samples are representative, roughly 50% of the outer highland crust consists of ferroan anorthosite (the remainder is mainly Mg-rich rocks; see section 6.3.4).

The lunar ferroan anorthosites evidently formed as coarse-grained igneous rocks. The coarse grain size suggests that they are *intrusive* rocks, formed during slow cooling deep below the surface. The high concentration of plagioclase feldspar suggests that they are also *cumulate* rocks, produced by the separation of just-formed crystals (in this case, plagioclase feldspar) from the remaining melt. Although the vast majority of ferroan anorthosites are severely brecciated (Fig. 6.30), the few samples that show vestiges of their former igneous texture tend to be coarse-grained, with large subhedral to euhedral plagioclase crystals surrounded by smaller anhedral pyroxene or olivine (Fig. 6.31). For example, the anorthosite portion (about 100 g) of Apollo 16 breccia 60135 has remnants of original blocky plagioclase crystals up to 4.4 mm across, which separated from the melt (*cumulus* plagioclase), surrounded by pyroxene that grew from the remaining melt (*adcumulus* or *orthocumulus* pyroxene). The pyroxene crystals are as much as 5.0 mm across. Although these vestiges of the original igneous texture have survived, 60135 is a severely shocked rock in which most mineral grains have been shock-melted *in situ* (*Warren et al.,* 1983c). Other examples of ferroan anorthosites that retain vestiges of former coarse igneous (cumulate) textures include samples 60025 (*Ryder,* 1982), 62236 (*Nord and Wandless,* 1983), and 62237 (*Dymek et al.,* 1975a).

The Apollo 15 "Genesis rock" (15415), which is by far the largest (269 g) ferroan anorthosite from a site other than Apollo 16, has a unique texture (*Ryder,* 1985). Plagioclase makes up about 99% of the rock and occurs as extremely coarse (up to 3 cm across) anhedral or polygonal grains. This unusual texture may have been produced by thermal metamorphism at least a few kilometers deep in the crust after the

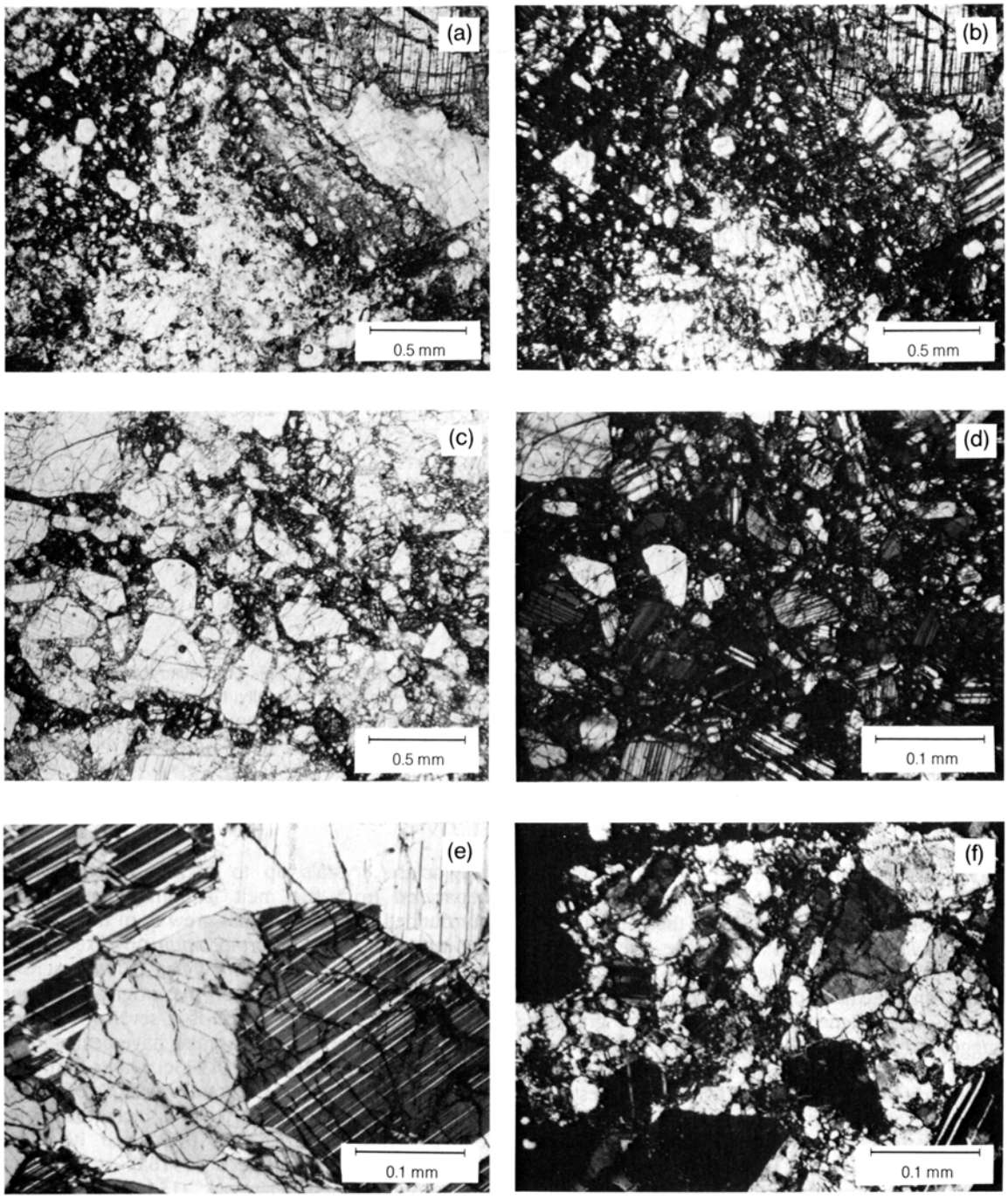

Fig. 6.30. Photomicrographs of typical ferroan and other anorthosites: **(a)** and **(b)**, severely brecciated and crushed areas in ferroan anorthosite 62236 [note relatively unbrecciated, pyroxene-rich area (gray) in lower left]; **(c)** and **(d)**, ferroan anorthosite 62237, showing "stringers" of pulverized mafic silicates (gray) among larger plagioclase fragments (white); **(e)** ferroan anorthosite 15415, showing coarsely crystalline texture; **(f)** alkali anorthosite 12073c, showing texture resulting from severe crushing followed by thermal annealing. All views in transmitted light and crossed polarizers, except **(a)** and **(c)**, which are with uncrossed polarizers.

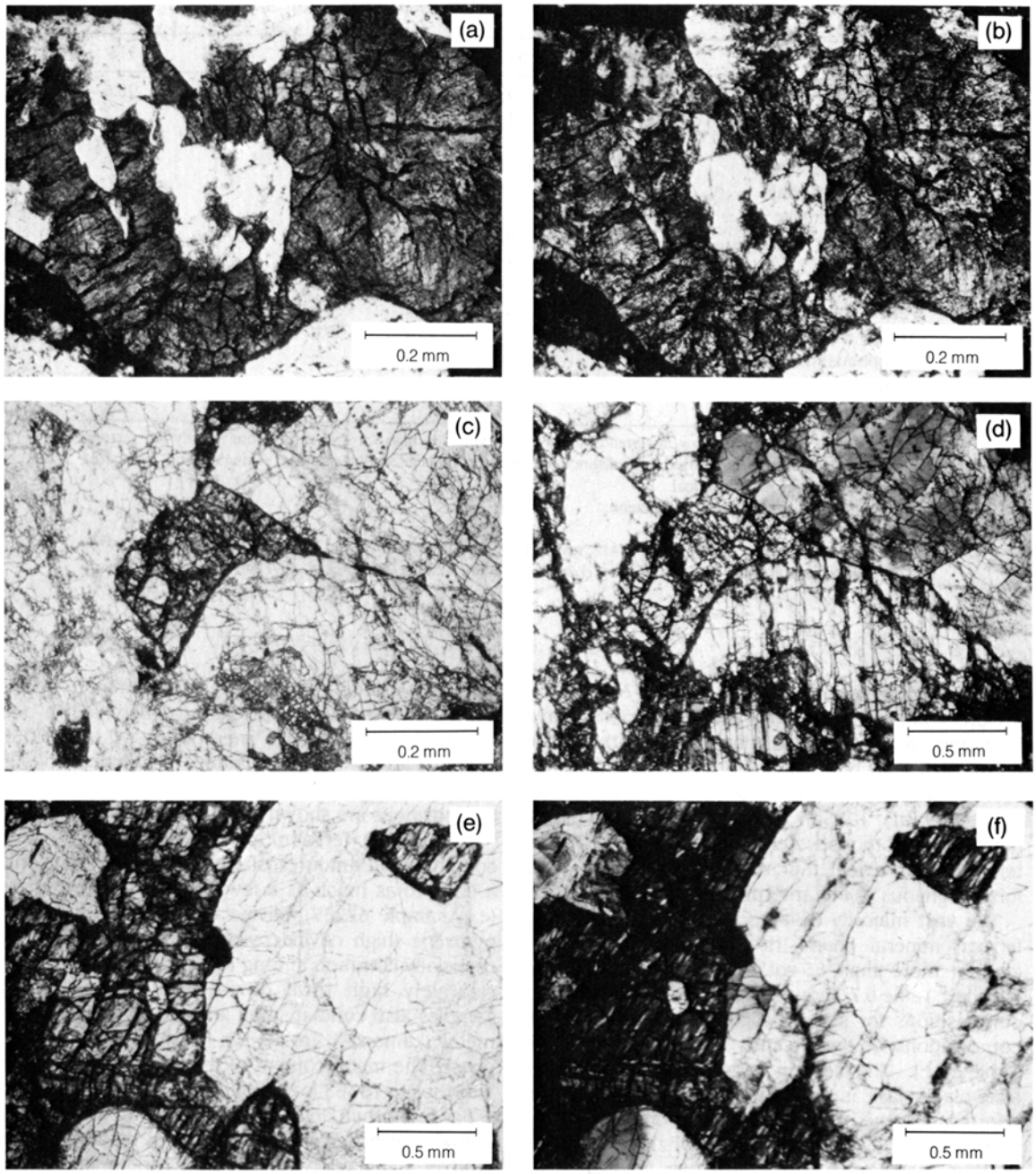

Fig. 6.31. Photomicrographs of areas of ferroan anorthosite samples containing *mafic* minerals (olivine and pyroxene). These minerals show relict *cumulate* textures produced by accumulation of crystals from a melt, most notably the smooth, arcuate boundaries between coarse pyroxenes (dark gray) and plagioclase. Images **(a)** and **(b)** show a small clast composed of augite, plagioclase, and low-Ca-pyroxene from the lunar meteorite ALHA81005. Based on its "ferroan" composition, this clast is thought to be an atypically pyroxene-rich fragment of an anorthosite. Images **(c)** and **(d)** show part of sample 62237, in which small pyroxenes are surrounded by large plagioclase crystals. Images **(e)** and **(f)** show another clast, composed of plagioclase and low-Ca pyroxene, which is also presumed to be an atypically pyroxene-rich fragment of an anorthosite, from sample 66035. Note that exsolution lamellae in the dark-gray pyroxene are visible as light, discontinuous diagonal bands in **(f)**. Images **(a,c,e)** were photographed with uncrossed polarizers; **(b,d,f)** are the same views, but photographed with crossed polarizers.

TABLE 6.7. Modal mineralogy (in vol.%) of some monomict ferroan anorthosites.

	15363	15415	60015	62236	62237	65315
Plagioclase	85	99	98.6	85	85	98.5
Olivine	tr	tr?	—	4	14	tr
Primary (?) hypersthene	12	tr	—	—	—	—
Inverted pigeonite*	—	tr?	1.3	10	1	1.4
Pigeonite lamellae†	—	tr	—	—	—	—
Primary (?) augite	2	tr	tr	1	tr	tr
Total pyroxene	~14	(tr)	~1.3	~11	~1	~1.4
Ilmenite	—	tr	tr	tr	tr	—
Cr-spinel	—	—	tr	tr	tr	—
FeNi metal	0.4	tr	tr	—	—	—
Troilite (FeS)	0.1	—	tr	tr	tr	—
Total opaque minerals	—	—	0.35	—	—	0.3
SiO_2 mineral(s)	—	tr	—	—	—	—
Apatite	—	tr?	—	—	—	—

* Primary igneous pigeonite now inverted into orthopyroxene + high-Ca pyroxene. Note: nearly all ferroan anorthosites are severely brecciated, and distinctions between brecciated (hypersthene + augite) and brecciated inverted pigeonite are problematical.

† Pigeonite lamellae within high-Ca pyroxene.

References: 15363, *Warren et al.* (1987); 15415, review by *Ryder* (1985); 60015 and 65315, *Dixon and Papike* (1975); 62236, *Warren and Wasson* (1978), *Nord and Wandless* (1983); 62237, *Dymek et al.* (1975a), *Warren and Wasson* (1978).

rock had originally solidified (*Stewart,* 1975). Similar textures, although involving smaller grains, have been observed in individual clasts found within more normal-textured but brecciated ferroan anorthosites such as 62236 (*Nord and Wandless,* 1983) and 62237 (*Dymek et al.,* 1975a). Most ferroan anorthosites, however, are too severely brecciated to preserve textures that reveal much information about their former igneous or metamorphic histories (Fig. 6.30)

The vast majority of large (i.e., >10 g) rocks with ferroan mineral chemistries are anorthosites that contain more than 85 vol.% of Ca-rich plagioclase feldspar. Table 6.7 shows a range of modal mineral compositions for several rock types. The chemical compositions of these same samples are listed in Table A6.11. The second most abundant mineral, after plagioclase, is usually pyroxene. In most ferroan anorthosites, the pyroxene is mainly original low-Ca pigeonite that has, since crystallizing from the igneous melt, exsolved to form two pyroxenes: an orthopyroxene host crystal with almost no Ca, containing blebs or lamellae of high-Ca augite (e.g., samples 60025, 62236, 66035; see Fig. 6.31). However, typical ferroan anorthosites are so severely brecciated that it may be impossible to determine the precise origin of the scattered pyroxene fragments they contain; some orthopyroxenes may be primary igneous minerals. In a few cases (e.g., sample 15415), the pyroxene in the ferroan anorthosite is predominantly augite. A small clast of cumulate-textured ferroan gabbro, identified in one of the lunar Antarctic meteorites (ALHA81005), contains augite that is definitely of primary igneous origin (*Warren et al.,* 1983d). Typical pyroxene compositions are shown in Fig. 6.32.

Most large ferroan anorthosite samples also contain small amounts of olivine, ranging from only a trace to as much as a few percent. In a few cases (e.g., sample 62237), olivine is more abundant than pyroxene (high olivine/pyroxene ratios seem to be especially common among ferroan anorthosites with relatively high total olivine + pyroxene). Many samples also contain small amounts of ilmenite, Fe-metal (kamacite), troilite, Cr-Fe-spinel, and a silica phase. The metal content of the small (0.5 g) ferroan anorthosite 15363 is exceptionally high (Table 6.7).

Far more than any other rock type, the widespread abundance of ferroan anorthosite is responsible for (and is a reflection of) extreme enrichment of the lunar crust in plagioclase feldspar. Many petrologists think that the ferroan anorthosites are cumulate rocks that formed by the extensive flotation of plagioclase on top of a primordial Moonwide "magma ocean," an outer layer that was molten (or partially molten) to a depth of several hundred kilometers, from about 4.4 to 4.6 b.y. ago (section 2.4.3). In this view, the ferroan anorthosites should have formation ages that fall within this

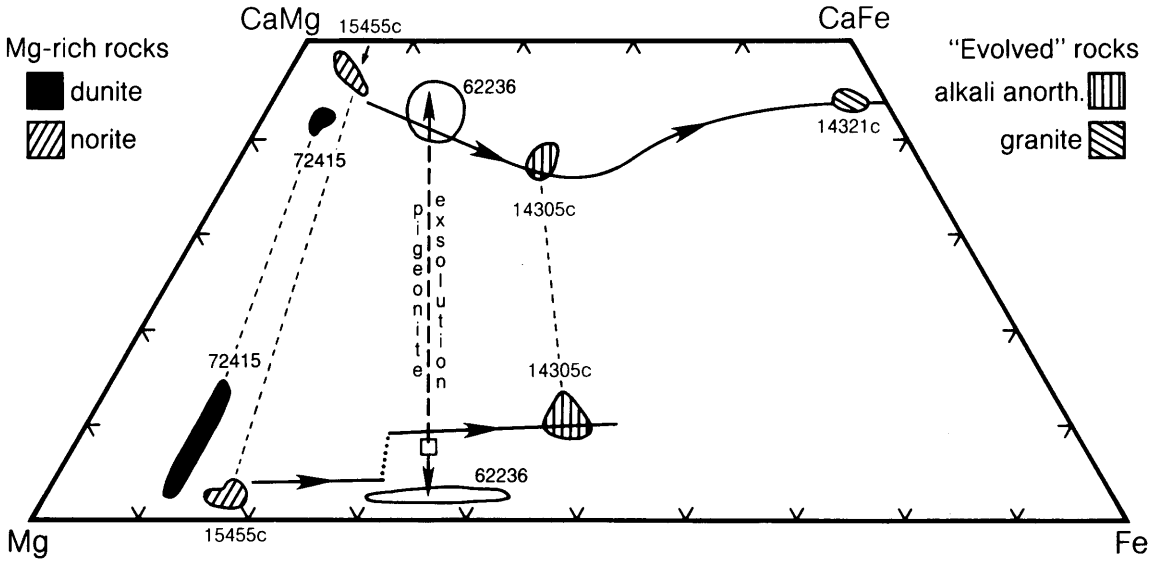

Fig. 6.32. Compositions (Mg:Fe:Ca atomic proportions) of pyroxenes from selected pristine highland intrusive rocks: dunite 72415 (*Dymek et al.,* 1975a), anorthositic norite 15455c (*Ryder and Bower,* 1977), ferroan noritic anorthosite 62236 (*Nord and Wandless,* 1983), alkali anorthosite 14305c (*Warren et al.,* 1983c), and granite 14321c (*Warren et al.,* 1983b). Square symbol indicates estimated composition of typical 62236 pyroxene (pigeonite) prior to its exsolution into orthopyroxene (lower in Ca) and augite (higher in Ca). Note that the compositions of most of these lunar pyroxenes closely match positions on the pyroxene evolution trends (solid lines with arrows) observed for terrestrial pyroxenes formed by crystal settling in a single large igneous body, the Skaergaard intrusion, Greenland (*Deer et al.,* 1978).

time interval. Unfortunately, few if any reliable crystallization ages have been obtained for ferroan anorthosites, mainly because their extremely low abundances of Rb and REE make it difficult to apply standard age-dating techniques based on the Rb-Sr and Sm-Nd systems. The severe brecciation suffered by most ferroan anorthosites (and indeed, by nearly all monomict highland rocks) also hampers efforts to measure crystallization ages. Most of the "isotopic clocks" used in age dating involve elements (e.g., K, Rb, Ar) that are easily mobilized and expelled by shock and heating associated with impact events, and ages derived from these isotopic systems tend to reflect the time of the last severe shock suffered by the rock rather than its original crystallization age (*Unruh et al.,* 1977; *Nyquist,* 1982).

However, some age measurements are at least consistent with the magma ocean model. Ferroan anorthosites tend to have extremely low $^{87}Sr/^{86}Sr$ ratios (*Nyquist,* 1977), implying that they have been separated from any significant concentrations of Rb for a length of time that is comparable with the age of the Moon. More recently, *Lugmair* (1987) has reported a Sm-Nd age of 4.44 ± .02 b.y. for a ferroan anorthosite, sample 60025. *Hanan and Tilton* (1987) reported a Pb-Pb model age of 4.51 ± .01 b.y. for the same sample. Any age for a plutonic lunar rock such as 60025 should be interpreted with caution, because rather than dating igneous crystallization it might date isotopic closure during prolonged global cooling of a primordial "magma ocean."

6.3.4. Mg-rich Rocks

The precise compositional range of the Mg-rich rock group is not well defined. Rocks in this group range from olivine-rich rocks (*dunite*) all the way to rocks composed of pyroxene and Na-rich plagioclase (*sodic ferrogabbro*) (Fig. 6.23). As originally applied, the term "Mg-rich" covered all coarse-grained highland rocks that could be distinguished from the ferroan anorthosites by such chemical indicators as higher Mg/(Mg+Fe) and/or Na/(Na+Ca) ratios (*J. Warner et al.,* 1976a). Subsequently, many petrologists have come to suspect that there are fundamental genetic distinctions even within this group, and that different rocks have been produced by separate and dissimilar magmas (e.g., *James and Flohr,* 1983). For these reasons, some extreme highland rock types such as dunite, gabbronorite,

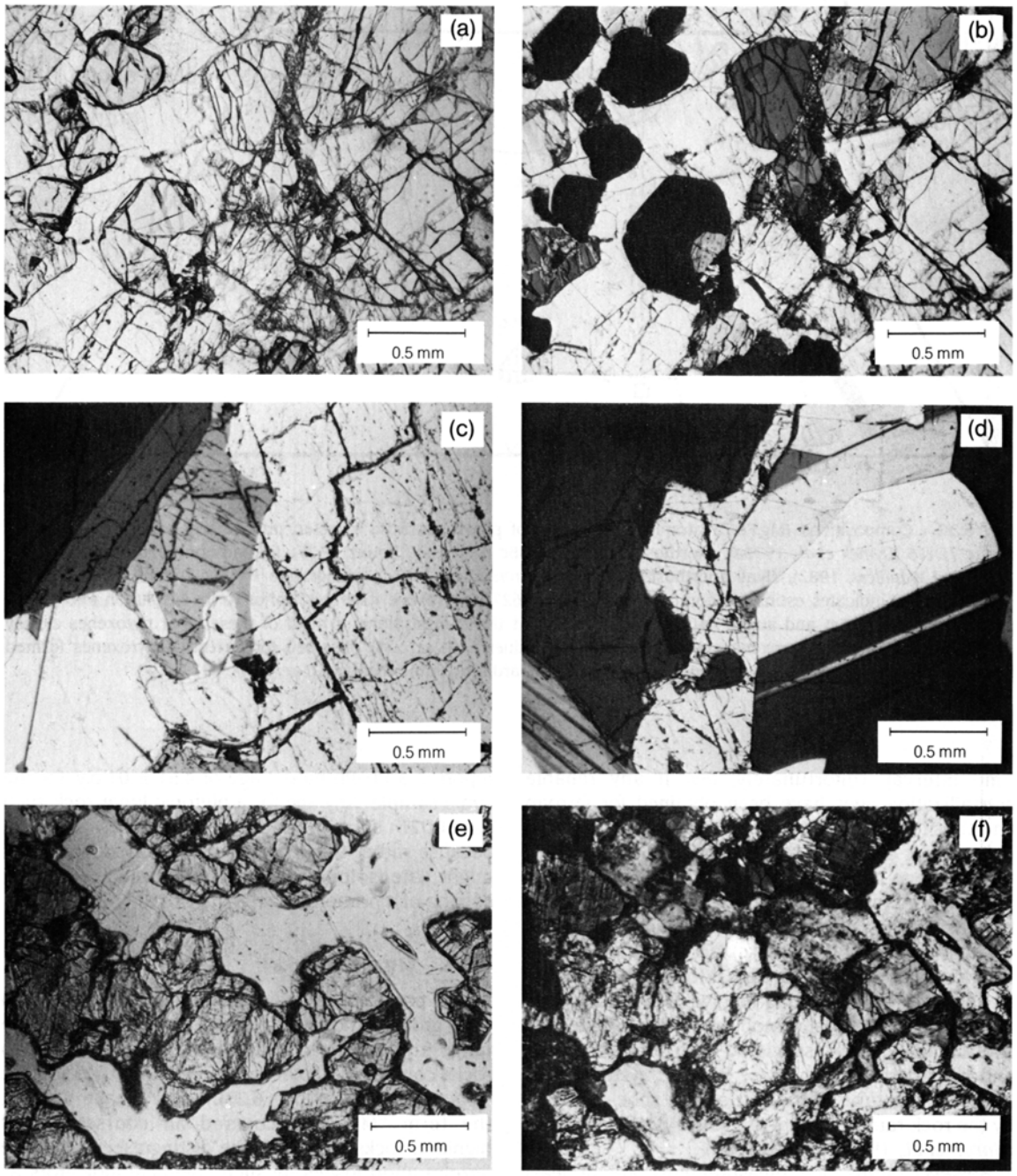

Fig. 6.33. Photomicrographs of Mg-rich pristine highland rocks: **(a)** and **(b)**, olivine-plagioclase-spinel cumulate clast from sample 67435. The plagioclase (white) is a single crystal that poikilitically encloses near-euhedral olivine (gray) and spinel (black in **(b)**). Note small crush zone that cuts diagonally across the field of view. Images **(c)** and **(d)** show troctolite 76535, composed mainly of plagioclase and olivine, which has a coarse granulitic texture. These views show some of the numerous small grains of trace minerals found in interstitial areas, which *Dymek et al* (1975a) interpret as the result of crystallization of residual trapped melt after deposition of the olivine-plagioclase cumulate. Images **(e)** and **(f)** show a gabbro fragment from sample 61224 (*Marvin and Warren,* 1980). Plagioclase (white in **(e)**) has recrystallized to feathery aggregates of tiny crystallites.

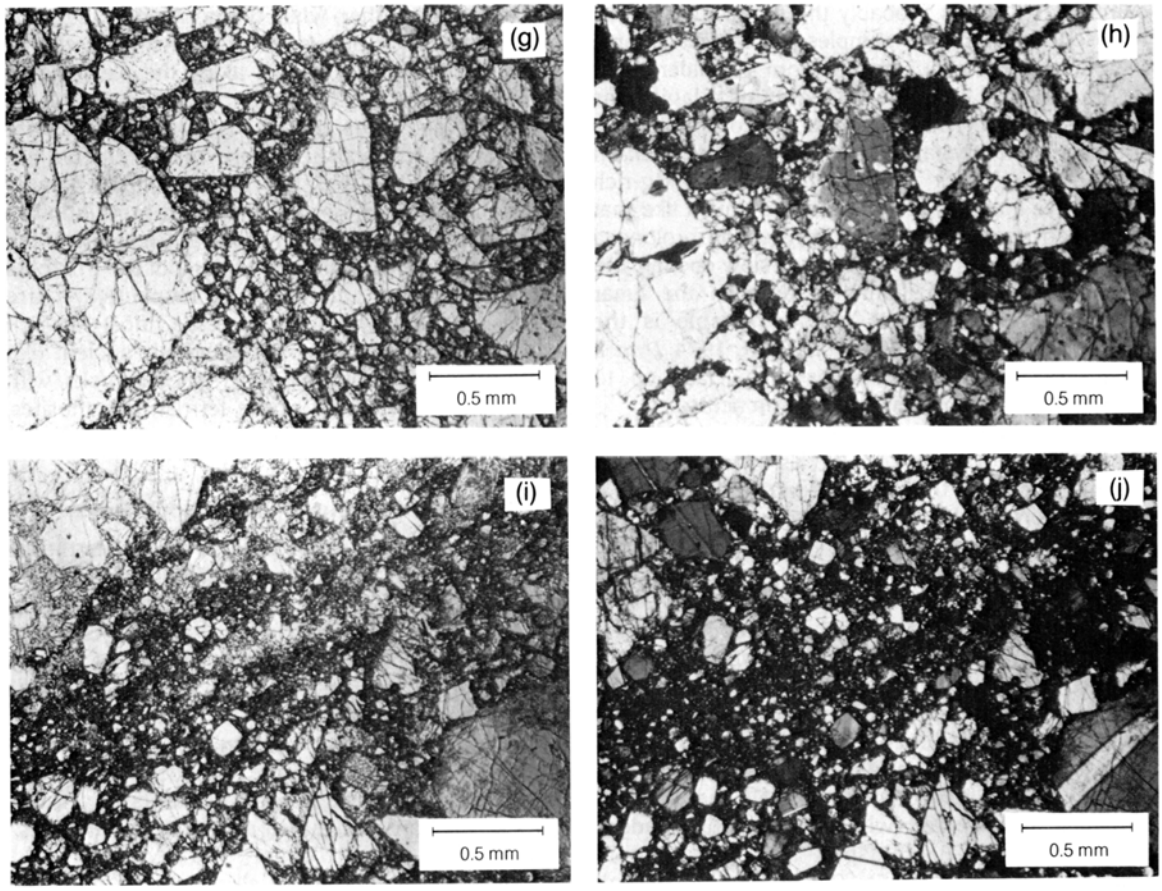

Fig. 6.33. (continued) Images **(g)** and **(h)** show the nearly monomineralic, brecciated dunite 72415, with various degrees of comminution of original extremely coarse olivine crystals. Images **(i)** and **(j)** show a clast of norite, composed of plagioclase and low-Ca pyroxene, from sample 77035, with a similarly cataclastic (crushed) texture. All pictures were taken in transmitted light. Images **(a,c,e,g,i)** are with uncrossed polarizers; images **(b,d,f,h,j)** are the same views, photographed under cross-polarized light, except for **(d)**, which shows a cross-polarized view different from **(c)**.

alkali anorthosite, and especially granite are sometimes excluded from the Mg-rich category. However, given the genetic implications sometimes attached to the term Mg-rich, and the rudimentary nature of current knowledge about highland petrogenesis, we have included both dunite and gabbronorite (which may be related) in the Mg-rich group. We consider alkali anorthosite and granite in the category of "other rock types" (section 6.3.5).

Most Mg-rich rocks are either highly magnesian *anorthositic troctolites* (plutonic rocks composed dominantly of plagioclase and olivine) or moderately magnesian *norites* (plutonic rocks composed dominantly of plagioclase and low-Ca pyroxene). The third most common type of Mg-rich rock is *gabbronorite,* which differs from norite by having much high-Ca pyroxene instead of (or in addition to) the normal low-Ca pyroxene (*lames and Flohr,* 1983). Two of the larger samples of Mg-rich rocks are *ultramafic,* i.e., composed dominantly of olivine and/or pyroxene. One, the dunite (sample 72415), is a nearly monomineralic olivine cumulate (*Dymek et al.,* 1975a). The other, a *feldspathic lherzolite* (sample 67667) (*Warren and Wasson,* 1979b; *Hansen et al.,* 1980), is rich in high-Ca pyroxene and is therefore a type of gabbronorite.

Mg-rich rocks are common at all Apollo sites where many fragments of pristine highland rocks have been found. Like the ferroan anorthosites, most Mg-rich rocks are brecciated, but those that are relatively uncrushed tend to preserve textures that strongly suggest that these rocks have also originated as igneous cumulates (Fig. 6.33). The coarsest-grained lunar rock with clear vestiges of an igneous

cumulate texture is probably the norite represented by a series of Apollo 17 samples (the largest, sample 78235, weighs 199 g) collected from a boulder about 2/3 m in size. This norite contains plagioclase crystals up to 10 mm across, accompanied by orthopyroxene crystals up to 7 mm across (*Jackson et al.,* 1975; *Dymek et al.,* 1975a). A few Mg-rich rocks have a coarse granular texture, much like that of ferroan anorthosite 15415, suggesting prolonged thermal metamorphism (or at least slow cooling and equilibration) many kilometers deep in the lunar crust (*Stewart,* 1975). A prime example is the Apollo 17 troctolite 76535 (*Gooley et al.,* 1974; *Dymek et al.,* 1975a), which contains plagioclase up to 10 mm across and olivine up to 8 mm across.

Table 6.8 shows the mineral abundances in several Mg-rich rocks. The major minerals in Mg-rich rocks are the same as those in ferroan anorthosites. A combination of plagioclase feldspar, pyroxene, and olivine usually makes up more than 99% of the rock. However, in the Mg-rich rocks, plagioclase is frequently more Na-rich, the mafic silicates are generally more magnesian and more abundant, and the Ca-poor pyroxene tends to be primary orthopyroxene rather than pigeonite. Figure 6.32 shows typical pyroxene compositions. A wider variety of trace minerals occurs in the Mg-rich rocks than in the ferroan anorthosites. Troctolite 76535 alone contains Cr-Fe spinel, Fe-Ni metal (both kamacite and taenite), whitlockite, apatite, baddeleyite (ZrO_2), K-Ba-feldspar, and "pyrochlore" [$(Na,Ca)_2(Nb,Ta)_2O_6(OH,F)$; *Dymek et al.,* 1975a]. Other accessory minerals observed in Mg-rich rocks include Mg-Al spinel (which may form up to 15% of the rock, e.g., the 67435 troctolite clast shown in Figs. 6.33a,b), ilmenite (which may form several percent of the rock), troilite, farringtonite [$Mg_3(PO_4)_2$], armalcolite, zircon, zirconolite, and silica minerals (*Prinz and Keil,* 1977; *Ryder and Norman,* 1979; *James,* 1980).

Mg-rich rocks have a greater diversity in bulk composition than do the KREEP rocks or the ferroan anorthosites (Fig. 6.27; Table A6.12). One interesting aspect of this diversity is the observation that the Mg-rich troctolitic rocks from Apollo 14, whose major-element compositions are similar to the Mg-rich troctolitic rocks collected during other missions (e.g., Apollo 17), tend to have radically higher contents of incompatible trace elements (*Warren et al.,* 1981). The scatter of compositions shown in Fig. 6.27 probably reflects the removal or concentration of different minerals that are forming from melt(s) as they undergo fractional crystallization. For example, the troctolites presumably accumulated as crystals formed from melts evolving along the boundary where plagioclase and olivine were crystallizing together, while the norites accumulated from more silica-rich melts (or possibly from the same melt at a later stage), along the plagioclase-pyroxene boundary (Fig. 6.27).

Isotopic age measurements for Mg-rich rocks are summarized in Table 6.9. These measurements are extremely difficult because of the limited sample sizes and the severe shock-produced brecciation of most samples. Often the results are equivocal; the Rb-Sr and Sm-Nd results for the age of the troctolite 76535 (4.51 b.y. and 4.26 b.y., respectively) are surprisingly discrepant. In any case, most Mg-rich rocks—including 76535—are extremely ancient (i.e., more than 4.2 b.y. old). No older igneous rocks, with the probable exception of the ferroan anorthosites, are known from either the Moon or the Earth.

6.3.5. Other Pristine Highland Rock Types

More exotic rock types, such as alkali anorthosite and granite, are rarely observed in highland samples. Despite their rarity, they are of considerable interest because they greatly extend the range of chemical composition observed in lunar rocks and require more complex theories to explain their origin. These rocks display a wide range in composition, from anorthosite to norite to granite (Fig. 6.23). Because the anorthositic and noritic varieties tend to be uncommonly enriched in alkali elements (e.g., Na, K, Rb, Cs), they are designated as "alkali anorthosites," "alkali norites," etc.

In terms of total volume, all these rock types are only minor components of the lunar crust. Alkali anorthosite and granite tend to be disproportionately abundant among the rocks returned by the Apollo 12 and 14 missions (although Apollo 12 returned few highland rocks). These two missions landed only about 180 km from one another, but over 1000 km from the next closest sampling site (Apollo 16; see Fig. 2.1). Surface spectra obtained from orbit (see section 10.2) indicate that the Apollo 12-Apollo 14 region has exceptionally high surface concentrations of incompatible trace elements (i.e., KREEP). It is therefore not surprising that these two missions yielded unusually high proportions of such "evolved" rock types as alkali anorthosite and granite. Even in this region, however, simple mixing-model calculations based on the observed compositions of returned polymict breccias indicate that alkali anorthosite and granite are only minor components of the crust. They are vastly outweighed by other rock types such as KREEP and troctolite.

Like the ferroan anorthosites, alkali anorthosites typically contain more than 85% plagioclase feldspar; the remainder is mainly pyroxene (Table 6.10). The key difference between the two types of anorthosite

TABLE 6.8. Modal mineralogy (in vol.%) of some monomict Mg-rich rocks.

	15455c	61224,6	67435c	67915c	72415	76535
Plagioclase	70	35	26	42	4	57
Olivine	—	—	69	—	93	37
Orthopyroxene	30	22	—	—	2	5
Pigeonite	—	—	—	5	—	—
High-Ca pyroxene	tr	43	—	23	1	tr
Mg-spinel	—	—	5	—	—	—
Cr,Fe-spinel	tr	tr	—	—	0.2	tr
Armalcolite	tr	—	—	—	tr	—
Ilmenite	tr	—	—	6	—	—
Rutile	tr	—	—	—	—	—
Pyrochlore	—	—	—	—	—	tr
Baddeleyite	tr	—	—	—	—	tr
Zirconolite	—	—	—	—	—	tr
FeNi metal	tr	tr	tr	tr	0.1	tr
Troilite (FeS)	tr	tr	tr	0.4	tr	tr
Unspecified SiO_2 minerals	tr	—	—	23	—	—
K-feldspar	tr	—	—	1.2	—	tr
Zircon	tr	—	—	—	—	tr
Apatite	—	—	—	—	—	tr
Whitlockite	—	—	—	—	tr	tr
Unspecified phosphates	tr	—	—	0.2	—	—

References: 15455c (norite), *Ryder and Bower* (1977), *James and Flohr* (1983); 61224,6 (gabbro), *Marvin and Warren* (1980); 67435c (spinel troctolite with obvious cumulate texture), *Prinz et al.* (1973); 67915c (sodic ferrogabbro), *G. J. Taylor et al.* (1980); 76535 (dunite), *Dymek et al.* (1975a); 76535 (troctolite), *Brown et al.* (1974), *Gooley et al.* (1974), *Dymek et al.* (1975a). For a good compilation of additional modes, see *James and Flohr* (1983).

TABLE 6.9. Sm-Nd and Rb-Sr isotopic age data (b.y.) for monomict highland rocks.

Sample	Lithology	Sm-Nd age	Rb-Sr age	Initial $^{87}Sr/^{86}Sr$
15386	KREEP basalt	3.85 ± .08	3.86 ± .04	0.70038 ± 10
Range	KREEP basalts (8)	—	3.83 - 3.93	0.6994 – 0.7006
14321c	granite	4.11 ± .20	4.00 ± .1 1	0.703 ± 8
15455c	Mg-rich norite	4.48 (?)	4.48 ± .12	0.698960 ± 30
67667	Mg-rich lherzolite	4.18 ± .07	4.18 (?)	0.699050 (?)
72255c	Mg-rich notire	no data	4.08 ± .05	0.699130 ± 70
72417	Mg-rich dunite	no data	4.45 ± .10	0.699000 ± 70
73255c	Mg-rich norite	4.23 ± .05	no data	no data
76535	Mg-rich troctolite	4.26 ± .06	4.51 ± .07	0.699000 ± 30
77215	Mg-rich norite	4.37 ± .07	4.33 ± .04	0.699010 ± 70
78236	Mg-rich norite	4.34 ± 4.43	4.29 ± .02	0.699010 ± 20
Avg.	Ferroan anorthosites (5)	4.44 ± .02	—	0.698949 ± 10*

* Least-squares-weighted mean and uncertainty of mean, based on 16 measurements for 15415, 60015, 60025, 61016c, and 64423,13,1. The listed mean does not include four values from *Nunes et al.* (1974a), which would drive it down to 0.698925 ± 10.

Data sources: *Carlson and Lugmair* (1988), *Shih et al.* (1985), and reviews by *Nyquist* (1977, 1982). The time constant for decay of ^{87}Rb is assumed to be 0.0142/b.y. (ages reported based on 0.0139/b.y. are adjusted × 0.979).

TABLE 6.10. Modal mineralogy (in vol.%) of some monomict "evolved" lithologies.

	Felsite 12033;507	Alk. A 14047c	Alk. N 14304c	Alk. A 14305c	Granite 14321c	Alk. GN 67975 c
Plagioclase	6	84	14	95	—	—
Ca-rich ternary feldspar	—	—	tr	—	—	41
Fayalitic olivine	1	—	—	—	tr	—
Orthopyroxene	—	—	*	—	—	32
Pigeonite	—	16	75*	2	—	—
High-Ca pyroxene	1	—	*	1	tr	13
Ilmenite	1	tr	—	tr	tr	1
FeNi metal	—	tr	tr	tr	tr	tr
Troilite (FeS)	tr	—	tr	tr	—	tr
Quartz	—	—	—	—	40	—
Unspecified SiO_2 minerals	33	—	tr	tr	—	11
K-feldspar	49	tr	tr	tr	60	tr
Zircon	—	—	—	—	—	0.3
Apatite	—	—	P	—	—	0.5
Whitlockite	—	—	P	2	—	tr
Unspecified Ca-phosphates	tr	—	2	—	—	—
Brownish glass	9	—	tr	—	—	—

* Pigeonite that has inverted into orthopyroxene + high-Ca pyroxene.

Abbreviations: Alk. = alkali; A = anorthosite; N = norite; GN = gabbronorite;"tr"= trace; P = present.
References: Mostly compiled by *James et al.* (1987), which is the original source for 67975c. For 12033,507, *Warren et al.* (1987).

is that the plagioclase in alkali anorthosites is Na-rich, whereas plagioclase in ferroan anorthosites is uniformly Na-poor. Alkali anorthosites also have much higher contents of K, Rb, Cs, and other incompatible trace elements such as REE than do ferroan anorthosites (Fig. 6.34; Table A6.13).

Pyroxenes in alkali anorthosites are either low-Ca (pigeonite) or high-Ca (augite), or both. They tend to be Fe-rich, similar to the pyroxenes found in recrystallized ferroan anorthosites. The pyroxene crystals usually consist of a single mineral; exsolution to form inclusions of a second pyroxene is only rarely observed and is seldom extensive. *Hubbard et al.* (1971) describe a small sample of "high-K" anorthosite (12033,85c) that contains 1% olivine (70% forsterite) and no pyroxene at all. Several samples also contain 2-3% of the phosphate mineral whitlockite (*Warren et al.*, 1983c).

The alkali anorthosites appear related to a group of more mafic (lower-plagioclase) rocks with similar mineral compositions; examples are *alkali norite* (*Goodrich et al.*, 1986) and *alkali gabbronorite* (*James et al.*, 1987). The latter rock contains plagioclase feldspar with a remarkably high K/Ca ratio (11-22% K-feldspar component within Ca-feldspar; see sections 5.1.2 and 5.1.5).

Typical mineral abundances for these rocks are listed in Table 6.10. Other minerals found in trace amounts among these alkali-rich rocks include ilmenite, zircon, apatite, K-Ba-feldspar, SiO_2 mineral(s), troilite, and Fe-metal.

By far the largest sample of an alkali-suite rock is a 1.6-g clast from breccia 14047; it contains 84% plagioclase and 16% pyroxene (*Warren et al.*, 1983a). The microscopic textures in this sample and in other samples of alkali lithologies typically reflect severe shock and/or thermal metamorphism (Fig. 6.35). The most "pristine" (or unaltered) texture observed among alkali lithologies is that of a small clast from breccia 12073 (*Warren et al.*, 1981); this texture resembles—and could easily be mistaken for—the monomict-breccia texture of a typical ferroan anorthosite (Fig. 6.30). Considering the small fragment sizes of the alkali rocks, it is conceivable that all of them are poorly representative and highly selective samples from a group of closely similar rocks with plagioclase contents of roughly 70-80%.

Lunar granites, and their finer-grained equivalents known as *felsites*, are much richer in K-feldspar and SiO_2 minerals than are other lunar rocks. Rocks intermediate in composition between granites and the anorthosite-norite-troctolite-gabbro group (e.g.,

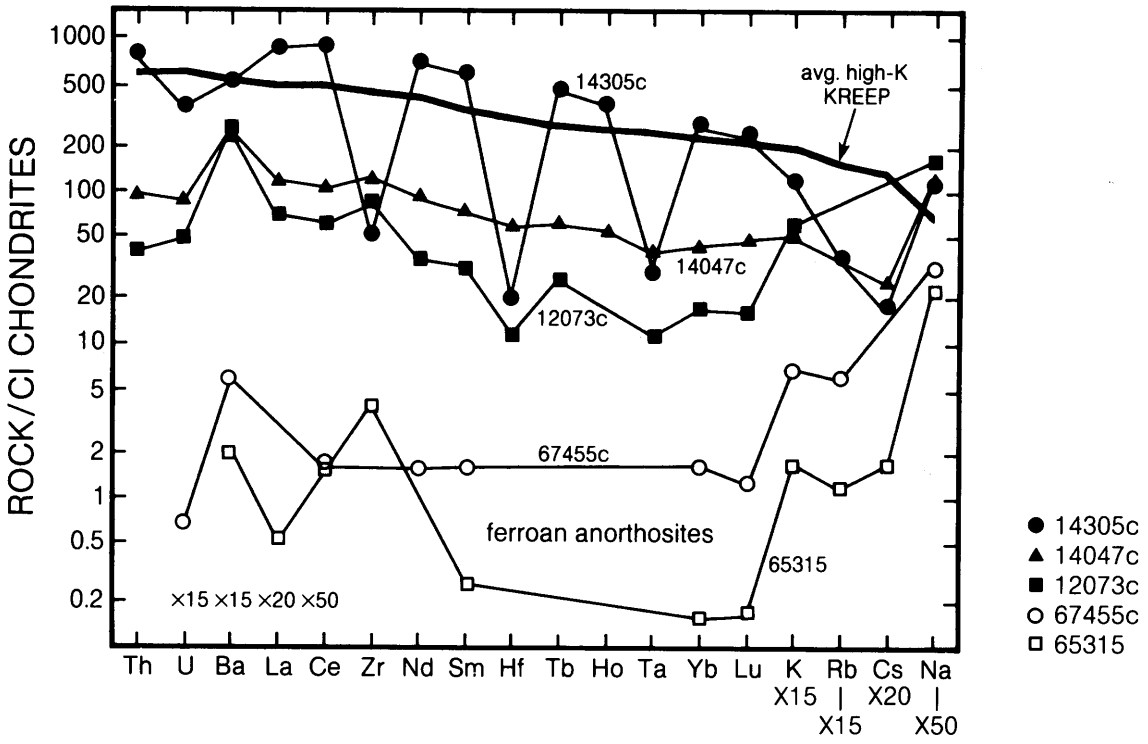

Fig. 6.34. Plots of incompatible-element contents in monomict alkali and ferroan anorthosite breccias. Element abundances are normalized to CI chondrite meteorites (*Anders and Ebihara,* 1982). Alkali anorthosites (filled symbols) have higher incompatible-element abundances than ferroan anorthosites (open symbols). Alkali anorthosite data: 12073c and 14047c from Table A6.13; 14305c from *Warren et al.* (1983c). Data for the two ferroan anorthosites (open symbols) are from Table A6.11 and encompass, at least for the REE, virtually the entire range of compositions observed among ferroan anorthosites. A lower-case "c" after the sample number indicates that a clast from within the sample was separated and analyzed.

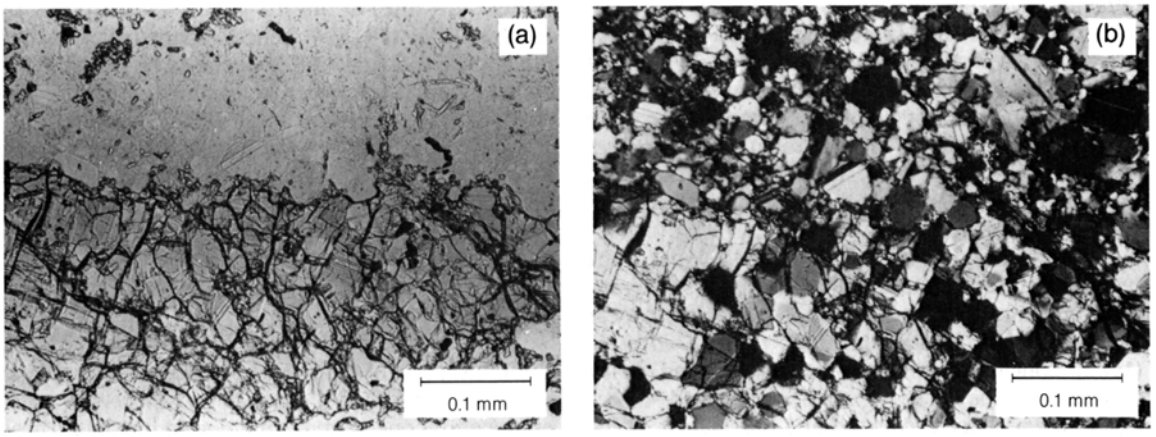

Fig. 6.35. Photomicrographs of alkali anorthosite 14047c. **(a)** The top half of this view shows an area typical of this sample; the bottom half shows the shattered, recrystallized remains of a single former large low-Ca pyroxene crystal (transmitted light). **(b)** Same view under cross-polarized transmitted light, showing the slightly granulitic texture and variable orientation of fragments of the shattered pyroxene.

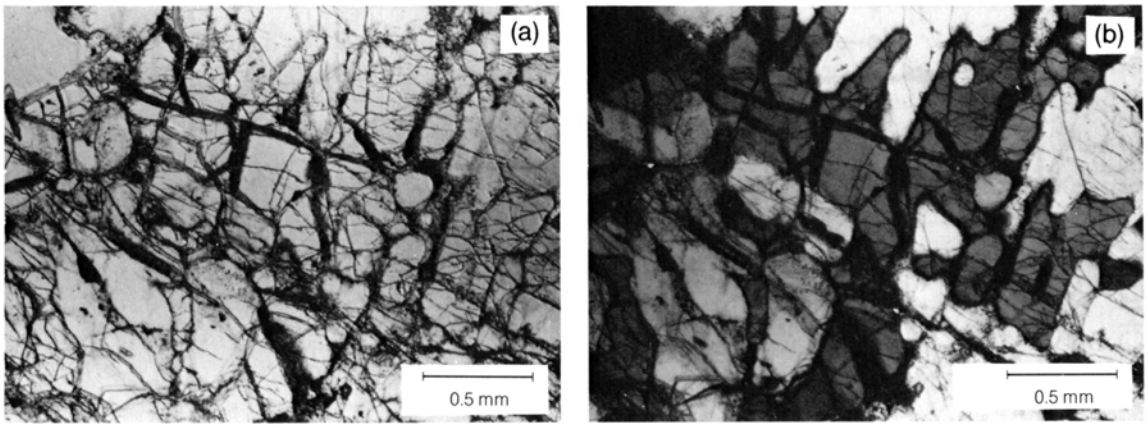

Fig. 6.36. Photomicrographs of an unusually well-preserved area of the brecciated "large" (1.8 g) granite clast from sample 14321. **(a)** "Graphic" intergrowth of quartz (dark grey) and K-feldspar (light grey and white; transmitted light). **(b)** Same view in transmitted light with crossed polarizers.

such terrestrial rocks as diorite, andesite, syenite, tonalite, etc.) are virtually unknown from the Moon. One possible intermediate variety, the "quartz monzodiorite," observed only as clasts in breccia 15405, seems to be a coarse-grained variety of KREEP (see above).

Mineral compositions for typical granites and felsites are shown in Table 6.10. The granites, and even the finer-grained felsites, typically consist mostly of graphic intergrowths of K-feldspar and a silica phase (*Shervais et al.,* 1983). The largest granite, a 1.8-g clast from breccia 14321 (*Warren et al.,* 1983b) is a typical example (Fig. 6.36). The mafic minerals (pyroxenes or olivine) are simply more Fe-rich members of the same types found in the Mg-rich rocks. As in all lunar rocks, and in sharp contrast to terrestrial granites, lunar granites have no hydrous minerals (e.g., mica or amphibole). The felsites often consist largely of thin veins of brownish glass (*James and Hammarstrom,* 1977; *Nord and James,* 1978; *Warren et al.,* 1987). Typical bulk chemical compositions are listed in Table A6.13.

The ultimate origins of these odd lunar rock types—alkali anorthosites, alkali norites, and granites—are still poorly understood. The granites appear to be young for pristine highland rocks. *Shih et al.* (1985) concluded from Rb-Sr, Sm-Nd, and Ar-Ar studies that the 14321 granite crystallized 4.1 b.y. ago and was later excavated and brecciated 3.9 b.y. ago. Most other granites and felsites are either too small to analyze or not pristine (e.g., the felsite component of the 82-g polymict breccia 12013). However, Rb-Sr measurements on a relatively undisturbed felsite clast from breccia 73215 indicate that 4.05 b.y. is a reasonable upper limit for its age (*Compston et al.,* 1977).

The granites and felsites are suspected to be the results of two processes: fractional crystallization accompanied by liquid immiscibility. If so, they could have formed as minor, late-stage components in subsurface igneous bodies that were producing larger volumes of more mafic rocks, i.e., Mg-rich rocks (*Shih et al.,* 1985; *Warren et al.,* 1987). No isotopic age measurements have yet been obtained on samples of the "alkali" lithologies, except for the high bulk-rock $^{87}Sr/^{86}Sr$ ratio (0.69963 ± 10) deter-mined for one Apollo 12 alkali anorthosite by *Hubbard et al.* (1971). A genetic connection between the alkali rocks and KREEP seems firmly established by their similar trace-element patterns (e.g., *Hubbard et al.,* 1971; *Warren et al.,* 1983a; *Shervais et al.,* 1984b; *James et al.,* 1987), as well as by geographic association. One of the original names for alkali anorthosite (*Hubbard et al.,* 1971) was, in fact, "KREEP anorthosite."

6.4. HIGHLAND POLYMICT BRECCIAS

All but a few of the samples collected in the lunar highlands are *polymict breccias* or *impact-melt rocks* produced by one or more meteoroid impacts. These rocks are mixtures of materials derived from different locations and different kinds of lunar bedrock. They contain varying proportions of two components: (1) broken or *clastic* rock fragments

(*clasts*), and (2) material melted by meteoroid impacts (*impact melt*). The latter material may occur in a range of forms from completely glassy to completely crystalline rocks. *Polymict breccias* consist chiefly of older rock fragments. *Impact-melt rocks* consist chiefly of the products of impact-produced melting, both glassy and crystalline.

The constituents of both fragmental polymict breccias and impact-melt rocks are derived from preexisting highland igneous rocks, plus a little meteoroid debris. However, the multiple impacts to which these components have been subjected have destroyed much of the direct evidence for what these precursors were, and all that remains are small rock fragments, mineral fragments, or molten mixtures. Some of the individual fragments in breccia samples are themselves fragments of older breccias and impact-produced melt rocks. Age determinations for these rocks can be very complex, and are discussed separately for each type of polymict breccia described in this section. [Note that all radiometric ages described in this section have been recalculated using the following decay constants: (^{87}Rb) = 1.42×10^{-11}/yr; (^{40}K) = $(0.581 + 4.962) \times 10^{-10}$/yr.]

As with all lunar samples, in no case do we have any polymict samples collected directly from bedrock. Many specimens of polymict rocks were collected as isolated samples from the lunar surface, and therefore nothing is known directly about their parent units. Other samples were chipped from displaced boulders of polymict breccia, where at least some local stratigraphic context is available from astronaut observations and photographs.

Polymict rocks show a wide diversity of textures, grain sizes, and chemical compositions. These features reflect the original nature and history of the individual components, the effects of the last impact that assembled the components, and the results of such subsequent processes as *lithification* (conversion of loose material into solid rock) and metamorphism (recrystallization). Lithification can result from the same impact that assembled the fragments if enough interstitial molten material is included, or by the application of heat and pressure at some later time. In many cases, lithification is so weak that the sample is very friable and falls to pieces with little handling.

Breccias consist of two textural components: (1) the *clasts* (individual fragments) and (2) the *matrix* that contains them. Clasts may be a wide variety of materials: fragments of igneous rocks or older breccias, or the shock-metamorphosed or melted derivatives of either. Generally, but not always, the clasts are internally at least as consolidated as the matrix and often more so.

The matrix material forms the host for the fragments and is finer grained. Three kinds of matrix are distinguished: solidified *melt* (crystalline or glassy), *clastic* (fragmental), or *a metamorphosed* clastic/melt mixture. A melt matrix consists of material that is entirely distinct from the clasts, although it may have formed in the same impact. Clastic and metamorphosed matrices are arbitrarily defined on the basis of grain size (usually as having grain sizes less than 25 μm). Breccias with these matrices generally have a wide range of fragment sizes, and the matrix fragments have populations and histories similar to those of the larger clasts.

A single large meteoroid impact can produce a variety of polymict rocks that range from totally molten and crystalline materials to masses of unconsolidated fragments. These materials may then be reworked by later impacts and incorporated into new breccias, many of which are therefore polygenetic. It is therefore almost impossible to trace a breccia sample, or one of its fragments, to a particular impact or a specific parent crater. The exceptions are some samples collected from rather small craters, e.g., glass-lined craters at the Apollo 15 landing site.

6.4.1. Nomenclature and Classification

At the time of the Apollo missions, little work had been done on terrestrial impact craters, so a ready-made and generally accepted classification for impact-produced polymict rocks did not exist. As a result, the nomenclature for lunar polymict rocks, most of which are fragmental or crystalline breccias, was built up rapidly during the Apollo missions on a piecemeal basis, without benefit of much prepublication discussion between different workers. Consequently the nomenclature and classification of lunar polymict rocks is confusing, duplicative (many different names are applied by different workers to the same samples) and often irrational (many terms are neither inclusive nor exclusive). Furthermore, the nomenclature changed as genetic interpretations developed and were modified. At first, there was a general impression that ejecta blankets were deposited hot, which gave rise to the incorrect belief that many crystalline samples were metamorphosed because of contact with, or burial in, layers of hot ejecta. Hence, the term "recrystallized breccia" was originally applied to rocks we now consider to have been formed instead by the crystallization of impact melts produced in a single impact event.

Stöffler et al. (1980) attempted to produce a more consistent, unified classification and nomenclature for lunar highland rocks, including polymict rocks, incorporating the recommendations of a Nomenclature Committee established by the Lunar and

TABLE 6.11. Classification, characteristics, and examples of highland polymict breccias (adapted from *Stöffler et al.*, 1980).

Class	Main Characteristics	Examples
Fragmental breccia	Angular clasts in a porous, clastic matrix of rock, mineral, and rare glass debris. Some melt clasts may be cogenetic with assembly (suevite). Most are friable.	14063, 67015, 67455
Glassy melt breccia and impact glass	Coherent glassy or devitrified glass matrix with (melt breccia) or without (impact glass) clasts.	60115, 68815, 60095, 79175
Crystalline melt breccia (impact melt breccia)	Rock or mineral clasts or both in an igneous (extrusive)-textured matrix (ophitic, subophitic, poikilitic, dendritic, etc.). May be fine- or coarse-grained, and clast-rich to clast-poor.	15455, 62295, 76015
Clast-poor impact melt	Igneous (extrusive)-textured rocks but containing meteoritic siderophile contamination. Textures can be slightly more heterogeneous than igneous rocks, and rare clasts may be present. Compositions can be unlike possible igneous-generated ones.	14310, 68415
Granulitic breccia and granulite	Rock or mineral clasts or both in an equilibrated, granoblastic to poikiloblastic matrix. Clasts may not be obvious, and poikilitic textures may mimic (or even be) siderophile contamination.	79215, 77017, 67955, 78155
Dimict breccia	Veined texture of intrusive dark fine-grained crystalline melt breccia with coarser-grained light-colored breccia consisting of plutonic or metamorphic fragments or both. In some cases the dark-light relationship is mutually intrusive.	61015, 62255, 64475
Regolith (soil) breccia	Lithified regolith. Regolith fragments including impact glass and volcanic debris with a glassy matrix. Commonly retain some solar wind gases through lithification process.	14318, 15299, 60019, ALHA 81005

Planetary Sample Team. These recommendations have been widely adopted, and their classification for polymict rocks is used here with slight modifications (Table 6.11). Table 6.12 is a list of the many previous names used (also adapted from *Stöffler et al.*, 1980).

The present classification leans heavily on more recent information from terrestrial impact craters; individual terms are based largely on observed textures and other objective features rather than on genetic or other interpretations. Additional characteristics (composition, detailed texture, grain size, visible shock effects) can be used as modifiers. While this system is a major improvement over the original state of affairs, it still represents a compromise between purely nongenetic and commonly used genetic terms, and it is therefore not entirely inclusive or exclusive.

The composite (and often reworked) nature of polymict lunar rocks makes their classification to some extent dependent upon the size of a sample. For instance, small samples of a fragmental breccia might consist of individual pieces of metamorphosed crystalline rock, impact melt rock, or plutonic igneous rock. Several representative breccia samples are shown in hand-sample (macroscopic) photographs (Fig. 6.37) and in thin-section (microscopic) photographs (Fig. 6.38).

This descriptive classification is not entirely independent of the genesis of a sample. In particular, a distinction is made between the mechanical *assembly* of the components of a breccia and their *lithification* into coherent rocks. These processes may or may not take place in a single impact event. Figure 6.39, adapted from a concept of *Simonds et al.* (1976), shows the relationships for those breccias in which the same impact event produces both assembly and lithification. In these breccias, lithification is promoted mainly by the large amount of melt produced by shock-heating during impact. Such a breccia is a mixture of impact-produced melt (hot) and clastic material (cooler). When mixed, these materials thermally equilibrate in a short time (less

TABLE 6.12. Some of the more common previous names for polymict rocks (much simplified after *Stöffler et al.*, 1980).

Present Class	Previous Names	References
Fragmental breccia	Light matrix breccia (LMB)	*J. Warner et al.* (1973)
	Feldspathic breccia	*Chao et al.* (1972a)
	Clastic breccia	*Stöffler et al.* (1979)
Glassy melt breccia	Agglutinate	*Vaniman et al.* (1976)
	Glassy breccia	*R. Warner et al.* (1976c)
	Vitric matrix breccia	*Stöffler et al.* (1979)
Crystalline melt breccia	Annealed Fra Mauro breccia	*Chao et al.* (1972a)
	Metamorphosed breccia	*J. Warner et al.* (1973)
	Recrystallized noritic breccia	*Vaniman et al.* (1976)
	Crystalline matrix breccia	*Phinney et al.* (1977)
	Thermally metamorphosed breccia	*James* (1977)
	Pyroxene poikiloblastic breccia	*Delano et al.* (1973)
Clast-poor impact melt	High-alumina basalt	*Kushiro et al.* (1972)
	Fra Mauro basalt	*Ridley et al.* (1972)
	Basaltic impact melt	*Ryder and Norman* (1980)
Granulitic breccia	Polymict metamorphic breccia	*Stöffler et al.* (1974)
	Granulitic impactite	*J. Warner et al.* (1977)
	Recrystallized ANT rocks	*R. Warner et al.* (1978a)
Dimict breccia	Partially molten breccia	*LSPET* (1973a)
	Black and white rock	*J. Warner et al.* (1973)
	Dike breccia	*Stöffler et al.* (1979)
Regolith breccia	Dark matrix breccia (DMB)	*Wilshire and Jackson* (1972)
	Vitric matrix breccia	*Stöffler et al.* (1974)
	Soil breccia	*R. Warner et al.* (1978a)

than 100 sec; *Onorato et al.*, 1976) and then cool more slowly and uniformly. The equilibrium temperature produced after mixing is largely a function of the melt/clast ratio; breccias with more hot melt than cold clasts have higher equilibrium temperatures. The value of this temperature determines the amount of recrystallization that will occur during the subsequent slow cooling; it has a dominant effect on the overall texture and therefore on classification. As discussed below, regolith breccias and granulitic breccias, for which assembly and lithification are separate and distinct events, do not plot on the diagram. *Dimict breccias* (with two distinct components) might be considered a special case of impact-melt breccias.

Craters in the lunar highlands are formed in target rocks that have previously been multiply impacted, reworked, and mixed together. The relationship between sample type and impact-crater features is sketched in Fig. 6.40. Multiple impacts cause the highland polymict rocks produced by the later impacts to contain rocks and chemical components derived from a broad spectrum of lunar surface materials. This feature is illustrated by the comparative rare earth element concentration diagrams in Fig. 6.41. There is a wide and overlapping range of chemical compositions between fragmental breccias, glassy breccias, and melt rocks.

6.4.2. Fragmental Breccias

Polymict fragmental or *clastic* breccias are almost entirely composed of discrete fragments. Some monomict breccias are also fragmental (see section 6.3). Many specimens are porous and tend to fall apart very easily. Fragmental breccias consist of a variety of angular fragments of rocks or single mineral crystals embedded in a matrix of finely-comminuted similar materials (Fig. 6.37a). The individual fragments are bonded together only at limited points of contact, probably by a very thin layer of glass (*Nord et al.*, 1975). Deformation during lithification of these breccias has been minor; such

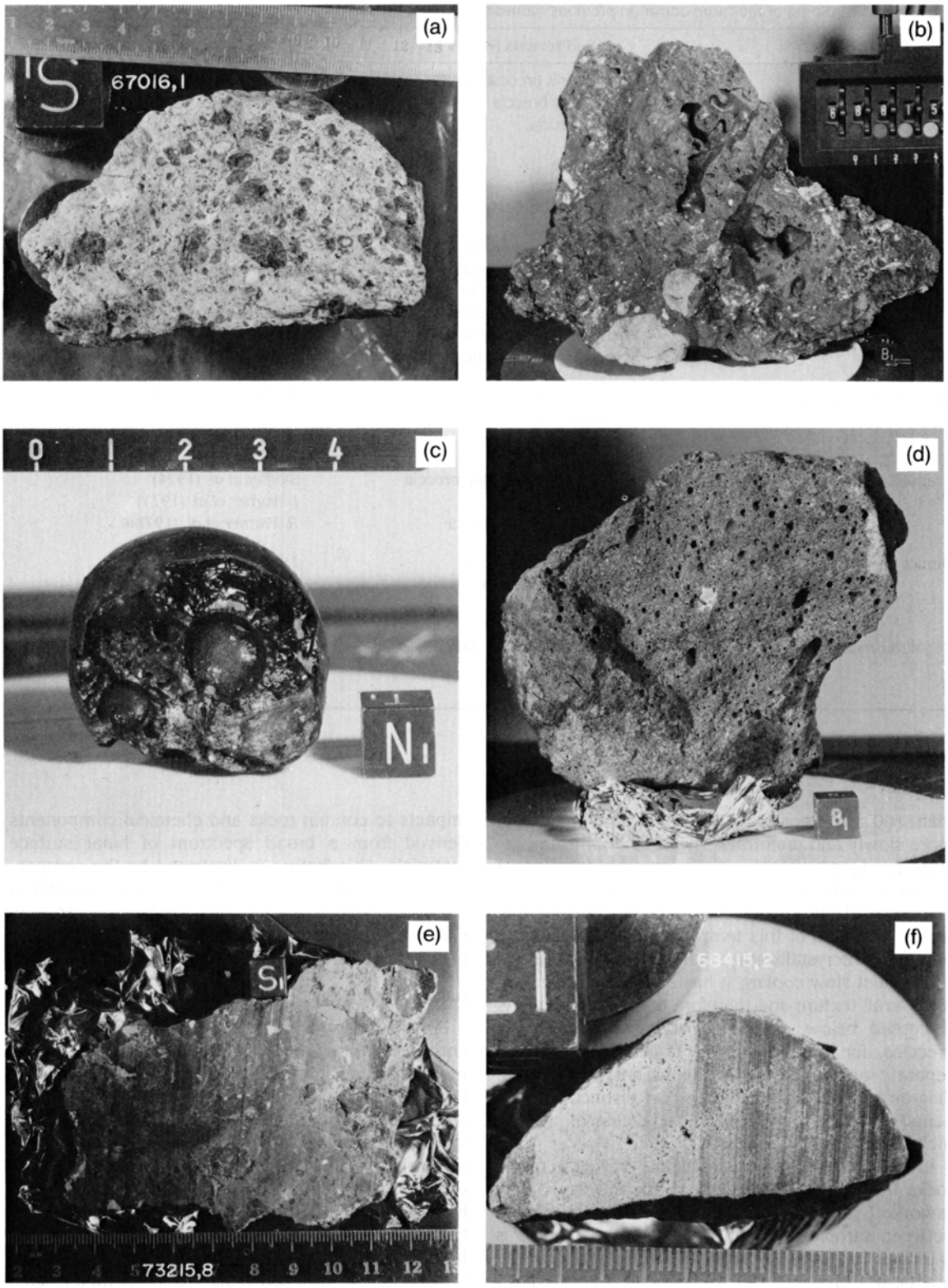
(a)
67016,1
(b)
(c)
N1
(d)
B1
(e)
S1
73215,8
(f)
68415,2

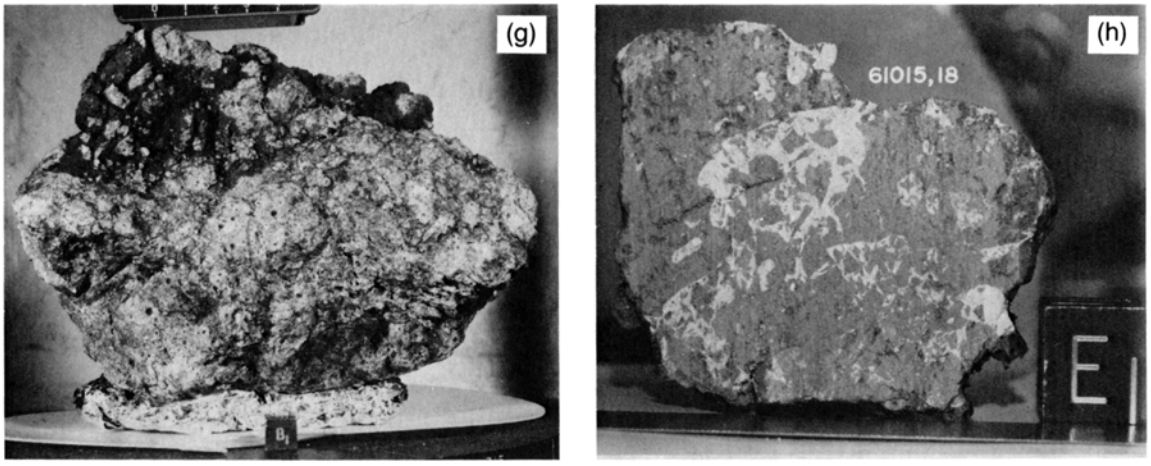

Fig. 6.37. Macroscopic views of lunar polymict breccias, showing the range of textures in this group of rocks. **(a)** Fragmental breccia 67016, sawn face, showing dark and light clasts in a finer fragmental matrix. Cube is 2 cm (NASA Photo S-75-32783). **(b)** Irregular glassy breccia 68815, broken face, showing clasts and irregular gas channels. Cube is 1 cm (NASA Photo S-72-37155). **(c)** Glass sphere 60095, showing broken surface and internal gas-produced vesicles. Cube is 1 cm (NASA Photo S-72-39424). **(d)** Crystalline melt breccia 77135, broken surface, showing numerous gas-produced vesicles and a lack of large conspicuous clasts. Cube is 1 cm (NASA Photo S-72-56391). **(e)** Fine-grained, schlieren-rich crystalline melt breccia 73215. Cube is 1 cm (NASA Photo S-73-38455). **(f)** Clast-free impact melt 68415, sawn surface showing a lack of prominent clasts but containing numerous very small vesicles. Slab is about 5 cm long (NASA Photo S-75-32778). **(g)** Granulitic (poikiloblastic) breccia 77017, showing adhering and intruding dark glass. Cube is 1 cm (NASA Photo S-73-17772). **(h)** Dimict breccia 61015, sawn face, showing mutually intrusive relationships of dark fine-grained melt and white cataclastic anorthosite. Slab is about 3.5 cm wide (NASA Photo S-75-20878).

delicate features as *deformation twins* (twin-crystal structures produced by pressure) are frequently preserved. The matrices, and many individual clasts, are contaminated with meteoritic siderophile elements (see section 6.3).

By definition, fragmental breccias do not preserve any physical features normally associated with the near-surface lunar regolith (see Chapter 7). Such features as glass-mineral agglutinate particles, glass spheres, or solar-flare tracks (e.g., *MacDougall et al.,* 1973) are absent.

Most known fragmental breccias were collected at the Apollo 16 landing site, but some prominent examples were collected from the Apollo 14 and Apollo 17 sites as well. The Apollo 16 fragmental breccias are highly enriched in plagioclase feldspar and, as a result, they contain more than 30% Al_2O_3. Nearly all the specimens were collected from the rim of North Ray Crater, and they are probably derived from a subsurface unit in the North Ray area. Some samples were chipped from boulders of essentially similar rock. At the Apollo 14 site, a few fragmental breccias collected from the rim of Cone Crater are less feldspathic. At the Apollo 17 site, a fragmental breccia makes up the matrix of Boulder 1 at Station 2. It therefore seems likely that a large part of the upper highland crust consists of deposits of fragmental breccia, which vary in composition between different regions.

Petrography and chemistry of fragmental breccias. Fragmental breccias consist of clasts of a variety of materials—other breccias, igneous rocks, and single mineral grains (Figs. 6.37a and 6.38a,b). Glass is present in some specimens, but most are glass-poor. The clasts are generally angular; they range in size from submicroscopic to several centimeters across, and they have varying intensities of shock metamorphism. *Stöffler et al.* (1980) distinguished two subclasses of fragmental breccias, according to the presence or absence of glassy melt particles with the same composition as the bulk rock, which were presumed to have been generated in the same impact that formed the breccia. This distinction has not often been attempted; *Norman*

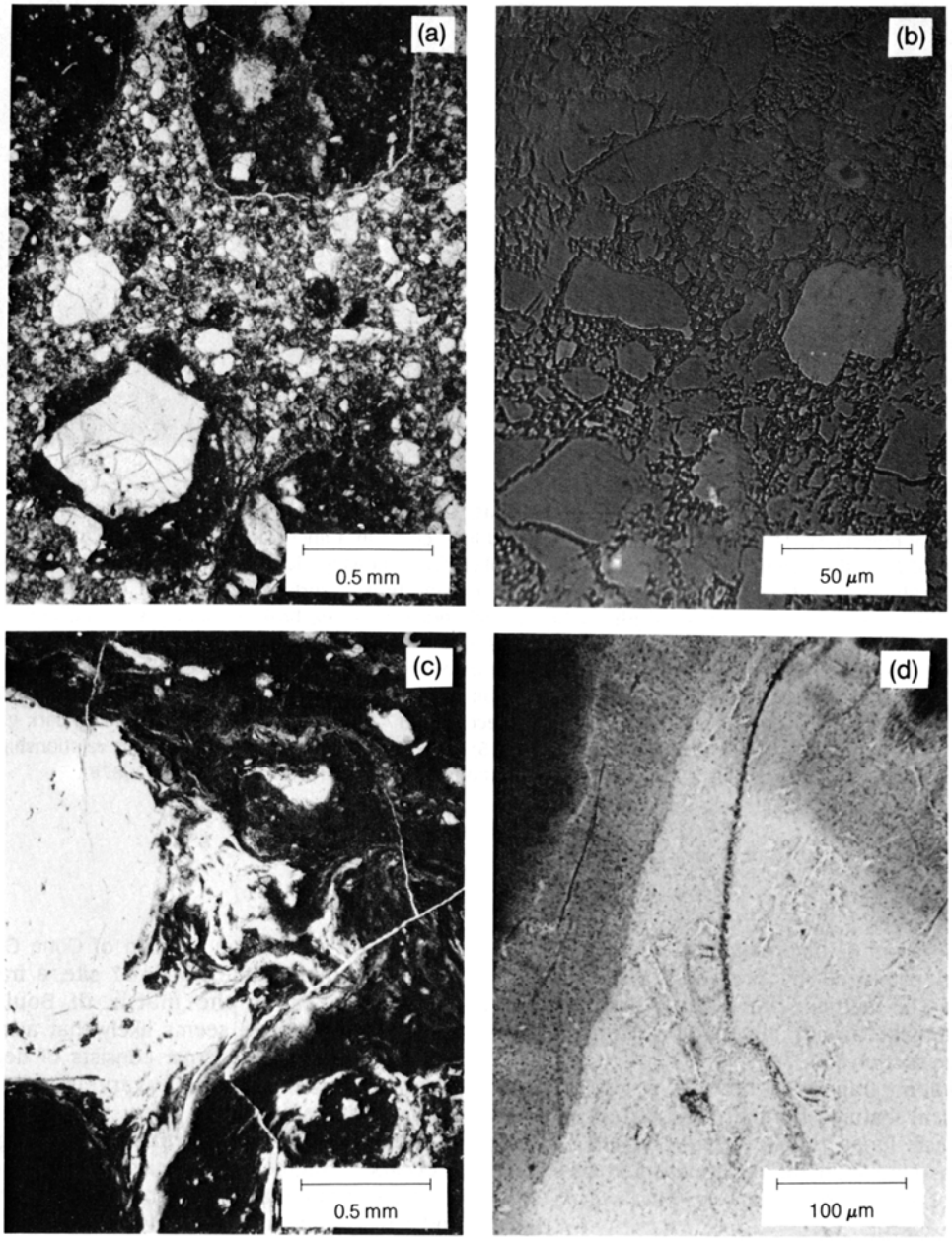

Fig. 6.38. Photomicrographs of lunar polymict breccias, showing the rarige of microscopic textures developed in this group of rocks. **(a)** Fragmental breccia 67016 in transmitted, plane-polarized light, showing dark melt clasts and mineral fragments. **(b)** Fragmental breccia 67016, the same sample as in **(a)**, photographed in reflected light, showing the fragmental and porous nature of the matrix, which is mainly plagioclase fragments (dark gray) with less abundant mafic grains (pyroxene and olivine, lighter gray). **(c)** Glassy breccia 68815 in transmitted, plane-polarized light, showing the irregular swirled texture produced by flow structure in the glass and occasional clasts. Clear glass is clast-free and undevitrified; dark areas of glass are clast-rich, and the glass is at least partly devitrified or crystallized. **(d)** Glassy crystallization front in breccia 66095 in transmitted, plane-polarized light. Clear areas are undevitrified glass; darkest areas are massive, spherulitic, devitrified glass. The intermediate zone shows a fibrous texture with crystals perpendicular to the contacts.

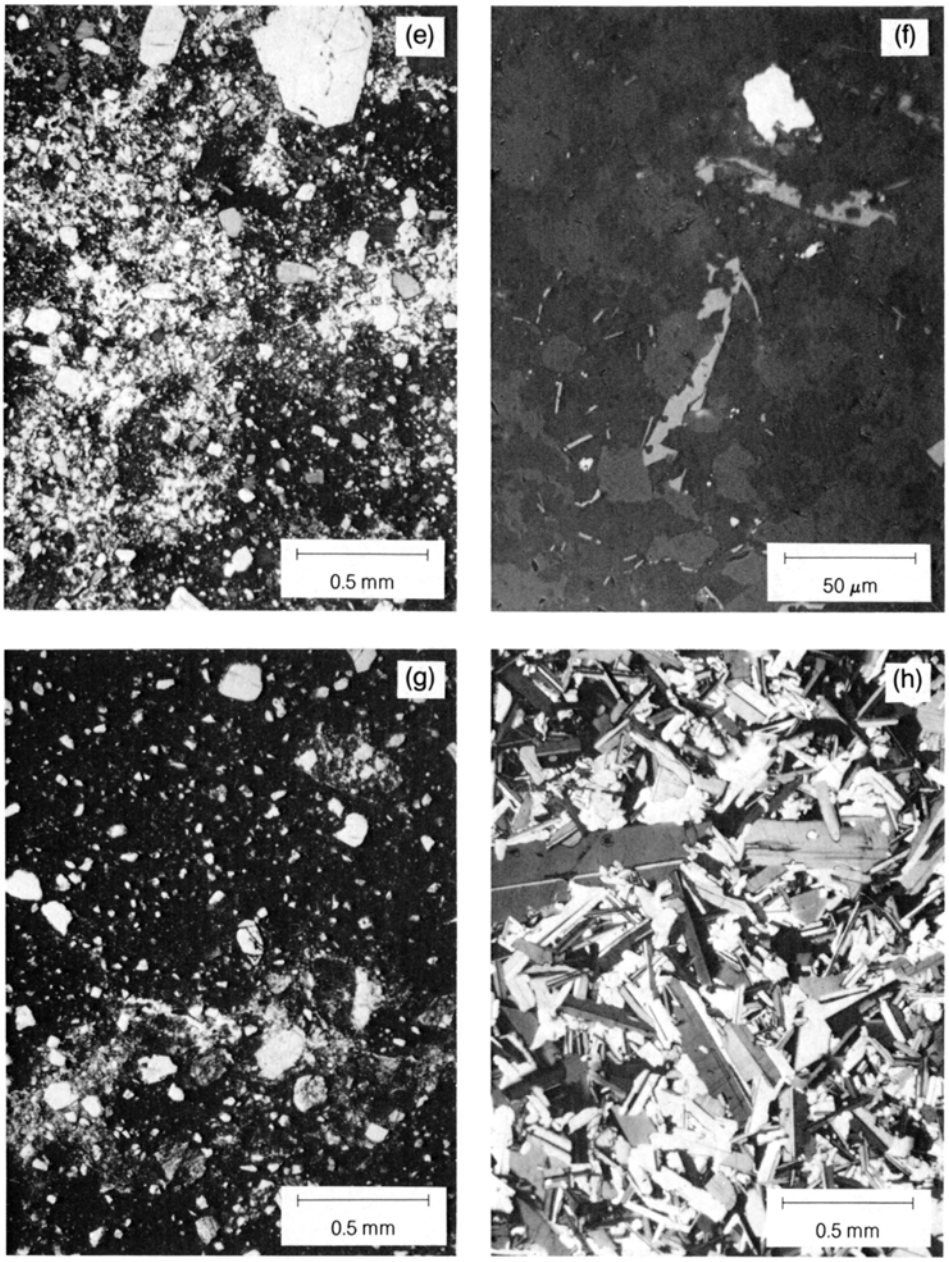

Fig. 6.38. (continued) **(e)** Poikilitic crystalline melt breccia (impact melt) 65015 in transmitted light with crossed polarizers. Distinct small clasts, mainly plagioclase, are common. Millimeter-sized zones of constant color (white, gray, black) are large pyroxene crystals (oikocrysts) in which numerous smaller crystals are embedded. **(f)** Intergranular area (*mesostasis*) of poikilitic melt particle 15423,40 in reflected light, showing late-stage crystallization products. Tiny very dark gray areas (mainly triangular) are interstitial residual silicic glass; dark gray is plagioclase; medium gray is pyroxene; tiny to moderate-sized very pale gray crystals are ilmenite; white bleb near top is Fe-Ni metal. **(g)** Very fine-grained (*aphanitic*) impact melt 73215 in transmitted, plane-polarized light. Flow lines of heterogeneous glass (*schlieren*) occur lower in the photo, and rounded mineral clasts are common. Individual groundmass crystals are too small to be distinguished at this scale, and the groundmass therefore appears massive and dark. **(h)** Crystalline (subophitic/ophitic) clast-poor impact melt 68415 in transmitted light with crossed polarizers. Lath-shaped (striped) crystals are plagioclase; the most abundant interstitial mineral is olivine.

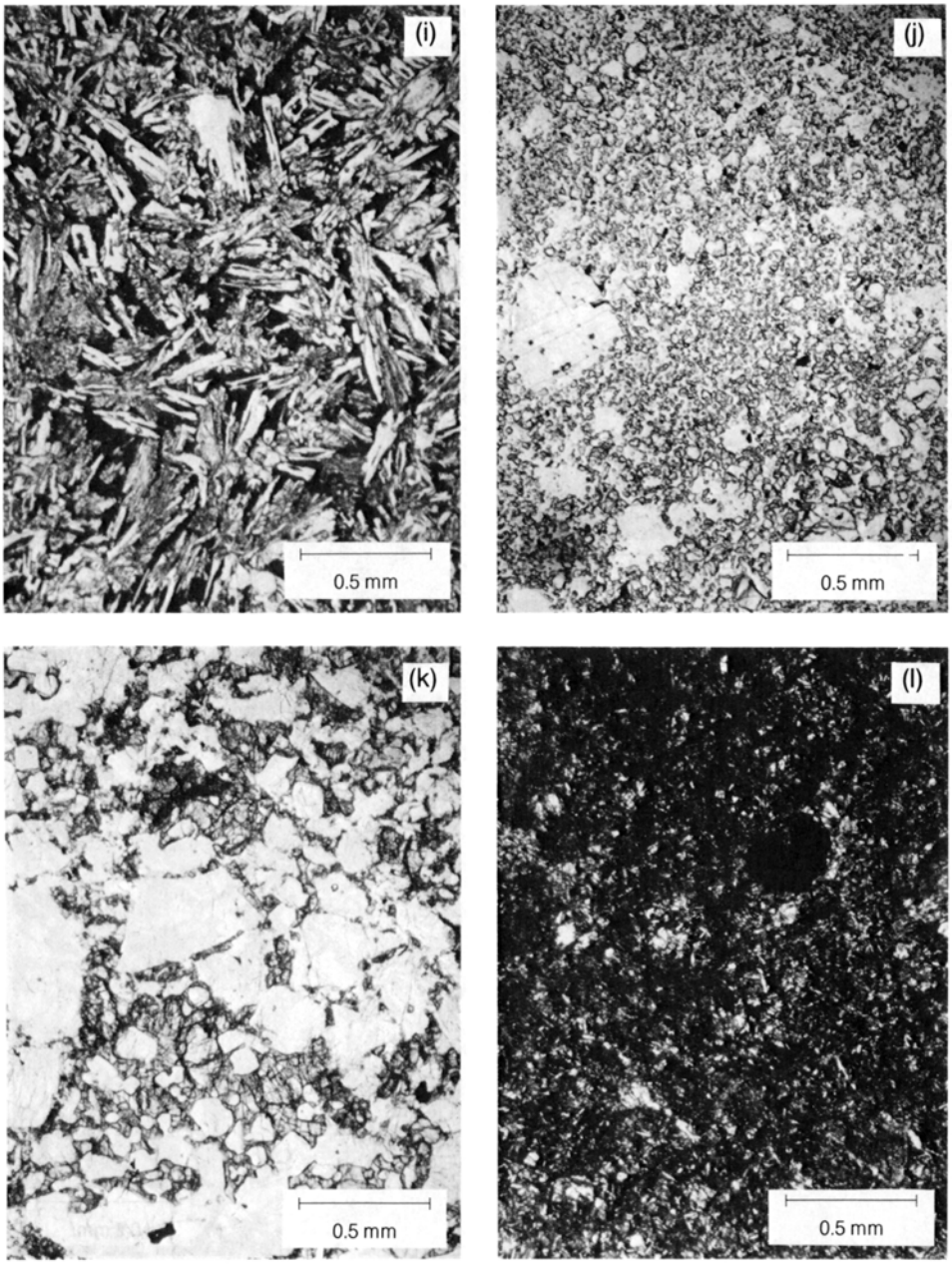

Fig. 6.38. (continued) **(i)** Crystals in glass (*vitrophyre*)*:* Clast-poor impact melt 62295 in transmitted, plane-polarized light. Skeletal (hollow) olivine crystals are embedded in a glassy groundmass (black). Clasts are very rare. **(j)** Recrystallized (*granulitic*) breccia 79215 in transmitted, plane-polarized light. Sample is a fine-grained variety. The tiny grains are mainly olivine and pyroxene, and the bulk of the sample (including most of the obvious mineral clasts) is made up of plagioclase. **(k)** Recrystallized (*granulitic*) breccia 77017 in transmitted, plane-polarized light. The texture formed by small stubby plagioclase crystals (white) embedded in larger pyroxene crystals (gray) is *poikiloblastic.* More than one episode of brecciation can be recognized in this specimen. **(l)** Melt-rich component (dark-colored) of dimict breccia 61015 in transmitted, plane-polarized light. Melt is very fine-grained (tiny plagioclase laths are visible) and glassy (dark groundmass), and contains some vesicles. Clasts are visible in this view, but they make up only a small proportion of the rock.

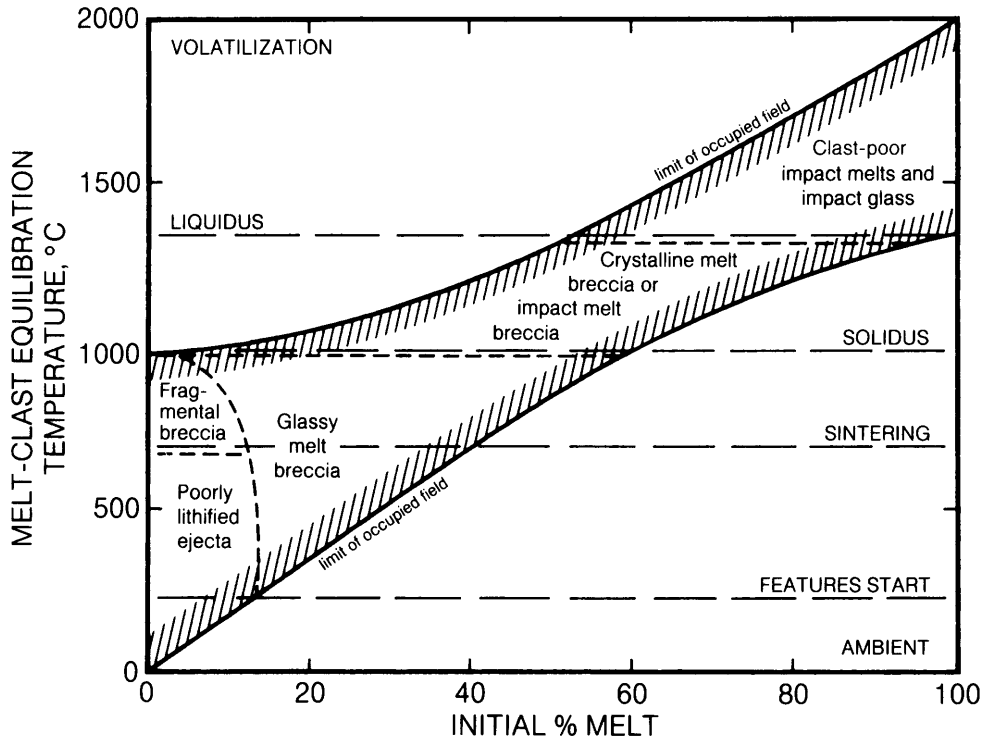

Fig. 6.39. Generalized scheme showing the relations between petrographically distinct impact breccias produced and lithified in a single impact event as a function of the amount of melt originally present and the equilibrium temperature attained between clasts and melt (figure modified from *Simonds et al.,* 1976). The textures of resulting breccias are assumed to be controlled by the initial process of rapid thermal equilibration between clasts and the enclosing melt. Subsequent cooling rates will have some, but much less, effect on matrix textures. Fields in which different breccias occur on the diagram are approximate, and the locations of liquidus, solidus, and other transformation boundaries will vary with bulk composition. Dimict breccias, granulitic breccias, and regolith breccias do not plot as classes on this diagram. Regolith breccias could be classified as glassy melt breccias or fragmental breccias, but they differ in that they are commonly lithified from loose fragments of lunar soil by an impact event that is separate from (and later than) those that produced the assemblage of fragments. Similarly, lithification of granulitic breccias is usually the result of recrystallization long after assembly of the fragments. Dimict breccias can be considered a special case of crystalline melt breccias.

(1981) identified such genetically-related melt fragments in breccia 67016, as did *Marvin et al.* (1987) in breccia 67015.

The Apollo 16 fragmental breccias consist mainly of plagioclase feldspar. They contain three dominant types of rock fragments: (1) cataclastic anorthosite, (2) granulitic breccia, and (3) fragment-rich feldspathic impact-melt rocks (*James,* 1981; *Stöffler et al.,* 1981, 1985; *R. Warner et al.,* 1976a; and others). The impact-melt clasts are dark, while the anorthosites and granulites are light colored.

The impact-melt clasts have significant variations in mineral and chemical composition. In sample 67455, a fairly typical specimen, half the mineral grains larger than 40 μm are plagioclase and about 10% are olivine and pyroxene (*Minkin et al.,* 1977). Fragments of cataclastic anorthosite make up about 12% of this rock, granulites about 8%, and impact melts about 8%.

However, the Apollo 16 fragmental breccias are not all the same. Sample 67015 contains a more diverse assemblage of fragments, including (1) anorthositic norites that are related to ferroan anorthosites and (2) less aluminous KREEPy impact melts (*Marvin and Lindstrom,* 1983; *Marvin et al.,* 1987; see section 6.3). *Stöffler et al.* (1985) studied the modal and textural characteristics of many of these Apollo 16 fragmental breccias from North Ray Crater and found that the relative proportions of different rock types in the lithic fragments vary

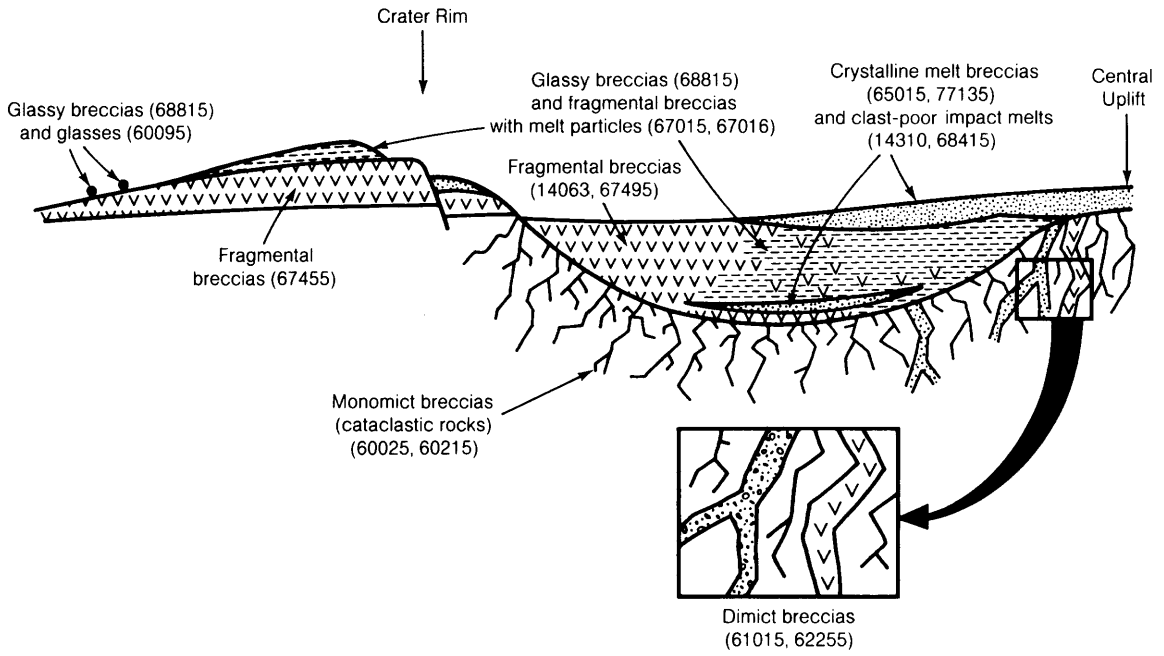

Fig. 6.40. Cross-section of an ideal lunar crater showing the relations of different polymict breccia types and possible monomict breccias to the geological environment of the crater (adapted from *Stöffler,* 1981). Numbers indicate actual lunar samples that are examples of the different breccia types. In reality, most lunar polymict breccias are the result of a series of impacts, and in almost all cases the target for each new breccia-producing impact is already a polymict breccia.

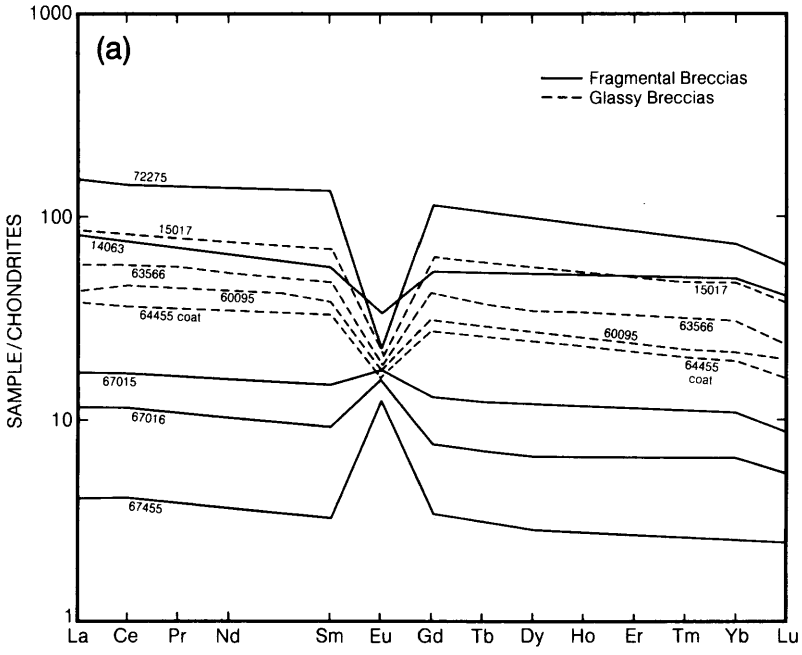

Fig. 6.41. Representative rare earth element (REE) distribution diagrams for lunar polymict breccias: **(a)** fragmental and glassy breccias.

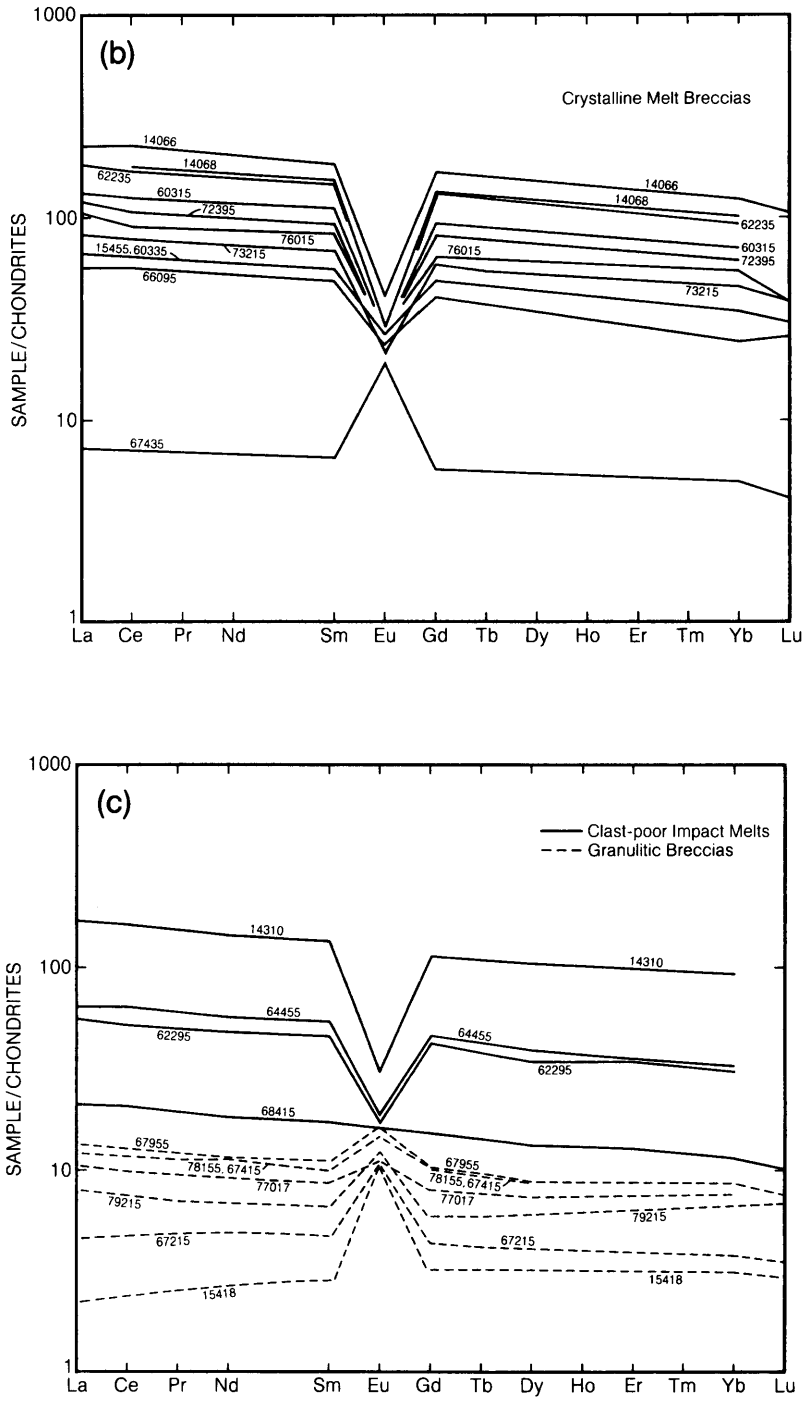

Fig. 6.41. (continued) **(b)** Crystalline melt breccias; **(c)** clast-poor impact melts and granulitic breccias. REE abundances are normalized to chondritic meteorites and are plotted on a logarithmic scale. The distributions show a general enrichment in light REE (curves are higher at the left side of the diagram) with either positive or negative Eu anomalies. In a few cases, the Eu point is omitted and the connecting lines have not been completed because their inclusion would clutter the diagram.

TABLE 6.13. Frequency % of lithic clasts (grain size: 0.05-4 mm) in Apollo 16 Stations 11 and 13 fragmental breccias measured by sectioned area in thin sections (*Stöffler et al.,* 1985).

Sample	n	1	2	3	4	5	6	7	8	9	10	11
63588,4	90	15.3	34.6	1.3	—	22.7	—	3.1	—	1.8	21.1	—
63595,4	88	22.5	13.9	20.8	0.6	6.5	3.8	2.8	—	—	29.0	—
67455,57	111	10.9	35.9	33.2	—	5.4	—	0.6	10.5	—	3.5	—
67455,61	139	5.2	63.4	24.4	—	—	—	2.8	1.4	—	2.8	—
67495,3	93	18.9	27.4	44.9	—	3.5	—	1.1	—	—	4.2	—
67517,3	156	5.4	86.9	6.3	—	—	—	—	—	1.4	—	—
67526,4	79	5.2	87.2	7.6	—	—	—	—	—	—	—	—
67527,1	30	1.8	85.0	13.2	—	—	—	—	—	—	—	—
67528,1	68	21.2	56.5	11.7	—	1.3	—	—	—	—	4.7	4.7
67545,4	36	—	90.2	9.8	—	—	—	—	—	—	—	—
67457,1	65	46.0	5.5	41.5	—	—	—	—	—	—	7.0	—
67549,5a	57	—	2.6	59.1	0.9	10.2	—	—	—	—	—	27.2
67549,5b	79	—	3.8	39.0	3.4	14.5	—	—	—	—	—	39.4
67639,2	121	18.2	15.4	62.6	—	—	—	3.7	—	—	—	—
67645,3	79	20.1	18.1	55.8	—	—	—	2.5	—	—	3.4	—
67647,2	79	1.3	3.8	88.4	—	—	—	5.7	—	—	0.8	—
67649,5	35	—	20.0	74.1	—	—	—	—	—	—	5.9	—
67655,1	55	14.1	63.6	—	—	—	—	20.8	—	0.1	0.8	0.7
67656,3	31	19.1	18.5	62.4	—	—	—	—	—	—	—	—
67657,7	58	51.5	40.9	7.6	—	—	—	—	—	—	—	—
67669,27	24	—	47.4	50.2	—	—	—	2.3	—	—	—	—
67706,2	121	7.9	15.6	73.1	0.3	—	—	0.3	—	—	2.4	0.4
67707,17	96	24.8	13.9	61.0	—	—	—	0.3	—	—	—	—
67768,3	65	24.6	42.5	32.0	—	—	—	—	—	—	0.9	—
67975,80,13	358	16.4	29.3	0.9	51.2	0.9	—	0.8	—	—	0.6	
		2213										
Weighted average		14.4	35.7	30.6	8.4	2.6	0.15	1.7	0.6	0.2	3.4	2.3
Error (95% confidence):		±1.6	2.0	2.0	1.2	0.5	~0.07	0.4	~0.2	0.08	0.7	0.5

n = number of analyzed clasts; 1 = granulitic rocks and breccias; 2 = recrystallized cataclastic anorthosite; 3 = feldspathic microporphyritic melt breccia (MB); 4 = mafic microporphyritic MB; 5 = intergranular MB; 6 = micropoikilitic MB; 7 = fine-grained subophitic-ophitic-intersertal MB; 8 = coarse-grained subophitic-ophitic-intersertal MB; 9 = vitric or partly devitrified (impact) glass; 10 = devitrified (variolitic) glass; 11 = unrecrystallized cataclastic anorthosite. Weighted average (bottom) is based on n.

considerably from sample to sample (Table 6.13). However, it is obvious that the heterogeneity and the coarse fragment size in these samples produce variations even among determinations on the same sample. *Stöffler et al.* (1985) also found differences in the compositions of metal grains in the matrices of different samples.

The Apollo 16 fragmental breccias are all highly aluminous and have similar, but not identical, chemical compositions (Tables A6.14-A6.16). The Mg/Fe ratios vary substantially, although all the samples are rather ferroan when compared to the full range of lunar highland samples. The bulk composition of the Apollo 16 breccias seems to be dominated by ferroan anorthosites and other ferroan plutonic highland rocks (e.g., *Stöffler et al.,* 1985). Most of the incompatible elements are provided by a small component of KREEPy and magnesian impact melts.

The Apollo 14 fragmental breccias (samples 14063, 14064, and 14082/14083) contain much less plagioclase and hence have lower alumina contents than do the Apollo 16 samples (Table A6.14). These samples have been described briefly by *Warner* (1972), *Steele and Smith* (1976), and *Ryder and Bower* (1976). They contain a wide range of fragment types; fine-grained KREEPy impact melts and troctolitic breccias are prominent. Other fragment types include fine-grained or glassy melt rocks, granulites, norites, anorthosites, and rare mare basalts.

The only large fragmental breccia (sample 72275) recognized among Apollo 17 samples formed the matrix of Boulder 1 at Station 2. It is a highly complex rock that appears to be the crushed remnants of a mixture of KREEPy basalt and fine-grained KREEPy impact melts, which make up other parts (and samples) of a single boulder (*Ryder et al.,* 1975). Some fragments have melt rinds, a feature

that could have been produced by inflight agglomeration of the fragment and melt during ejection from the impact crater. A few other clasts, norites and granulites, are also present. The dominance of the KREEPy basalts in this sample is reflected in its chemical composition (Tables A6.14-A6.16).

The fragments of single minerals in the fragmental breccias range widely in composition, both within and between individual samples. This situation demonstrates the diverse nature of the source materials and the polymict origin of the rock. It also shows that the rocks have not been thermally metamorphosed since their assembly; intense metamorphism at high temperatures would tend to homogenize the different mineral grains to a single equilibrium composition. The mineral fragments generally resemble crystals in the coarser-grained rock fragments such as ferroan anorthosites. In some cases, they suggest unsampled rock types. For example, the Apollo 14 fragmental breccias contain some coarsely-exsolved pyroxenes apparently derived from slowly-cooled plutonic norites; however, no fragments or other samples of the parental norites themselves have been discovered.

Ages of fragmental breccias. Fragmental breccias consist of discrete fragments with diverse origins and ages; some of them have been dated by radiogenic isotope methods. None are younger than 3.9 b.y. and some are older. Interpretation of these results is complicated by the fact that a fragmental breccia may have two different "ages": One is the time that the fragments were assembled, the other is the time when the fragments were lithified (solidified into a rock). These two events may be simultaneous or they may be separated by a significant interval of time. To make things more complicated, neither event can generally be dated by radiogenic isotope methods because heating during either event is generally not intense enough to reset the original isotopic systems to the new time.

However, the ages of these events can sometimes be dated. *Malvin et al.* (1987) identified some melt clasts in Apollo 16 breccia 67015 that had been hot and plastic during assembly and were therefore produced by the impact that assembled the breccia. These clasts were dated at 3.9 b.y. (^{40}Ar-^{39}Ar method), an age that is common for melt fragments in these and other rocks. Because no fragments younger than 3.9 b.y. have been identified among Apollo 16 fragmental breccias, it has been assumed that these breccias were assembled by a major impact 3.9 b.y. ago.

Coatings of glass are observed on some breccia samples, apparently splashed onto them by later impacts in the vicinity of the sample. Because these coatings cannot be older than the time when the breccias were lithified (and may be much younger), they could provide minimum age estimates for the time of lithification. Unfortunately, little reliable information on the age of these coatings is available.

There are few age data for rock fragments in the Apollo 14 fragmental breccias. The KREEPy melt clasts that dominate these breccias are 3.8 b.y. old (*Bernatowicz et al.,* 1978), not significantly different from ages of other Apollo 14 rocks, and there is no compelling reason to believe that their chronology is significantly different from that of other highland rocks. The age of the fragmental breccia that forms the matrix of Boulder 1 at Station 2 at the Apollo 17 site is at present known only to be younger than its clasts, which have been dated at 3.9 b.y. (*Leich et al.,* 1975; *Compston et al.,* 1975).

Origins of fragmental breccias. Fragmental breccias were assembled and lithified while cool, in most cases about 3.9 b.y. ago. Because they do not contain any near-surface (regolith) components, their components must have been derived from considerable depth during the formation of substantial craters that penetrated the regolith, and the breccias themselves were assembled as large, blanket-like deposits around these craters.

The composition and characteristics of the Apollo 16 fragmental breccias have led many workers to believe that many of them represent material from the Descartes Formation, which is, in turn, thought to be a large deposit of ejecta from the Nectaris Basin (e.g., *Stöffler et al.,* 1985; *James,* 1981; *Norman,* 1981). This interpretation is consistent with orbital geochemical data. However, the KREEP-bearing Apollo 16 breccias may be derived from the younger Cayley Plains unit, which may be ejecta from the Imbrium Basin (*Stöffler et al.,* 1985; see section 10.6.5). The mild lithification observed in both breccia types could have taken place immediately after deposition or it may have been produced much later, possibly during their excavation by the formation of North Ray Crater in the immediate vicinity (e.g., *Nord et al.,* 1975). Because large basin-forming impacts such as the Imbrium and Nectaris events were common during the intense lunar bombardment that waned about 3.9 b.y. ago, and because the bulk of ejecta from any impact crater is deposited cold, it seems quite likely that a major portion of the upper part of the lunar crust consists of material similar to the Apollo 16 feldspathic fragmental breccias.

The origin of the Apollo 14 fragmental breccias is much less clear, mainly because their bulk chemistry is less well established and the context of the samples at the site is less well known. The Apollo 14 breccias contain some fragments of deeper crustal rock types as well as KREEPy melts, and their overall

bulk compositions may not be too different from those of the local, near-surface regoliths. The breccias suggest that there may be remnants of the upper lunar crust in the Fra Mauro region, from which both the regoliths and Apollo 14 impact melts were made.

The Apollo 17 fragmental breccia (the Boulder 1, Station 2 matrix) appears to have been produced by a much smaller impact than that which formed the Apollo 16 fragmental breccias, because it is dominated by materials (basalt and impact melt) that originally crystallized at the lunar surface.

6.4.3. Glassy Melt Breccias and Impact Glasses

Glassy materials produced by meteoroid impacts vary widely, depending on the amount of glass present. These materials range from extremely clast-rich breccias with glassy matrices (*glassy melt breccias*) to glass-rich bodies that are clast-poor or clast-free (*impact glasses*). Glassy melt breccias are polymict; they show a wide range of fragment types and there may be more than one generation of glass involved in their formation and lithification. The shapes of samples of glassy melt breccias are generally irregular and some are slaggy (Figs. 6.37b and 6.38c). Impact glasses appear to have formed and cooled in single impacts. Many samples are ovoid and some are hollow. A distinctive feature of most impact glasses is the presence of a free melt surface (Fig. 6.37c), in contrast with most breccias, including glassy melt breccias, which have mechanically broken surfaces.

The distinction between glassy melt breccias and impact glasses on the one hand, and crystalline melt breccias or clast-poor impact melts (which are also formed by meteoroid impact) on the other (sections 6.4.4 and 6.4.5), is the degree of crystallization of the melt. Impact melts that have been slowly cooled are largely crystalline, and they show textures indicating that their crystals formed in equilibrium with the melt at high temperatures. The glassy melt breccias and impact glasses can be considered as impact melts that were cooled too rapidly for crystallization to occur. *Devitrified glasses,* in which microscopic crystals have formed in the solidified glass, are also included in the category of glassy rocks.

There are several ways to distinguish between impact-produced glasses and glasses formed by volcanic processes. Volcanic glasses contain only rare broken rock and mineral fragments and are homogeneous. They also lack the high contents of siderophile elements that indicate meteoritic contamination (see section 6.1.7 and Chapter 8). An additional, simple distinction is that all sampled lunar glass particles more than a few millimeters across are impact-produced, not volcanic. Examples of impact glasses that form coatings on chemically unrelated rocks are common. In these cases, the impact glass has been splashed onto nearby exposed rocks or the rock was entrained during flight of the melt.

Petrography and chemistry of glassy breccias and impact glasses. These rocks form a diverse group whose members share the common characteristic of a glassy (vitric) groundmass. In impact glasses, this groundmass may constitute virtually the entire rock.

Glassy melt breccias contain fragmental minerals and rocks; *schlieren* (flow layering) and vesicles are common in the glassy groundmass. Some samples are slaggy or cindery. Glassy melt breccias can be distinguished from *regolith breccias* formed near the surface because they have little or no surface-produced agglutinates (section 7.1.3), solar wind gases, or glass spheres. However, such distinctions are difficult in some cases. The groundmass glass can be heterogeneous and may have several different generations, but many samples have a dominant "latest" glass groundmass. These groundmass glasses form veins and protrusions throughout the rock.

Few detailed studies of glassy breccias have been made. One sample (68815, weighing 1789 g), which was chipped from a boulder at the Apollo 16 landing site, consists of many lobes of glass (Fig. 6.37b). *Brown et al.* (1973) described it as a "fluidized lithic breccia." The glasses vary in composition, color, and banding. The clasts in 68815 are commonly angular and consist dominantly of fine-grained impact melts that are much less aluminous (about 22% Al_2O_3; *Brown et al.,* 1973) than either the glass (26-30% Al_2O_3) or the average composition of the rock (about 27% Al_2O_3; Table A6.17). Two larger clasts are apparently *granulitic* breccias. The overall chemical composition of this breccia is similar to that of local soils at the Apollo 16 site.

Impact glasses occur as relatively small particles, generally less than a few centimeters across. They characteristically have at least one surface where the glass was chilled. Impact glasses are rarely optically homogeneous on scales of more than a few millimeters; heterogeneous and *schlieren-rich* glasses dominate. In shape, impact glasses range from spheres to ovoids to angular, blocky fragments with vesicles. Some occur as individual pieces resembling volcanic "bombs."

Most impact glasses have been found as coatings or drapings on rocks. These impact glasses have been found at most Apollo sites, and those from the

Apollo 16 site have been the most studied (*See et al.,* 1986; *Morris et al.,* 1986; *Borchardt et al.,* 1986). The glass drapings have sharp boundaries against the host rock, and differ from the host rock in chemical composition. These coatings were clearly not formed by fusion of the rock (i.e., they are not analogous to the fusion crusts found on meteorites). Instead, the glass seems to have been splashed onto the rocks, probably from nearby meteoroid impacts.

The presence of distinct crystallization fronts (Fig. 6.38d) in both glass bombs and melt splashes indicates that devitrification (subsolidus crystallization) has occurred (*See et al,* 1986). Other samples have intersertal textures (with interstitial glass), indicating crystallization from a melt. In some samples, such textures may perhaps even be dominant, implying that the specimen should be classified as an impact melt. However, the outwardly glassy appearance of the samples and the presence of smooth exterior surfaces make it more convenient to include them with the impact glasses.

Rock and mineral fragments are common as inclusions in impact glasses. Among such inclusions, mineral fragments, particularly plagioclase, are most abundant (>80%), and various types of anorthosite predominate among the lithic clasts. Some fragments of earlier-formed impact-melt rocks and polymict breccias are also present, but the inclusion population is biased toward plagioclase. Most crystals have textures indicating that they are either unshocked or only moderately shocked and heated (<30 GPa; <300° C).

At the Apollo 15 landing site, glass coatings and some glass spheres are common. A few glass samples were collected from the glassy linings of small craters about a meter or two in diameter. These samples have not been studied in detail, but preliminary examination shows that they have petrographic characteristics similar to those of the Apollo 16 glasses. At both the Apollo 15 and 17 landing sites, neither the glassy breccias nor the impact glasses can be considered as purely highland samples. Most samples, both petrographically and chemically, have a major mare basalt component, and many were collected from the mare plain itself. Large (5-10 cm) samples of impact glasses are uncommon from the Apollo 11-14 missions, and the few specimens have not been well characterized.

Chemical compositions of some glassy melt breccias and impact glasses are listed in Tables A6.17-6.19. The Apollo 16 impact glasses are fairly homogeneous individually, but there is considerable chemical variation among samples (24-30% Al_2O_3; 2-6% FeO; *See et al.,* 1986) (Fig. 6.42). Most of the samples form a group that is chemically unlike local regoliths in having higher Mg/Fe ratios and lower Al_2O_3 contents. These samples appear to be mixtures of anorthosite and a low-Sc type of very-high-alumina (VHA) impact melt (for a discussion of VHA, see section 6.4.4). A second group of samples is rather like the local regoliths and is comparatively enriched in a higher-Sc type of VHA impact melt or anorthositic norite. They also contain a minor high-Ti component (mare basalt?), which is absent from the first group (*Morris et al.,* 1986). All the glassy specimens, regardless of their chemical composition, are very enriched in meteoroid material, averaging over 7%, as indicated by their siderophile element abundances, which is higher than most regoliths or other breccias (Table A6.19). This meteoroid component apparently comes from chondritic meteoroids (*Morris et al.,* 1986). Impact glasses from the Apollo 15 site are chemically similar to the local regoliths and also have high meteoroid siderophile contamination. Their chemical composition indicates that most of the Apollo 15 glasses have a significant amount of mare basalt in them.

Ages of glassy melt breccias and impact glasses. Virtually no age-measurement data have been obtained for glassy melt breccias, and their ages of formation can only be constrained loosely from their surface exposure ages (see section 7.3) and from the ages of the clasts they contain. Most samples appear to be less than 1 b.y. old.

Impact glasses collected from the surface at the Apollo 16 landing site appear to be late additions; they have been on the lunar surface for less than 107 years, as estimated from micrometeoroid erosion rates and from the preservation of thin glass coatings on them (*Hörz et al.,* 1975). The dominant group of impact glass samples from the Apollo 16 site has surface exposure ages of 1.5 to 2 m.y. The other group, with regolith-like chemical compositions, has exposure ages of about 50 m.y. (*Morris et al.,* 1986). *Borchardt et al.* (1986) dated several samples from North Ray Crater using ^{40}Ar-^{39}Ar techniques, and found them all to be younger than the 3.9 b.y. age estimated for the Cayley Formation, from which they were presumably derived. Their formation ages ranged from 0.37 up to 3.8 b.y., but their surface exposure ages were restricted to 40-50 m.y.

Chronological data for other glasses are virtually nonexistent. However, the presence of mare components in the Apollo 15 samples, as well as the geological constraints, limit them to less than 3 b.y. old. The surface exposure ages are much younger than that, e.g., the glass coating on sample 15205 is about 1 m.y. old (see summary in *Ryder,* 1985).

Origins of glassy breccias and impact glasses. The production of glass, rather than crystalline materials, from a melt requires rapid

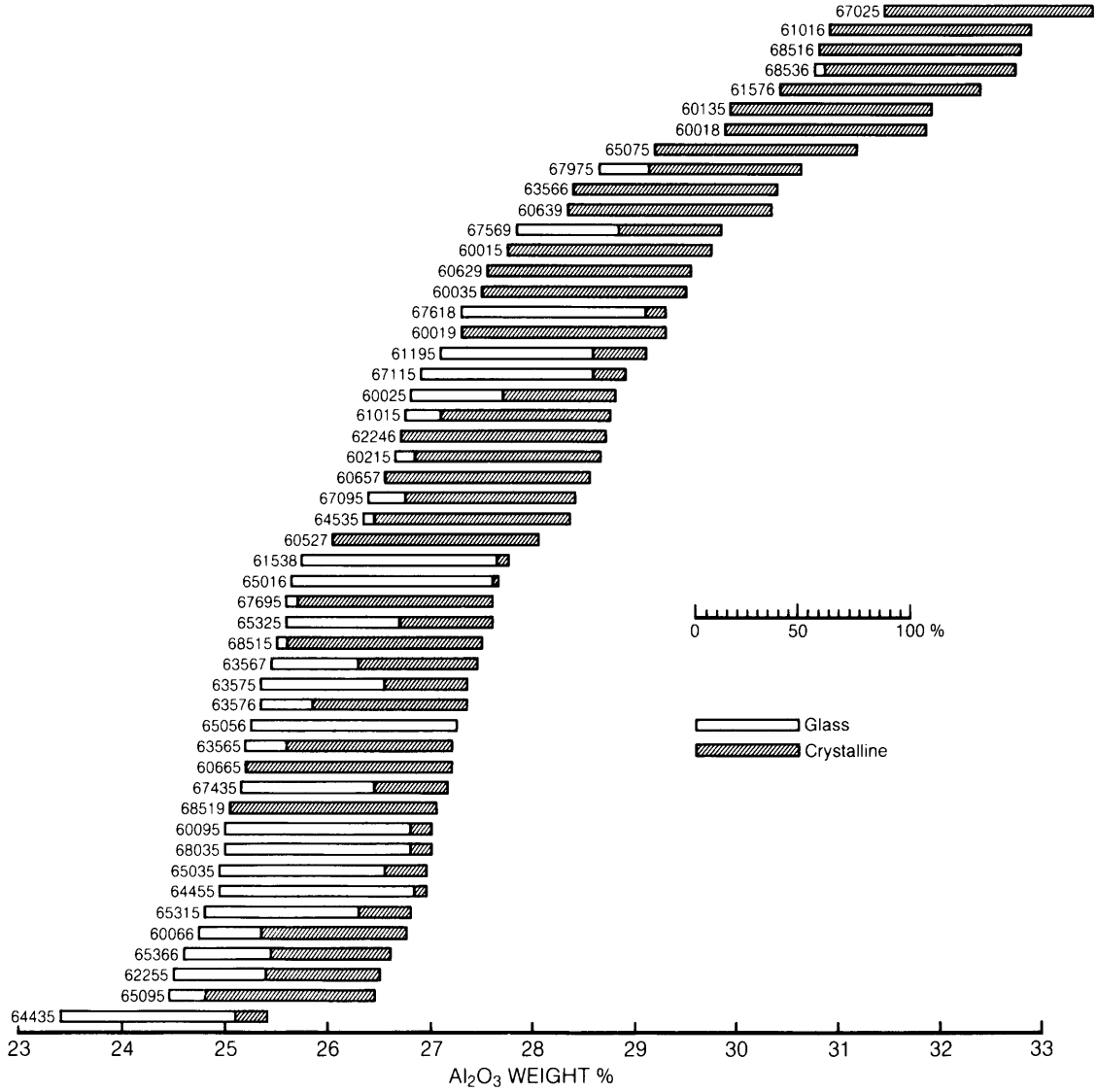

Fig. 6.42. Diagram showing alumina contents of impact glasses from the Apollo 16 site (*See et al.,* 1986), comparing Al_2O_3 contents of the crystalline and completely glassy (*holohyaline*) portions of the samples. The midpoint of each bar represents the bulk Al_2O_3 content of the sample. Impact glasses with more alumina (e.g., >30%; upper right) are generally more crystalline than those with less alumina (e.g., <25%).

cooling. Rapid cooling can be achieved in small cooling units, i.e., small volumes of original melt. Many glasses in the glassy polymict samples are smaller than a few centimeters in size, although some may be much larger. Such small, and therefore rapidly cooled, volumes of impact melt could be produced either in small impacts or in the most distant (distal) or uppermost portions of the ejecta blankets from larger impact craters.

Too little is known of the chemistry and petrology of most samples of glassy melt breccias and impact glasses to be sure of the origin of any particular sample. However, most samples show strong chemical similarities to the local regolith, suggesting that they have been produced by fairly small-scale craters that did not penetrate the existing regolith. These samples do not seem to be totally exotic to their collection sites. At the Apollo 15 site, the

impact glasses are chemically identical to local regolith. Others were collected as linings from small craters, so their origin is not in doubt.

In samples from all the Apollo sites, the glass coatings differ in composition from the coated host rocks, and they were therefore not derived from them. Furthermore, many of the glassy coatings on lunar rocks occur on several sides of the host rock, indicating that they were not splashed onto one side of a passive surface rock at some distance from the crater. Instead, most of the glasses were deposited onto their hosts inside growing crater cavities or during ballistic flight, so that more than one side of the rock was coated. The glass coatings were then "piggy-backed" on the rocks to their collection sites (*See et al.,* 1986).

The surface exposure ages of the Apollo 16 impact glass samples fall into two groups: about 2 m.y. and about 50 m.y. They seem to have been produced or exposed by the South Ray Crater and the North Ray Crater events, respectively (*See et al.,* 1986; *Morris et al.,* 1986; *Borchardt et al.,* 1986). Additional age data (e.g., *Borchardt et al.,* 1986) show that not all the glasses were produced by the North Ray Crater event; some are older than 50 m.y. The South Ray Crater group, however, might have been produced from that event itself (*See et al.,* 1986), since all of them have exposure ages of about 2 m.y. Chemical analysis indicates that most of these Apollo 16 glasses are not identical with the local regolith, but they appear to be dominated by subregolith materials of the Cayley Plains (*Morris et al.,* 1986; *Borchardt et al.,* 1986). This is consistent with the observation that they lack materials (agglutinates, glass droplets, etc.) formed and reworked at the lunar surface. However, these glasses were still formed by relatively small (<2 km diameter) craters in post-Imbrian times (section 4.4).

6.4.4. Crystalline Melt Breccias or Impact-Melt Breccias

Crystalline melt breccias are coherent rocks that contain obvious clastic material in a finer-grained groundmass that has formed by the crystallization of a silicate melt. The clasts range from a few percent to more than half the rock (Table 6.14); as the amount of clastic debris increases, the ground-mass tends to be more glassy and these samples grade somewhat arbitrarily into the glassy melt breccia group.

Many of the clasts show evidence of shock metamorphism or of resorption by the melt. The melt breccias invariably have high siderophile element contents resulting from meteoroid contamination. Vesicles are abundant in some samples. In short, these breccias have clearly been produced by the crystallization of clast-laden, impact-produced melts (*Simonds et al.,* 1976; *Onorato et al.,* 1976), although the older literature commonly refers to them as recrystallized or metamorphic breccias.

The chemical compositions of crystalline melt breccias span virtually the entire range of compositions observed in highland samples, with about 15% to 30% Al_2O_3 (Table A6.20). Crystalline melt breccias are common at all the lunar highland sites and they have also been found among the regolith particles of highland origin in the Apollo 11 and 12 samples (e.g., the Type-A norites of *Marvin et al.,* 1971).

Petrography and chemistry of crystalline melt breccias. Many samples of crystalline melt breccias have a grossly homogeneous appearance and show a generally even distribution of clasts (Fig. 6.37d). The textures of the crystalline ground-mass in such samples tend to be poikilitic to subophitic. Only rarely is anything approaching a porphyritic texture observed, and then only in the most feldspathic samples. The crystalline ground-mass is generally fine- to medium-grained, with poikilitic pyroxenes typically no larger than a millimeter across (Fig.6.38e,f). Other. samples are more heterogeneous, with clasts occurring as *schlieren* in the groundmass (Fig. 6.37e). These heterogeneous samples tend to be finer-grained than homogeneous samples and may even be partly glassy (Fig. 6.38g). They may also have a higher percentage of clasts. Many descriptions of crystalline melt breccias have been published (e.g., *Dymek et al.,* 1976; *Simonds,* 1975; *Simonds et al.,* 1976; *James,* 1976; *Ryder and Bower,* 1976). *Vaniman and Papike* (1980) reviewed the mineralogy and chemistry of highland melt rocks, including crystalline melt breccias.

In most samples of crystalline melt breccias, the clasts are predominantly of plagioclase; pyroxene, olivine, and rock fragments are present in lesser amounts. The chemical composition of the clasts is more refractory than that of equivalent minerals in the groundmass that have crystallized from the melt. Plagioclase clasts are more calcic and the mafic mineral clasts more magnesian than the ground-mass minerals (Fig. 6.43). In samples with a coarser-grained groundmass, the amount of clastic material tends to be less abundant, more refractory, and contains fewer rock (lithic) fragments. For example, the aphanitic (fine-grained) melt breccias at the Apollo 17 site contain abundant clasts of a diverse rock population. The coarser poikilitic-subophitic melt breccias contain few clasts and, among these, lithic fragments are scarce (*Spudis and Ryder,* 1981).

TABLE 6.14. Mineral modes (vol. %) of crystalline melt breccias (impact melt breccias).

Phase	14066	60315	60335	62235	66095	73215	77135
Melt	(84)	(96)	(84.2)	(86.5)	(88.5)	(68.1)	(87.9)
Feldspar	—	43.2	56.5	34.1	45.0	—	41.1
Hi-Ca px	—	4.9	13.4	6.0	{30.6}	—	{30}
Low-Ca px	—	39.0	0.6	36.3		—	
Olivine	—	6.1	9.0	6.0	10.2	—	15.1
Silica	—	—	—	—	—	—	—
Ilmenite	—	2.1	0.3	2.8	—	—	1.4
Ulvöspinel	—	—	—	—	—	—	—
Mg, Al-spinel	—	—	—	—	—	—	—
Fe-Ni metal	—	0.7	0.1	1.2	1.2	—	0.2
Troilite	—	—	0.8	0.1	0.1	—	0.1
Phosphate	—	—	<0.1	—	—	—	—
Mesostatis	—	—	3.6	—	—	—	—
Glass	—	—	—	—	1.4	—	—
Clasts	(16)	(4)	(15.8)	(13.5)	(11.5)	(31.9)	(12.1)
Feldspar	6.0	3.0	15.0	9.0	8.5	23.7	6.2
Olivine	0.7	1.0	—	—	—	{8.2}	—
Pyroxene	2	—	—	0.5	0.1		2.0
Lithic	7	—	0.8	4.0	2.9	0	3.9

14066: *Juan et al.* (1972); 60315, 60335, 62235, 66095, 77135: *Vaniman and Papike* (1980); 73215: *James* (1976).

In general, the crystallized groundmass of these breccias consists dominantly of plagioclase and a low-Ca pyroxene. Depending on the bulk chemistry and crystallization conditions, olivine and a variety of accessory minerals may also be present (Table 6.14). Small amounts of ilmenite or ulvöspinel are almost universally present. Globules of Fe-Ni metal and sulfide are also common (Fig. 6.38f). In the more common poikilitic groundmass, plagioclase crystals tend to be small (less than a few tenths of a millimeter) and stubby, and dozens of them may be embedded in the larger pyroxene (normally pigeonite, less commonly augite) or olivine crystals. In the subophitic textures, the plagioclase crystals form grains that are more comparable in size to the pyroxene or olivine crystals. Ilmenite crystals tend to be lath-like, rather than anhedral as in metamorphic (recrystallized) lunar rocks. A glassy mesostasis is observed between the larger crystals in some groundmasses, especially in the more KREEP-rich samples. This mesostasis may contain Fe-rich mafic minerals, a silica phase, and minor minerals such as zircon (Fig. 6.38f).

Chemically, the crystalline impact-melt breccias tend to have abundances and patterns of incompatible element (e.g., REEs) that indicate the presence of a significant amount of KREEP component (Table A6.21 and Fig. 6.41). In some crystalline impact-melt breccias, KREEP is particularly abundant, e.g., in the Apollo 12 and Apollo 14 samples. In these samples, the KREEP abundance is roughly inversely related to alumina content, which is derived from the highland plutonic component. Therefore, in the more feldspathic varieties from the Apollo 16 site, KREEP is a relatively minor component. All samples are contaminated with meteoritic siderophile elements (Table A6.22).

Crystalline melt breccias and clast-poor impact melts (section 6.4.5) fall into distinct compositional groups. Four main groups have been recognized among the Apollo 16 melts. Very tightly-clustered compositional groups may represent samples derived from single impacts. Informal designations and acronyms have been applied in a nonrigorous fashion to different groups (*BVSP*, 1981). The LKFM (low-K Fra Mauro) group is a common one; the term is applied to samples that contain about 15-19% Al_2O_3 and have abundances of light REEs that are about 100-150× those in chondritic meteorites. Increasing REE and K contents give rise to the IKFM (intermediate-) and HKFM (high-) groups. More aluminous compositions (20-25% Al_2O_3) with lower REE contents have been called VHA (very-high-alumina) "basalts" (although they are not truly basalts in the traditional sense of lavas extruded from the planetary interior).

Ages of crystalline melt breccias. A large proportion of the material in crystalline melt breccias has been totally melted or degassed during formation. Under these extreme conditions, the isotopic systems used for age dating can be completely "reset," and meaningful crystallization ages can be

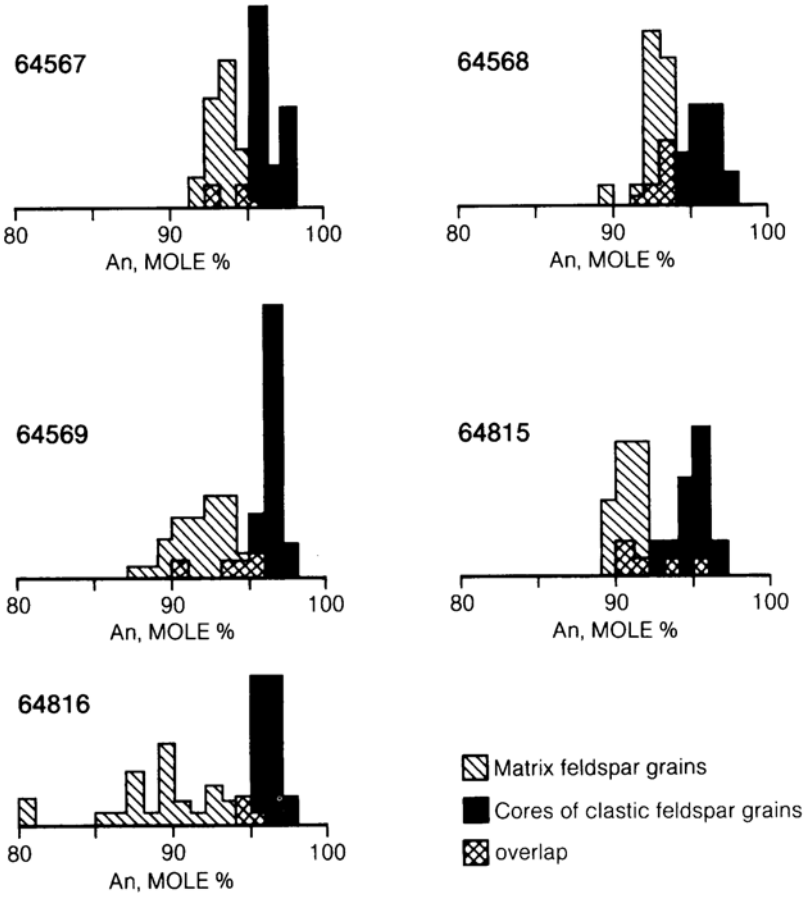

Fig. 6.43. Histograms of plagioclase compositions (mol.% anorthite, An) in Apollo 16 crystalline melt breccias. The included fragments of feldspar crystals from impact-shattered bedrock (clastic plagioclase; black bars) are more refractory (more Ca-rich) than groundmass plagioclases (diagonal ruling), which have crystallized from an impact-produced melt. Overlap of populations is shown by the criss-cross pattern. From *Simonds et al.* (1973).

obtained, particularly for the coarser-grained examples, which contain few original clasts. Dating the clast-rich varieties is more difficult. The clasts themselves, being relatively cold when mixed with the melt, act to cool the melt quickly. As a result, the crystalline groundmass is fine grained, and the necessary mineral separations are difficult or impossible. Furthermore, the clasts tend to be poorly reset or incompletely degassed, leading to inaccurate measurements. To minimize these complications, the ^{40}Ar-^{39}Ar dating method is more commonly used than the Rb-Sr method for these rocks. There is some indication that the Rb-Sr systems in at least some of the melt rocks were open during impact melting, so that Rb could migrate in and out of the rock (e.g., *Reimold et al.,* 1985), a condition that would make Rb-Sr measurements even more unreliable.

Representative ages for crystalline melt breccias are listed in Table 6.15; the table also lists Al_2O_3 as a rough guide to composition. Most samples, irrespective of chemical composition, have ages around 3.9 b.y., which is a common age for highland breccias in general. No sample is very far out of this range, implying that the available samples all formed during the period of large impacts that produced the mare basins. Even though such large young impact craters as Copernicus, Tycho, and King must have produced large volumes of crystalline melt breccias at much later times, these materials are not represented in the Apollo collections.

Origin of crystalline melt breccias. Crystalline melt breccias are of impact-melt origin as shown by their clasts, their nonigneous chemical compositions, and the presence of meteoroid contamination (see also section 6.3). Studies of large terrestrial impact craters (*Simonds et al.,* 1976) indicate that a large volume of completely melted rock forms near the point of impact, where the shock pressures are highest. This melt immediately moves outward across the developing crater, picking up cold debris (clasts) as it moves, and eventually forming a sheet within the crater or even spilling outside it (section 4.1.2 has a detailed discussion of this process).

TABLE 6.15. Representative crystallization ages (b.y. ago) of crystalline melt breccias.

Sample	~%Al_2O_3	$^{40}Ar/^{39}Ar$ whole rock	Ref.	Rb-Sr isochron	Ref.
14068	13	3.80±.01	9		
15455	17	3.87±.04	5		
60315	17	3.97±.03	1		
		3.86±.01	2		
64567	21	3.86±.05	8		
65015	20	3.92*	3	3.85±.02	4
		3.96±.04	1		
67715	30	4.09±.01	7		
73235	21	3.88±.04	10		
76315	18	3.92±.04	8		
76055	16	3.99±.07	11	3.78±.04	6
		3.92±.05	12		
		3.91±.04	13		

* Plagioclase, not whole rock.

(1) *Kirsten et al.* (1973); (2) *Schaeffer et al.* (1976); (3) *Jessberger et al.* (1974); (4) *Papanastassiou and Wasserberg* (1972); (5) *Alexander and Kahl* (1974); (6) *Tera et al.* (1974); (7) *Jessberger* (1983); (8) *Turner and Cadogen* (1975); (9) *Heusser* (1985); (10) *D. Phinney et al.* (1975); (11) *Kirsten and Horn* (1974); (12) *Turner et al.* (1973); (13) *Huneke et al.* (1973).

In this mixture, the hot melt and colder clasts come to an equilibrium temperature at which some clasts are preserved and the melt crystallizes into different minerals (often fine-grained) rather than chilling into a glass. In many cases it is difficult to distinguish a crystalline groundmass that has formed from a melt from one that has formed by later devitrification of solid glass. This difficulty makes the distinction of a crystalline melt breccia from a glassy melt breccia arbitrary in some cases (see also section 6.4.3).

Some crystalline melt breccias have compositions similar to upper-crustal or local compositions, implying origin from near-surface rocks involved in relatively small impacts. However, several groups, particularly those with basaltic compositions and moderate KREEP contents (e.g., the LKFM group), do not. The origin of these latter melts has not been fully explained. Part of the problem is that, while terrestrial crystalline impact-melt rocks can be chemically modeled by mixing compositions corresponding to the observed clasts, the lunar ones commonly cannot. This condition implies that these melts contain a chemical component not represented by the observed clasts.

A strong case can be made that at least some of these samples represent melts generated in large basin-forming impacts, which involved deeper levels of the lunar crust. Possible examples are (1) samples 15445 and 15455 (from Imbrium?; *Ryder and Bower,* 1977; *Ryder and Wood,* 1977), (2) the Apollo 17 poikilitic melts (from Serenitatis?; *Ryder and Wood,* 1977), which definitely represent an important part of the local massifs at the Apollo 17 site, and (3) perhaps the Apollo 16 poikilitic melts as well.

6.4.5. Clast-poor Impact Melts

Clast-poor impact melts are coherent. They contain very few, if any, clasts, so that their textures are almost wholly igneous. Most samples are fine-grained and resemble conventional volcanic rocks. They are much less common than melt breccias. Their chemical compositions span almost the entire range observed in highland rocks that contain more than about 15% Al_2O_3.

Because both clast-poor impact melts and conventional volcanic rocks crystallize from a silicate melt, it is not always easy to distinguish between them. Clast-poor impact-melt rocks have been identified by some workers (e.g., *Kushiro et al.,* 1972; *Crawford and Hollister,* 1974) as conventional, internally-generated igneous rocks; in these descriptions the rare included fragments were described as xenocrysts. The distinction between such impact melts and conventional igneous rocks produced by partial melting of the interior of the Moon is especially important when attempting to understand lunar petrogenesis. In general, a distinction can be made on the basis of siderophile-element abundances that indicate meteoroid contamination in the impact melts (see also section 6.3), although even that criterion has been questioned (*Crawford and Hollister,* 1974; *Delano and Ringwood,* 1978). The microscopic textures in impact melts are rather more heterogeneous and nonuniform than those of internally-generated igneous rocks. Chemically, most lunar impact melts have compositions that are unlike melts that could be expected to be produced by partial melting of the lunar interior; in particular, the impact melts tend to be more aluminous than internally-derived melts. Because most impact melts are fine-grained, this high aluminum content cannot easily be attributed to the accumulation of large plagioclase crystals during crystallization of an earlier and less-aluminous magma.

Petrography and chemistry of clast-poor impact melts. *Vaniman and Papike* (1980) reviewed highland melt rocks, including clast-poor impact melts. Clast-poor impact melts tend to have a range of fine-grained crystalline textures that are generally ophitic, and rarely vitrophyric or intersertal (Figs.6.38h,i). Some impact-melt rocks have a slightly porphyritic texture with larger plagioclase crystals. The textures of impact-melt rocks are more

TABLE 6.16 Mineral modes (vol.%) of clast-poor impact melts.

Phase	14276	14310	62295	64455	65055	67747	67559	68415
Feldspar	64.6	59.0	35.5	59.9	68.5	67.2	83.1	82.2
High-Ca px	4.0	6.1	—	{32.7}	{27.6}	{8.0}	{13.8}	4.4
Low-Ca px	25.0	26.8	—					7.5
Olivine	—	—	28.3	6.5	—	16.3	—	3.1
Silica	—	—	—	—	—	—	—	—
Ilmenite	1.2	1.8	—	—	0.8*	0.7*	0.1	
Ulvöspinel	<0.1	<0.1	—	—	0.7	—	—	—
Mg, Al-spinel	—	—	6.5	—	—	—	—	—
Fe-Ni	0.3	0.1	<0.1	0.2	0.7	0.3	0.1	0.2
Troilite	<0.1	<0.1	—	0.3	0.4	0.4	0.3	—
Phosphate	0.5	0.3	—	—	—	—	—	—
Mesostasis	3.5	4.4	—	0.4	2.0	7.0	2.0	2.1
Glass	—	—	30	—	0.2	—	—	—
Accessories (<0.1 %)	schreibersite armalcolite tranquillitite K-Ba feldspar	schreibersite armalcolite tranquillitite	schreibersite	schreibersite akaganeite				

* Includes armalcolite.

14276, 14310, 68415: *Gancarz et al.* (1972); 62295: *Walker et al.* (1973a); 64455 *BVSP* (1981); 67747, 67559: *Reimold et al.* (1985); 65055 *Vaniman and Papike* (1980).

heterogeneous than those in normal igneous rocks. In particular, impact-melt rocks have a much wider range in grain size within a single thin section, ranging from ragged plagioclase phenocrysts to irregular granular clots. Small, open, crystal-lined cavities (*vugs*) are common.

The minerals in clast-poor impact-melt rocks are virtually the same as those that make up normal, internally-derived lunar igneous rocks. Nearly all impact-melt rocks contain plagioclase and pyroxene (normally a low-Ca variety), and olivine is present in some samples. Minor minerals vary with the bulk chemistry. A common feature (shared with clast-bearing impact melts but not with volcanic basalts) is the presence of Ni-Fe metal/sulfide globules. Modal (mineral %) data for selected samples are given in Table 6.16; these data reflect the variety of compositions shown by the chemical data (Tables A6.23-A6.25).

A single bulk chemical composition may be represented by more than one sample. For instance, the only clast-poor melt composition among the Apollo 14 samples is represented by several different specimens, including 14310 and 14276. Sample 14310 was originally thought to be an igneous KREEP basalt, but its textures are more heterogeneous than those of a basaltic lava, it is not in fact clast-free, and it is enriched in meteoroid siderophile elements. This cluster of similar samples has a composition in which incompatible-element abundances are only slightly lower than Apollo 14 regolith samples and the Mg/Fe ratio is similar. However, these samples differ from the regolith in having higher Al_2O_3 and lower FeO and MgO.

At the Apollo 16 site, several samples from separate locations (e.g., samples 67559 and 60635) have compositions similar to samples 68415 and 68416, which were chipped from a single boulder. This composition appears to be similar to that of the regolith from the nearby Descartes Highlands, and it is much more aluminous than the Apollo 14 samples. Other Apollo 16 impact-melt samples, such as 64455 and the distinctive 62295, differ from each other, from the 68415 sample group, and from the local regolith compositions.

Ages of clast-poor impact melts. During formation, virtually all the components of clast-poor impact melts were totally molten and/or degassed, resetting the isotopic systems used for age-dating measurements. Thus, it is comparatively easy (especially in comparison with other highland breccias) to acquire consistent, meaningful crystallization ages by a variety of radioactive isotopic systems. Several such determinations have been made, and often duplicated, in different laboratories. Some of these ages are compiled in Table 6.17, which includes Al_2O_3 contents as a general guide to the chemistry of the sample. Most impact melts correspond closely to the 3.9-b.y. ages for glassy breccias. This correspondence suggests that the

TABLE 6.17. Representative crystallization ages (b.y. ago) of clast-poor impact melts.

Sample	~%Al_2O_3	$^{40}Ar/^{39}Ar$ whole rock	Ref.	Rb-Sr isochron	Ref.
14276	21			3.80±04	1
14310	20	3.82±06	2	3.79±04	1
		3.83±04	6	3.85±06	11
		3.85±05	4	3.86±03	5
		3.85±05	4	3.86±03	12
62295	21	3.84±05	6	3.92±06	5
67747	26			3.94±05	7
67559	28			3.84±05	7
60635	28			3.83±03	8
68415	28	3.75±04	2	3.76±01	9
		3.80±06	10		
		3.80±04	13		
65795	28			3.89±04	8

(1) *Papanastassiou and Wasserburg* (1971); (2) *Stettler et al.* (1973); (3) *Schaeffer et al.* (1976); (4) *York et al.* (1972); (5) *Mark et al.* (1974); (6) *Turner et al.* (1973); (7) *Reinhold et al.* (1985); (8) *Deutsch and Stöffler* (1987); (9) *Papanastassiou and Wasserburg* (1972); (10) *Kirsten et al.* (1973); (11) *Murthy et al.* (1972); (12) *Compston et al.* (1972a,b); (13) *Huneke et al.* (1973).

impact melts were also formed during the period of large, basin-forming impacts. However, some impact melts are around 3.85 b.y. old, almost as "young" as the 3.75-b.y.-old 68415 sample group. Relict clasts in the melts, even if not petrographically detectable, still cause problems with the isotopic systems because they may not be completely melted or outgassed. Relict plagioclase fragments, in particular, can preserve ages of older events.

Origin of clast-poor impact melts. Clast-poor impact melts evidently crystallized from impact-produced silicate liquids that were once entirely above their liquidus temperatures (~1300°-1200° C). Either these melts contained no clastic debris to start with, or virtually all the clastic material present dissolved into the melt before the melt had cooled below the liquidus temperature and had started to crystallize. The slightly heterogeneous textures (resulting from relict, heterogeneously-distributed nucleation sites), the common nonmagmatic chemical compositions (some of which are similar to brecciated rocks and regoliths in the highlands), and the presence of meteoroid siderophile elements precludes a normal magmatic origin and is consistent with an impact-melt origin.

Many impact melts evidently crystallized in units about the size of typical lava flows, because their crystal sizes (and therefore the inferred cooling rates) are similar. Similar clast-poor impact melt rocks are found in some of the larger terrestrial impact craters, where they typically occur with clast-bearing impact-melt rocks stratigraphically above and below them.

Production of an impact-melt sheet more than a few meters thick requires a crater at least a few kilometers in diameter. The correspondence between the chemical composition of lunar impact melts and the compositions of upper crustal rocks or even regoliths suggests that at least some of the impact-melt samples we have are not derived from basin-scale impact melts, but from melts produced in smaller craters. The Apollo 16 group that includes sample 68415, in particular, appears to mimic very closely the composition of upper crustal materials presumed to be present in the Descartes Formation (see section 10.6.5).

6.4.6. Granulitic Breccias and Granulites

Granulitic breccias and *granulites* are coherent crystalline rocks that have apparently been derived by the recrystallization of other rock types by heating at temperatures over 1000° C for long periods of time. The recrystallization textures are characterized by rounded polyhedral grain shapes (i.e., *granoblastic* texture) or presence of small bead-like crystals within larger crystals (*poikiloblastic* texture), and an absence of typical volcanic textures (*Warner et al.,* 1977; *Lindstrom and Lindstrom,* 1986).

Granulitic breccias contain obvious mineral or rock clasts or relicts of clasts, whereas granulites do not. The granulites are much less abundant. Both rock types commonly consist of a mosaic of grains whose boundaries meet at angles of about 120°, a texture produced by thorough recrystallization (*Stewart,* 1975). Mineral compositions are also uniform and equilibrated. All samples are aluminous (>25-29% Al_2O_3); they have a range of Mg/Fe ratios, and they have very low abundances of the incompatible elements that are indicative of a KREEP component. All granulitic breccias and granulites are contaminated with meteoroid siderophile elements, indicating that they were produced in meteoroid impact melts before they were recrystallized.

Both granulitic breccias and granulites have been found at all the Apollo and Luna landing sites. They are also present among the lunar meteorites recovered from Antarctica. Among the Apollo samples, they are generally found as small individual rocks, as clasts in other breccias, or as isolated regolith particles. A small number of larger samples, in the range of 5-10 cm, have also been returned. Their bulk chemical compositions are feldspathic and their incompatible-element concentrations are low. In these respects, they strongly resemble

estimates of the average lunar upper-crustal composition and, for that reason, they may have a greater significance in lunar history than their apparent scarcity would suggest.

Petrography and chemistry of granulitic breccias and granulites. The textures of granulitic breccias and granulites are extremely varied, ranging from granoblastic to poikiloblastic, from homogeneous to heterogeneous, and from coarse- to fine-grained (Figs. 6.38j,k). Granulitic breccias tend to have fine-grained matrices, whereas poikiloblastic breccias tend to be coarse-grained throughout. Generally, the clasts are as recrystallized as the matrices. The distinction between poikiloblastic textures (metamorphic, recrystallized) and poikilitic textures (primary igneous) on the basis of texture alone is all but impossible, and several workers have interpreted some of these samples as igneous (67955: *Hollister,* 1973; 77017: *Ashwal,* 1975).

The granoblastic rocks are dominated by anhedral and equant plagioclase (70-80%); smaller pyroxenes (15-25%) and small anhedral olivines (absent to a few percent) occur within and between the larger plagioclase crystals. The poikiloblastic rocks tend to have blocky plagioclase grains, partially enclosed in larger pyroxene crystals (*oikocrysts*). Ilmenite is rare and generally subhedral. Olivine inclusions commonly form strings or "necklaces" inside large plagioclase crystals; the strings possibly indicate the location of premetamorphic grain boundaries. In most samples, pyroxene and olivine grains are of nearly constant composition and are unzoned (e.g., *McCallum et al.,* 1974; *Ashwal,* 1975; *Bickel et al.,* 1977; *Ryder and Blair,* 1982; *Lindstrom and Lindstrom,* 1986). In contrast, *Norman* (1981) found that the granulitic clasts in fragmental breccia 67016 have ranges of mineral compositions within individual clasts. Among granulitic breccias, the pyroxene and olivine grains have Mg/(Mg + Fe) ratios ranging from less than 0.50 to more than 0.85 (review in *Lindstrom and Lindstrom,* 1986).

Most of the granulitic breccias and granulites, including the poikiloblastic varieties, have major-element chemical compositions similar to anorthositic norites (Fig. *6.23; Warner et al.,* 1977; *Lindstrom and Lindstrom,* 1986). They have low abundances of the KREEP incompatible elements, and are contaminated with meteoroid siderophile elements. There are small but important differences in the major elements, as well as larger variations in the trace elements (Tables A6.26-A6.28). *Lindstrom and Lindstrom* (1986) divided the range of compositions into two groups: ferroan [Mg/(Mg + Fe) <0.7] and magnesian [Mg/(Mg + Fe) >0.7]. Although the major-element data do not show a clear break between the two groups, the element Sc appears to define the groups more precisely. Ferroan granulites have about twice as much Sc as do magnesian granulites. Ferroan granulites also tend to have lower abundances of the incompatible elements. There is no correlation of microscopic texture with composition.

Ages of granulites and granulitic breccias. There are few data on the ages of granulitic rocks. Most age measurements are based on the ^{40}Ar-^{39}Ar system applied to whole-rock samples because the rocks are too fine-grained to permit the mineral separations necessary for Rb-Sr or Sm-Nd internal-isochron age determinations. The available data suggest that the granulitic rocks formed as much as 4.3 b.y. ago, and that for some samples, the ^{40}Ar-^{39}Ar system was reset by heating at around 3.9 b.y. ago (review in *Warner et al.,* 1977). The lack of the KREEP component in the breccias suggests that they were assembled before KREEP became widely dispersed on the lunar nearside, an event or a series of events that had taken place by 3.9 b.y. ago. Granulitic rocks are also common components of feldspathic fragmental breccias, some of which are interpreted to have been assembled by 3.9 b.y. ago (section 6.4.2). The chronological data are much too sparse to establish any systematic differences in age between ferroan and magnesian granulitic rocks.

Origins of granulites and granulitic breccias. The clast-matrix structure of the granulitic breccias and the meteoroid contamination detected in most granulitic rocks demonstrates that they were derived from even older breccias. These older breccias were metamorphosed and recrystallized by prolonged heating to temperatures of more than 1000° C (*Stewart,* 1975; *Bickel et al.,* 1977; *McCallum et al.,* 1974). They appear to have been formed from KREEP-free or KREEP-poor precursor rocks that were present early in lunar history. The prolonged heating necessary to produce the observed textures is different from the effects produced by the intense bombardment about 3.9 b.y. ago, in which prolonged heating is not evident. The effects in the granulitic breccias could have resulted from burial at a depth of several kilometers, possibly during an earlier period of even higher impact flux, accompanied by increased heat flow from the lunar interior (*Warner et al.,* 1977). The younger ages, about 3.9 b.y., might represent cooling (i.e., "freezing in" of the isotopic systems) by excavation from depth during the 3.9-b.y. bombardment period.

The chemical and textural characteristics suggest that some of the granulites may have been derived from distinctive anorthositic norite precursors; most, however, are clearly polymict (*Lindstrom and Lindstrom,* 1986). The bulk chemical compositions of granulites are similar to the average lunar surface

compositions estimated from remotely-sensed data (*Taylor,* 1982), even more so than the Apollo 16 fragmental breccias. There appears to be no difference in regional distribution between the ferroan and magnesian granulitic rocks, but the available orbital measurements are not adequate to preclude regional differences.

6.4.7. Dimict Breccias

Dimict breccias are a relatively rare lunar rock type. They consist of two distinct lithologies combined into a single rock. In most examples, the two lithologies are mutually intrusive, i.e, neither one can be defined as the host rock. The samples generally resemble complex veins or dikes of dark and light components. The dark material is a fine-grained crystalline melt breccia or a nearly clast-free impact melt. The light-colored material is, in most cases, an anorthositic breccia whose main constituents are crushed and shattered (*cataclastic*) anorthosite fragments. Dimict breccias cannot be recognized in samples less than a few centimeters across, because the scale of mutual intrusion is on that order.

All of the few recognized dimict breccias are from the Apollo 16 site. (In an older classification as "black-and-white rocks," some similar Apollo 15 samples were included with them.) The dark crystalline melt breccia is similar in all samples and contains about 21% Al_2O_3 (*McKinley et al.,* 1984). The white portion varies from nearly pure cataclastic ferroan anorthosite to less aluminous breccias (nearly all containing more than 30% Al_2O_3; *McKinley et al.,* 1984; *James et al.,* 1984). They are estimated to be about 3.9 b.y. old, and they may have formed during the period of major bombardment. In these large impact events the melt could have been created and the older anorthositic breccia could have been shattered and remobilized at the same time. Available surface exposure ages suggest that all the dimict breccia samples were ejected about 2 m.y. ago by the South Ray Crater event. Several samples have glass coats.

Petrography and chemistry of dimict breccias. Detailed petrographic and chemical studies, reviewed by *McKinley et al.* (1984) and *James et al.* (1984), provide the basis for characterizing dimict breccias. The mutually intrusive character is best displayed by sample 61015 (Fig. 6.37h). Most of the contacts between the two lithologies are smoothly curving surfaces; some are shear planes. Not all samples can be shown to be mutually intrusive, and in some specimens the melt phase is perhaps more clearly the host.

The dark-colored impact melt lithology is a crystalline melt breccia such as those described in section 6.4.4. In most cases, the melt contains less than 5% of clastic material. The melt is fine-grained and consists of lath-shaped plagioclase crystals, generally equant olivine grains, and pyroxene. A glassy mesostasis, producing an intersertal texture, commonly occurs between the crystals (Fig. 6.381). The few clasts are mainly plagioclase, and lithic clasts are very rare. The melt composition is consistent at about 21% Al_2O_3 with light-REE incompatible-element contents of about 80-90x that of chondritic meteorites. This composition is remarkably constant and is similar to most impact melts found at the Apollo 16 site (Tables A6.20-A6.22). The dimict breccias, however, form a tighter compositional cluster than do the other impact melts of roughly similar composition. In addition, the Apollo 16 dimict breccias have Mg/(Mg + Fe) ratios of about 70, and all those analyzed show evidence of contamination from meteoroid siderophile elements.

The light-colored lithology is composed dominantly of cataclastic anorthosite, containing more than 95% plagioclase. Low-Ca pyroxene is more common than olivine or high-Ca pyroxene. In their chemistry and mineralogy, these anorthosites are similar to the pristine igneous anorthosites described in section 6.3.3. In dimict breccias, the compositional range of the mafic minerals (pyroxene, olivine) extends to more magnesian compositions, however, and this greater range suggests that these light portions are actually polymict. The textures of these anorthosites have been extensively modified by impact processes. The clasts are shattered, and the individual crystals are granulated and have undulatory (strain) extinction under polarized light. The anorthosites have typical low rare earth abundances and lack meteoroid contamination.

Ages of dimict breccias. There are no ages available for the dark crystalline melt breccia phase of dimict breccias, the lithology that offers the best possibilities for age dating. However, by analogy with chemically similar melts, they are presumably about 3.9 b.y. old. Two ^{40}Ar-^{39}Ar determinations for the anorthosites give good ages of 3.92 ± .02 b.y. and 3.91 ± .01 b.y. (*Jessberger et al.,* 1977). These ages probably date the intense heating and deformation of the anorthosites, i.e., the impact event. The original crystallization of the anorthosites presumably took place much earlier.

Origin of dimict breccias. Terrestrial analogs for lunar dimict breccias occur in the basement rocks below large impact craters, where impact-produced melt was injected into hot shocked rock to form complex dike-like bodies (e.g., *Stöffler et al.,* 1979). Such melt-rich dikes have been referred to as *pseudotachylite,* although this term has been loosely applied to a variety of superficially similar lithologies

in both impact and nonimpact settings. The lunar dimict breccias were probably created in the same way.

The tight chemical clustering of the Apollo 16 dimict breccias suggests that they formed in a single impact (*McKinley et al.,* 1984), but the crater of origin cannot yet be identified. Although the samples appear to be associated with South Ray Crater, this crater is too young and too small to be their source. The South Ray Crater event merely excavated them and scattered them around. *James et al.* (1984) suggested that they were produced in a crater of about 50-150 km in diameter. However, *Spudis* (1984) noted that their composition is not that of the local crust and advocated an origin in the Nectaris basin-forming event.

6.4.8. Regolith Breccias

Regolith breccias form at or very near the lunar surface as the result of impacts into regolith (see section 7.6). Such breccias contain identifiable regolith components, such as solar wind gases, glass spherules, or agglutinates (section 7.1.3). They range from friable clods to coherent, glass-bonded breccias. They may represent ancient regoliths, rather than the visible regolith developing at the surface today. Many of them are not merely the lithified equivalents of ordinary regolith. Their agglutinate content is low, and some appear to be coarser-grained than modern lunar soil. They are also less mature than most modern regoliths.

Most regolith breccias were collected from mare surfaces or contain a mare component. These samples are probably younger than 3.9 b.y. old (the earliest time of widespread mare volcanism) and they are not strictly highland samples. However; some regolith breccias contain only or mostly highland material, including 18 specimens from the Apollo 16 landing site (*McKay et al.,* 1986) and several from the Apollo 14 landing site (e.g., 14318, *Kurat et al.,* 1974). Pure highland regolith breccias are rare at other Apollo landing sites, but four examples collected as lunar meteorites in Antarctica (summarized in *Ryder,* 1987) contain only minor mare components.

6.5. SPECTRAL PROPERTIES OF HIGHLAND ROCKS

The dominant mineral in lunar highland rocks is Ca-rich feldspar (anorthite). Pyroxene is usually present in varying amounts and olivine and oxide minerals are minor components. All these mineral components of highland rocks have diagnostic absorption features in the near-infrared. The few highland rock and breccia spectra measured in the laboratory (e.g., *Charette and Adams,* 1977) all have absorption bands due to the presence of low-Ca pyroxene in varying amounts (exceptions are pristine samples of anorthosite, troctolite, and dunite). Several rocks also have distinct feldspar absorption features.

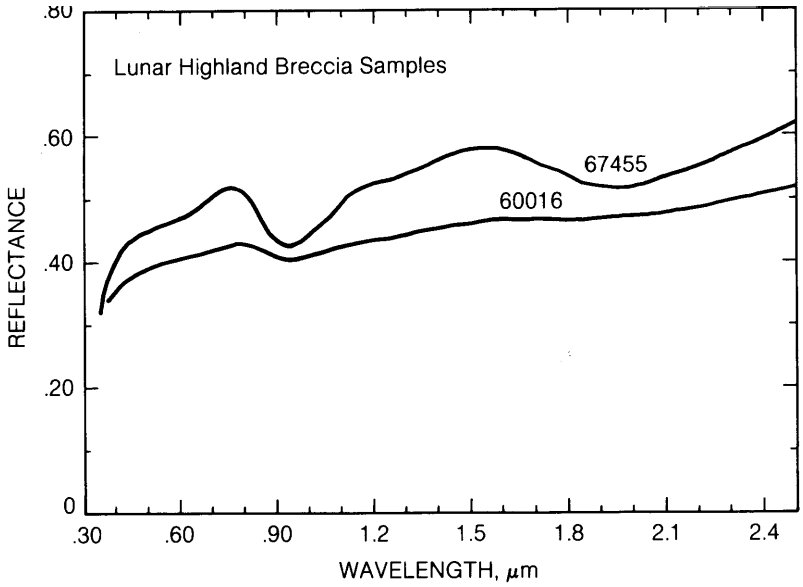

Fig. 6.44. Reflectance spectra as a function of wavelength for two lunar highland breccia samples, fragmental breccia 67455 (upper curve) and regolith breccia 60016 (lower curve). The absorption "valley" at about 0.93 mm reflects the presence of low-Ca pyroxene in the samples. Peaks in the regolith breccia are subdued. A very weak absorption feature at about 1.3 mm is due to crystalline feldspar.

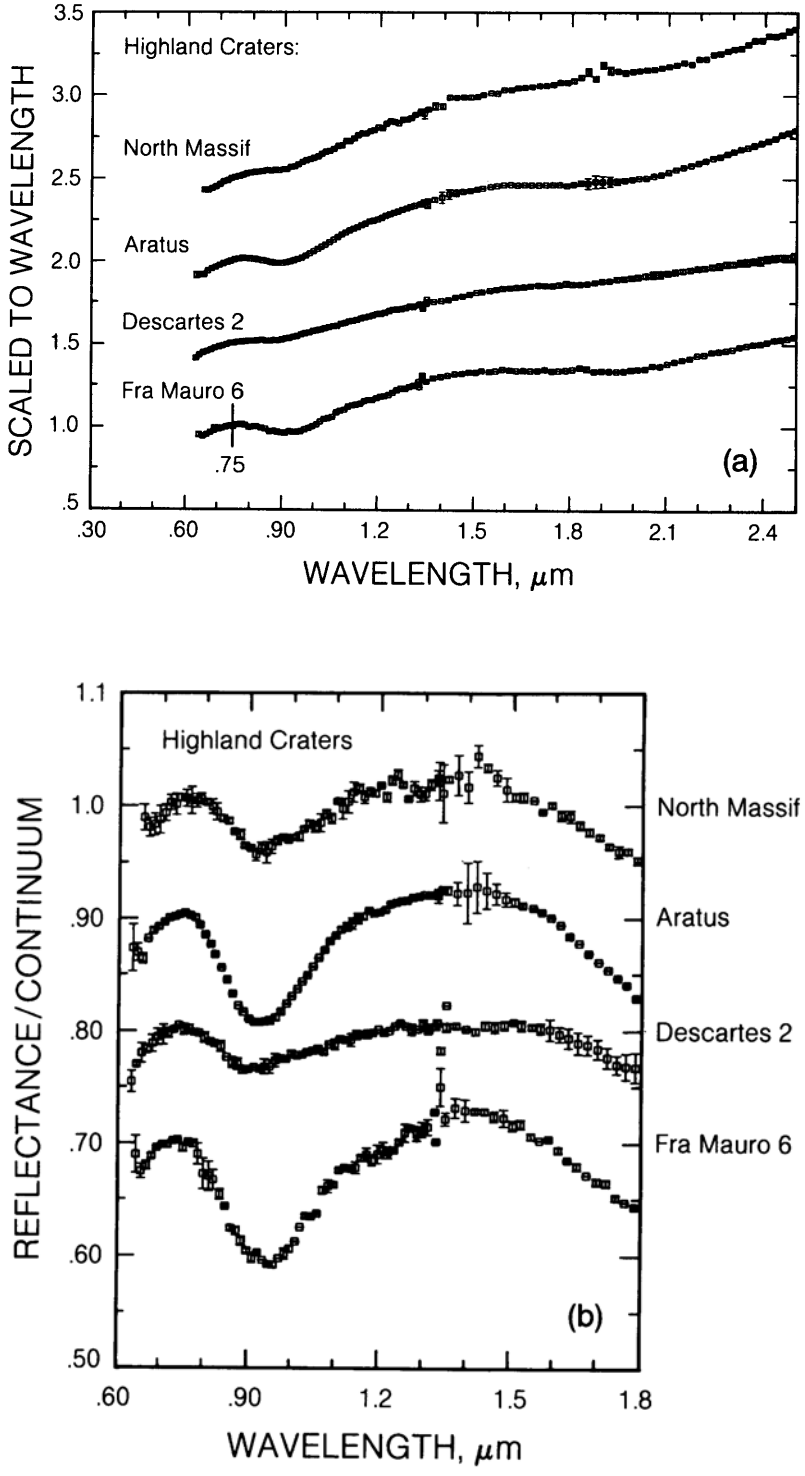

Fig. 6.45. (a) Scaled reflectance spectra, obtained with Earth-based telescopes, for small, fresh lunar highland craters or mountain regions. **(b)** Plots of residual absorption features of the spectra in **(a)** after removal of the sloping background continuum. (The continuum was approximated by a straight line tangent to the spectrum around the 1.0-mm absorption feature). Note the varying amounts of low-Ca pyroxene indicated by the varying depths of the 0.93-mm absorption feature. A similar variability can be (barely) distinguished in the 1.3-mm feature produced by crystal-line feldspar.

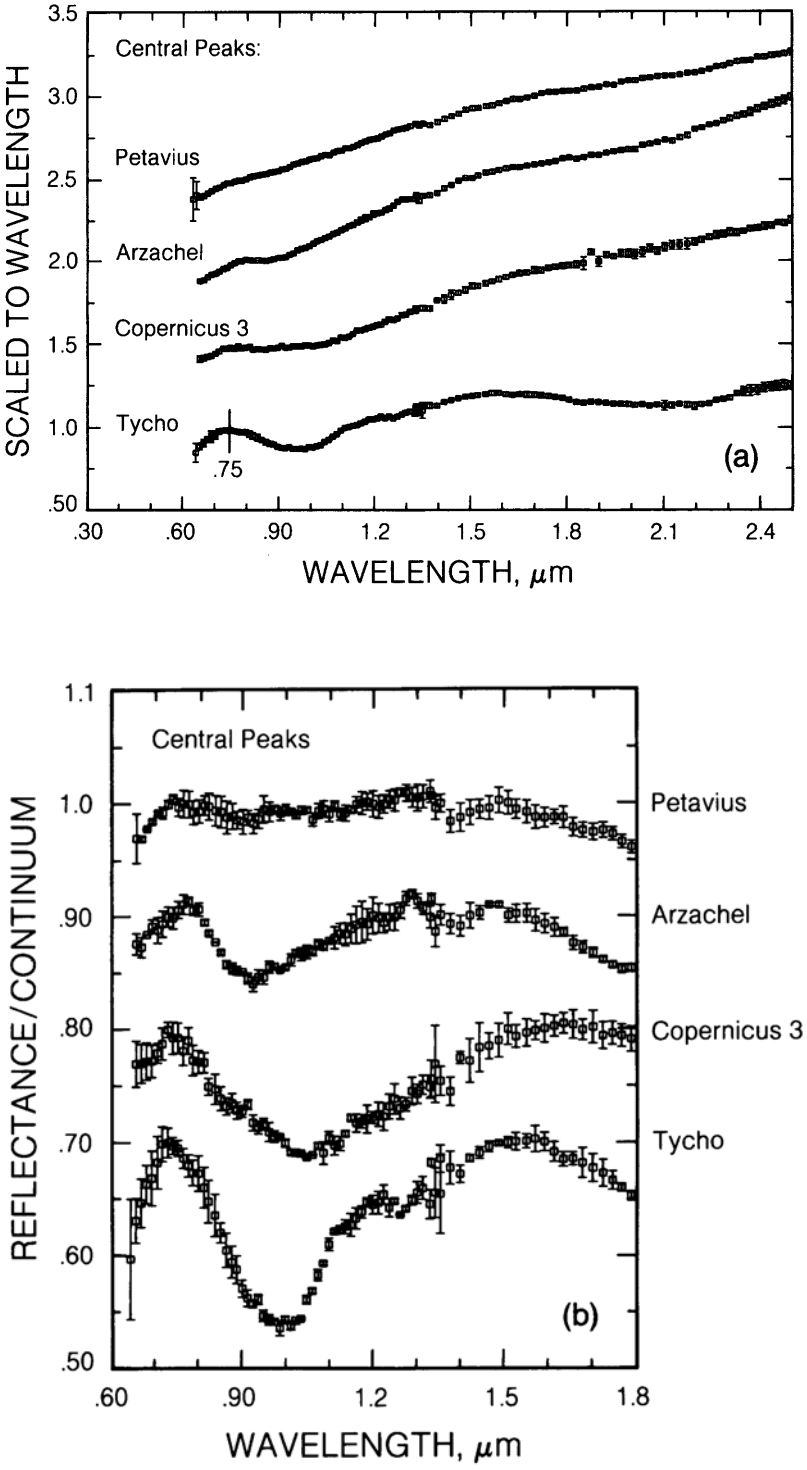

Fig. 6.46. (a) Scaled reflectance, obtained with Earth-based telescopes, of the central peaks of large lunar craters. **(b)** Residual absorption features of the spectra in **(a)** after removal of the sloping background continuum. The diverse spectra indicate that a wide range of different rocks have been uplifted from the deeper lunar crust to form the central peaks. The identified rock types and the major mafic (Fe, Mg-rich) silicate minerals that account for the spectral properties are, from top to bottom: anorthosite in Petavius (plagioclase with few mafic silicates); norite in Arzachel (abundant low-Ca pyroxene); troctolite in Copernicus 3 (abundant olivine); and gabbro in Tycho (abundant high-Ca pyroxene).

In principle, the strength of an infrared absorption band is a function of the abundance of the absorbing mineral, and the spectra can be used to estimate mineral percentages. However, in practice, the absorption bands of various mineral components of highland rocks do not combine in a linear fashion, and the more absorbing pyroxene tends to dominate the spectral character of a highland rock. Furthermore, feldspar that has been shocked to high pressure (e.g., ≥ 250 kbar), as is frequently the case in impact-produced breccias, has a featureless spectrum in the near-infrared (*Adams et al.,* 1979), quite unlike the spectrum of normal unshocked feldspar. The reflectance spectra of typical highland breccias are shown in Fig. 6.44. The bandcenters of the pyroxene features (e.g., the 0.93-μm band) result from the presence of low-Ca pyroxene as the major mafic mineral in these samples. The weaker feature near 1.3 μm is due to the crystalline feldspar component.

A complete survey of the spectral character of lunar samples has not been performed, so that the range of spectral types represented in the Apollo collection is still unknown. However, ground-based observations of the Moon, particularly of areas where fresh materials have been exposed by young impact craters, indicate that lunar materials are very heterogeneous on a large scale (*Pieters,* 1986). Figures 6.45 and 6.46 show near-infrared reflectance spectra (acquired with Earth-based telescopes) of small, fresh lunar craters (3-10 km in diameter) and of the central peaks in larger lunar craters. The small craters (representing excavation of the upper 1-2 km of lunar crust) yield spectra indicative of breccias containing varying amounts of low-Ca pyroxene and feldspar (compare Fig. 6.45b with 6.44). More deep-seated materials (from 5-10-km depth), which have been uplifted to form the central peaks of large craters, have diagnostic features indicating a diverse range of rock types on a regional scale.

APPENDIX: CHEMICAL DATA FOR LUNAR ROCKS

TABLE A6.1. Major-element concentrations in representative lunar mare basalts (wt.%).

	High-Ti				Low-Ti				
	Apollo 11 High-K 10049	Apollo 11 Low-K 10003	Apollo 17 70215	Apollo 17 Orange Gl. 74220	Apollo 12 Pigeonite 12064	Apollo 12 Olivine 12002	Apollo 12 Ilmenite 12051	Apollo 15 Pigeonite 15597	Apollo 15 Olivine 15545
SiO_2	41.0	39.8	37.8	38.6	46.3	43.6	45.3	48.0	45.2
TiO_2	11.3	10.5	13.0	8.8	4.0	2.6	4.7	1.8	2.4
Al_2O_3	9.5	10.4	8.8	6.3	10.7	7.9	10.0	9.4	8.6
Cr_2O_3	0.32	0.25	0.41	0.75	0.37	0.96	0.31	0.48	0.68
FeO	18.7	19.8	19.7	22.0	19.9	21.7	20.2	20.2	22.1
MnO	0.25	0.30	0.27	—	0.27	0.28	0.28	0.30	0.30
MgO	7.03	6.7	8.4	14.4	6.5	14.9	7.0	8.7	10.3
CaO	11.0	11.1	10.7	7.7	11.8	8.3	11.4	10.4	9.8
Na_2O	0.51	0.40	0.36	0.36	0.28	0.23	0.29	0.32	0.31
K_2O	0.36	0.06	0.05	0.09	0.07	0.05	0.06	0.06	0.04
Total	99.97	99.31	99.49	99.00	100.19	100.52	99.54	99.66	99.73
Ref.	a	a	a	a	a	a	a	a	a

	Low-Ti, aluminous					Very-low-Ti				
	Luna 16 21013,8	Apollo 14 14321 Gp. 5	Apollo 14 14053	Apollo 14 14321 Gp. 1	Apollo 14 VHK 14305,390	Apollo 17 70007,296	Apollo 17 78526	Luna 24 24174,7	Luna 24 24109,78	Apollo 15 Green Gl. 15426
SiO_2	—	—	46.4	—	—	—	—	46.0	—	44.1
TiO_2	5.1	2.6	2.6	2.2	2.2	0.4	0.9	1.1	1.3	0.37
Al_2O_3	13.3	11.8	13.6	12.7	13.0	10.3	11.0	12.1	11.6	7.8
Cr_2O_3	0.20	0.46	—	0.37	0.59	0.64	0.83	0.30	0.38	0.33
FeO	19.1	17.5	16.8	16.2	16.0	17.0	17.5	22.1	22.4	21.0
MnO	0.26	0.24	0.26	0.22	0.20	0.26	0.27	0.28	0.26	—
MgO	6.0	10.3	8.5	7.9	9.9	12.0	11.0	6.0	7.0	16.7
CaO	11.7	10.8	11.2	11.2	11.6	9.7	9.9	11.6	12.3	8.4
Na_2O	0.55	0.39	—	0.60	0.41	0.15	0.15	0.26	0.29	0.13
K_2O	0.21	0.01	0.10	0.16	0.80	0.01	0.02	0.02	0.02	0.03
Total	—	—	99.0	—	—	—	—	100.00	—	99.00
Ref.	b	c	a	c	d	e	e	g	f	a

References: (a) *BVSP* (1981); (b) *Ma et al.* (1979); (c) *Dickinson et al.* (1985); (d) *Shervais et al.* (1985b); (e) *Wentworth et al.* (1979); (f) *Ma et al.* (1978); (g) *Laul et al.* (1978b).

TABLE A6.2. Trace-element concentrations in representive lunar mare basalts (μg/g).

	High-Ti				Low-Ti				
	Apollo 11 High-K 10049	Apollo 11 Low-K 10003	Apollo 17 70215	Apollo 17 Orange Gl. 74220	A-12 Pigeonite 12064	A-12 Olivine 12002	A-12 Ilmenite 12051	A-15 Pigeonite 15597	A-15 Olivine 15545
Sc	80.9	—	85.9	—	63.1	38.3	58	—	42.0
V	—	63	50	—	119	175	102	—	168
Ni	—	—	3	—	6.9	63.9	5.9	30.0	68.9
Rb	6.2	0.62	0.36	1.11	1.05	1.04	0.91	1.13	0.75
Sr	161	161	121	209	135	101	148	111	104
Ba	330	108	56.9	76.4	70	67	73.6	52	46.7
La	28.8	15.5	5.22	6.25	6.76	6.02	6.53	4.86	4.93
Ce	82.8	47.2	16.5	19.0	17.5	17	19.2	13	13.9
Nd	62.8	40.0	16.7	17.8	16	12.3	15.4	9.3	9.8
Sm	22.3	14.4	6.69	6.53	5.51	4.24	5.68	3.09	3.29
Eu	2.29	1.81	1.37	1.80	1.16	0.84	1.23	0.84	0.89
Gd	29.3	19.5	10.4	8.52	7.2	5.65	7.89	4.4	4.48
Tb	—	—	—	—	1.27	—	—	0.69	—
Dy	33.4	12.9	12.2	9.40	9.03	6.34	9.05	4.51	4.68
Ho	—	—	—	—	1.72	—	—	0.86	—
Er	30.9	13.6	7.4	5.10	6	3.89	5.57	1.9	2.67
Tm	—	—	—	—	—	—	—	—	—
Yb	20.2	13.2	7.04	4.43	4.59	3.78	5.46	2.13	2.16
Lu	—	1.0	1.03	0.61	0.67	—	—	0.03	0.31
Hf	17.3	—	6.33	—	3.9	2.49	3.1	—	2.2
Zr	—	309	192	185	114	106	128	—	190
Th	4.03	1.1	0.34	—	0.84	0.75	1.0	0.53	0.43
U	0.81	—	0.13	0.16	0.22	0.22	0.26	0.14	0.13
Ref.	a	a	a	a	a	a	a	a	a

TABLE A6.2. (continued).

	Low-Ti, Aluminous					Very-low-Ti				
	Luna 16	Apollo 14 14321	A-14	A-14 14321	A-14 VHK	A-17	A-17	Luna 24	Luna 24	A-15 Green Gl.
	21013,8	Gp.5	14053	Gp.1	14305,390	70007,296	78526	24174,7	24109,78	15426
Sc	61	62	55	59	55	54	50	57	47	—
V	62	121	—	102	120	202	226	140	177	—
Ni	—	—	14	—	70	—	—	30	80	—
Rb	—	—	2.19	—	—	—	—	—	—	0.58
Sr	—	—	98	—	—	—	—	110	—	41
Ba	320	53	146	159	500	—	—	50	—	18
La	19.8	3.4	13.0	25	12.0	0.88	1.2	2.87	2.0	—
Ce	56	8	34.5	65	31	—	—	8.6	—	3.8
Nd	48	6.3	21.9	40	20	—	—	7.0	—	2.2
Sm	15.4	2.3	6.56	12.5	6.10	0.70	1.0	2.10	1.9	0.76
Eu	3.74	0.71	1.21	1.45	0.90	0.24	0.28	0.83	0.58	0.21
Gd	—	—	8.59	—	—	—	—	—	—	0.91
Tb	2.8	0.67	—	2.5	1.4	0.20	0.28	0.45	0.44	—
Dy	18	4.5	10.5	14.9	—	1.5	1.9	2.9	2.8	1.1
Ho	—	—	—	—	—	—	—	0.71	—	—
Er	—	—	6.51	—	—	—	—	—	—	0.8
Tm	—	—	—	—	0.75	—	—	—	—	—
Yb	9.1	3.2	6	8.3	5.35	1.1	1.4	2.00	1.9	0.93
Lu	1.28	0.61	—	1.21	0.82	0.19	0.23	0.31	0.29	0.14
Hf	11.6	1.9	9.8	8.7	3.7	0.62	0.6	1.4	1.1	—
Zr	—	70	215	320	—	—	—	50	—	—
Th	1.9	0.4	2.1	2.3	1.6	—	—	0.20	—	—
U	—	—	0.59	—	—	—	—	—	—	—
Ref	b	c	a	c	d	e	e	g	f	a

References: (a) *BVSP* (1981); (b) *Ma et al.* (1979); (c) *Dickinson et al.* (1985); (d) *Shervais et al.* (1985b); (e) *Wentworth et al.* (1979); (f) *Ma et al.* (1978); (g) *Laul et al.* (1978b).

TABLE A6.3. Composition (wt.%) of varieties of pristine lunar glasses arranged in sequence of increasing Ti-abundance.*

	1	2	3	4	5	6	7	8	9	10	11	12	13
SiO_2	48.0	45.5	43.9	46.0	45.1	45.2	44.8	46.0	43.7	45.3	44.3	44.1	42.9
TiO_2	0.26	0.38	0.39	0.40	0.41	0.43	0.45	0.55	0.57	0.66	0.91	0.97	3.48
Al_2O_3	7.74	7.75	7.83	7.92	7.43	7.44	7.14	9.30	7.96	9.60	6.89	6.71	8.30
Cr_2O_3	0.57	0.56	0.39	0.55	0.55	0.54	0.54	0.58	0.46	0.40	n.a.	0.56	0.59
FeO	16.5	19.7	21.9	19.1	20.3	19.8	19.8	18.2	21.5	19.6	20.2	23.1	22.1
MnO	0.19	0.22	0.24	n.a.	0.22	0.22	0.24	0.21	n.a.	0.26	0.23	0.28	0.27
MgO	18.2	17.2	16.9	17.2	17.6	18.3	19.1	15.9	17.0	15.0	19.5	16.6	13.5
CaO	8.57	8.65	8.44	8.75	8.43	8.15	8.03	9.24	8.44	9.40	7.40	7.94	8.50
Na_2O	n.d.	n.d.	n.d.	n.d.	n.d.	n.d.	0.06	0.11	n.d.	0.27	0.10	n.d.	0.45
K_2O	n.d.	n.d.	n.d.	n.d.	n.d.	n.d.	0.03	0.07	n.d.	0.04	n.d.	n.d.	n.d.

	14	15	16	17	18	19	20	21	22	23	24	25
SiO_2	40.8	40.5	39.4	38.5	37.9	38.8	37.3	37.2	35.6	35.6	34.0	33.4
TiO_2	4.58	6.90	8.63	9.12	9.12	9.30	10.0	12.5	13.8	15.3	16.4	16.4
Al_2O_3	6.16	8.05	6.21	5.79	5.63	7.62	5.68	5.69	7.15	4.81	4.6	4.6
Cr_2O_3	0.41	0.63	0.67	0.69	0.65	0.66	0.63	0.86	0.77	n.a.	0.92	0.84
FeO	24.7	22.3	22.2	22.9	23.7	22.9	23.7	22.2	21.9	23.7	24.5	23.9
MnO	0.30	0.25	0.28	n.a.	n.a.	0.29	n.a.	0.31	0.25	n.a.	0.31	0.30
MgO	14.8	12.6	14.7	14.9	14.9	11.6	14.3	14.5	12.1	13.0	13.3	13.0
CaO	7.74	8.64	7.53	7.40	7.41	8.55	7.62	7.04	7.89	6.49	6.9	6.27
Na_2O	0.42	0.39	0.41	0.38	0.36	0.39	0.31	0.28	0.49	0.50	0.23	0.05
K_2O	0.10	n.d.	0.04	n.d.	n.d.	n.d.	n.d.	0.29	0.12	n.d.	0.16	0.12

* These are the most primitive compositions within each of the groups (*Delano,* 1986).

n.a. = not analyzed; n.d. = not detected.

(1) Apollo 15 green C; (2) Apollo 15 green A; (3) Apollo 16 green; (4) Apollo 15 green B; (5) Apollo 15 green D; (6) Apollo 15 green E; (7) Apollo 14 green B; (8) Apollo 14 VLT; (9) Apollo 11 green; (10) Apollo 17 VLT (*R.D. Warner et al.,* 1979b); (11) Apollo 17 green (preliminary); (12) Apollo 14 green A; (13) Apollo 15 yellow; (14) Apollo 14 yellow; (15) Apollo 17 yellow; (16) Apollo 17 orange; (17) Apollo 17 orange (74220-type); (18) Apollo 15 orange; (19) Apollo 17 orange; (20) Apollo 11 orange; (21) Apollo 14 orange; (22) Apollo 15 red; (23) Apollo 14 red (preliminary); (24) Apollo 14 black; (25) Apollo 12 red (*Marvin and Walker,* 1978).

TABLE A6.4. Abundances of Ni (μg/g) and MgO (wt.%) in pristine lunar glasses demarcated according to their TiO_2 abundances* (after *Delano,* 1986).

	Ni(μg/g)	MgO (wt.%)	Ni/Mg ($\times 10^3$)
($TiO_2 \leq 1.0$ wt.%)			
Apollo 15 green A	170	17.2	1.64
Apollo 15 green B	150	17.2	1.45
Apollo 15 green E	170	18.3	1.54
Apollo 14 green B	185	19.1	1.61
Apollo 14 VLT	125	15.9	1.30
Apollo 11 green	135	17.0	1.32
Apollo 17 VLT	150	15.0	1.66
Apollo 17 green	188	19.5	1.60
Apollo 14 green A	115	16.6	1.15
Apollo 15 green C	90	18.2	0.82
($TiO_2 \geq 3.5$ wt.%)†			
Apollo 15 yellow	85	13.5	1.04
Apollo 14 yellow	82	14.8	0.92
Apollo 17 yellow	55	12.6	0.72
Apollo 17 orange	46	14.7	0.52
Apollo 17 orange (74220)	70	14.9	0.78
Apollo 17 orange	33	11.6	0.47
Apollo 11 orange	30	14.3	0.35
Apollo 14 orange	30	14.5	0.34
Apollo 15 red	<50	12.1	<0.69
Apollo 14 black	≤22	13.3	≤0.27

* Precision for Ni is typically ±10 μg/g with a detection limit of about 20 μg/g.

† No volcanic glasses have been found having TiO_2 abundances between 1.0 wt.% and 3.5 wt.%.

TABLE A6.5. Abundances of trace elements in the Apollo 17 pristine orange glass.

Element	Abundance	Reference	Element	Abundance	Reference
Li	12 μg/g	1,2,3,4	Ba	78 μg/g	3,4,6,15
F	60 μg/g	1,5	La	6.2 μg/g	1,4,8,9,15
P	200 μg/g	1,6	Ce	19 μg/g	1,3,4,9,15
S	725 μg/g	4,6,7	Pr	2.5 μg/g	1
Cl	20.2 μg/g	1	Nd	17.5 μg/g	1,3,4,15
K	625 μg/g	1,3,4,6	Sm	6.7 μg/g	1,3,4,8,9,15
Sc	46 μg/g	1,8,9	Eu	1.85 μg/g	1,3,4,9,15
V	131 μg/g	1,6	Gd	8.8 μg/g	1,3,4,15
Co	61 μg/g	1,6,8,9	Tb	1.6 μg/g	1,9
Ni	72 μg/g	1,4,6,9,10,11	Dy	9.3 μg/g	1,3,4,15
Cu	26 μg/g	1,6	Ho	1.9 μg/g	1
Zn	210 μg/g	1,4,6,8,10,11,12	Er	5.1 μg/g	1,3,4,15
Ga	16 μg/g	1,12	Yb	4.2 μg/g	1,3,4,8,9,15
Ge	230 ng/g	1,8,10,11,12	Lu	0.60 μg/g	1,3,4,9,15
As	15 ng/g	1	Hf	5.8 μg/g	1,9,13,14
Se	430 ng/g	10.11	Ta	1.2 μg/g	1,9
Br	88 ng/g	10	W	83 ng/g	1
Rb	1.2 μg/g	1,3,4,6,10	Re	0.04 ng/g	10,11
Sr	195 μg/g	1,3,4,6,	Os	0.04 ng/g	11
Y	46 μg/g	1,4,6	Ir	0.03 ng/g	8,11
Zr	185 μg/g	1,3,4,6,13,14	Au	1.1 ng/g	1,8,10,11,12
Nb	14 μg/g	1,4,6	Hg	7 ng/g	2,8
Pd	1.4 ng/g	11	Tl	9 ng/g	10,11
Ag	83 ng/g	10,11	Pb	2.5 μg/g	16
Cd	150 ± 100 ng/g	8,10,11,12	Bi	1 ng/g	10,11
In	20 ng/g	8,11,12	Th	480 ng/g	9,16
Te	60 ng/g	8,10	U	135 ng/g	1,2,4,8,10,11,16,17
Cs	60 ng/g	1,10			

References: (1) *Wänke et al.* (1973); (2) *Jovanovic and Reed* (1974); (3) *Philpotts et al.* (1974); (4) *Rhodes et al.* (1974); (5) *Goldberg et al.* (1976); (6) *Duncan et al.* (1974); (7) *Gibson and Andrawes* (1978a); (8) *Krähenbühl* (1980); (9) *Blanchard and Budahn* (1978); (10) *Morgan et al.* (1974); (11) *Morgan and Wandless* (1979); (12) *Wasson et al.* (1976); (13) *Ehmann and Chyi* (1974); (14) *Hughes and Schmitt* (1985); (15) *Masuda et al.* (1974); (16) *Tatsumoto et al.* (1973); (17) *Fleischer and Hart* (1974).

TABLE A6.6. Abundances of trace elements in the Apollo 15 pristine green glasses.

Element	Abundance	Reference	Element	Abundance	Reference
F	42 ± 21 μg/g	1	Ba	17 μg/g	4,7
S	330 μg/g	2	La	1.3 μg/g	3,4,7
K	145 μg/g	7	Ce	4.0 μg/g	4,7
Sc	39 μg/g	3,4,6	Pr	0.58 μg/g	4
V	163 μg/g	3,4	Nd	2.4 μg/g	4,7
Co	77 μg/g	3,4,5,6	Sm	0.82 μg/g	3,4,7
Ni*	170 μg/g	3,4,6	Eu	0.24 μg/g	3,4,7
Cu	5.4 μg/g	4	Gd	1.2 μg/g	4,7
Zn	16 μg/g	5,6	Tb	0.19 μg/g	3,4
Ga	4.2 μg/g	4.6	Dy	1.4 μg/g	4,7
Ge	58 ng/g	5,6	Ho	0.29 μg/g	4
Se	69 ng/g	5	Er	0.9 μg/g	4,7
Br	40 ng/g	5	Tm	0.15 μg/g	4
Rb	0.40 μg/g	4,5	Yb	0.97 μg/g	3,4,7
Sr	28 μg/g	8	Lu	0.15 μg/g	3,4,7
Y	8.7 μg/g	4	Hf	0.6 μg/g	3,4,7
Zr	24 μg/g	4,7	W	0.14 μg/g	4
Nb	1.8 μg/g	4	Re	0.02 ng/g	5
Ag	8.9 ng/g	5	Ir	0.29 ng/g	5,6
Cd	58 ng/g	5,6	Au	0.4 ng/g	5,6
In	1.1 ng/g	5,6	Tl	1.13 ng/g	5
Sn	0.13 μg/g	4	Pb	1.0 μg/g	4
Sb	0.12 ng/g	5	Bi	0.38 ng/g	5
Te	3.3 ng/g	5	Th	0.2 μg/g	4
Cs	24 ng/g	5	U	44 ± 7 ng/g	8

* Ni varies among the Apollo 15 green glasses. The variation is a result of magmatic fractionation processes. Refer to Table A6.4 for additional information.

References: (1) *Goldberg et al.* (1976); (2) *Gibson and Andrawes* (1978a); (3) *Ma et al.* (1981b); (4) *S.R. Taylor et al.* (1973a); (5) *Ganapathy et al.* (1973); (6) *Chou et al.* (1975); (7) *Wiesmann and Hubbard* (1975); (8) *Fleischer and Hart* (1974).

TABLE A6.7. Abundances of trace elements (μg/g) in the Apollo 15 pristine yellow/brown glass from two INAA investigations conducted at Oregon State University by R.A. Schmitt and coworkers.

Element	Ma et al. (1981b)	Delano (1986)
Sc	43.5 ± 0.2	41.5 ± 3.3
V	116 ± 2	118 ± 4
Co	65 ± 2	64 ± 5
La	9.4 ± 0.8	7.9 ± 0.9
Ce	—	23 ± 6
Sm	6.8 ± 0.4	6.0 ± 0.2
Eu	1.51 ± 0.02	1.51 ± 0.15
Tb	1.40 ± 0.06	—
Yb	4.6 ± 0.1	2.9 ± 0.5
Lu	0.62 ± 0.03	—
Hf	5.0 ± 0.3	4.8 ± 1.1
Ta	0.69 ± 0.05	0.70 ± 0.11

TABLE A6.8. References for surface-correlated volatile elements enriched in pristine lunar glasses.

B (1)	Br (3,12,16)
C (20)	Ag (6,12,19)
N (23)	Cd (6–8,12,14,18,19)
F (2–5)	In (6,7,14,19)
Na (6–8,18,21)	Sb (6,19)
S (2,8–10,18,21)	Te (14,19)
Cl (2,3,18,21,24)	I (16)
Ar (11,23)	Xe (16)
K (6,24)	Ir (14)
Cu (2,5)	Au (6,7,14,19)
Zn (2,5–9,12–14,18,19,21)	Hg (14,17)
Ga (2,5,7)	Ti (2,12,13,19,22)
Ge (6,7,14,19)	Pb (2,8,13,15,22)
Se (19)	Bi (6)

References: (1) *Meyer and Schonfeld* (1977); (2) *Meyer et al.* (1975); (3) *Jovanovic and Reed* (1974); (4) *Goldberg et al.* (1975, 1976); (5) *Wänke et al.* (1973); (6) *Chou et al.* (1975); (7) *Wasson et al.* (1976); (8) *Cirlin et al.* (1978); (9) *Butler and Meyer* (1976), *Butler* (1978); (10) *Grant et al.* (1974), *Thode and Rees* (1976), *Gibson and Andrawes* (1978a), *Ding et al.* (1983); (11) *Alexander et al.* (1980); *Chou et al.* (1973, 1974), *Eberhardt et al.* (1973), *Eugster et al.* (1980), *Huneke* (1978), *Podosek and Huneke* (1973), *Schaeffer and Husain* (1973), *Lakatos et al.* (1973); (12) *Morgan et al.* (1974); (13) *Allen et al.* (1975); (14) *Krähenbühl* (1980); (15) *Nunes et al.* (1974b); *Silver* (1974a,b), *Tatsumoto et al.* (1973), *Tera and Wasserburg* (1976), *Cirlin and Housley* (1977); (16) *Eugster et al.* (1980); (17) *Jovanovic and Reed* (1979); (18) *Cirlin and Housley* (1979); (19) *Morgan and Wandless* (1979, 1984); (20) *Epstein and Taylor* (1973), *Gibson and Moore* (1973c), *Sato* (1979), *Wszolek et al.* (1973); (21) *Clanton et al.* (1978); (22) *Reed et al.* (1977); (23) *Barraclough and Marti* (1985); (24) *Carusi et al.* (1972).

TABLE A6.9. Bulk compositions of some monomict KREEP rocks, the KREEP-like 14303 granite clast, a typical VHA basalt (probably not really a basalt, but an impact melt breccia), and an average composition for high-K KREEP breccias.

	Na_2O (wt.%)	MgO (wt.%)	Al_2O_3 (wt.%)	SiO_2 (wt.%)	K_2O (wt.%)	CaO (wt.%)	TiO_2 (wt.%)	FeO* (wt.%)	Li (μg/g)	P (μg/g)	S (μg/g)	Sc (μg/g)
15382 basalt	0.87	7.83	16.9	52.5	0.53	9.43	1.90	9.02	—	2400	—	19
15386 basalt	0.77	9.34	15	50.8	0.61	9.60	2.06	10.4	27.2	3054	900	22
15405 QMD clasts	0.89	3.60	12.6	56.4	2.06	8.10	1.85	13.5	40.9	1700	—	30
14303 'granite' clast	1.25	3.30	18.5	58	3.6	8.8	0.75	5.57	—	—	—	10.7
72275 basalt clasts	0.42	8.42	14.3	49.2	0.33	10.4	1.10	14.0	—	—	—	50
High-K KREEP breccias	0.86	10.6	16.6	47.9	0.83	9.51	1.67	10.6	56	3400	1100	23
61156 VHA (basalt ??)	0.40	9.59	23	45	0.108	13.4	0.63	7.83	10.5	960	1200	9.4

	V (μg/g)	Cr (μg/g)	Mn (μg/g)	Co (μg/g)	Ni (μg/g)	Cu (μg/g)	Zn (μg/g)	Ga (μg/g)	Ge (ng/g)	As (ng/g)	Se (ng/g)	Br (ng/g)
15382	60	1780	940	17	23	—	2.6	—	47	—	72	142
15386	62	2280	1200	23	12.5	—	3.5	6.2	61	—	—	—
15405	33	1370	1400	7.9	<2	—	5.6	—	250	—	96.5	170
14303	23	550	480	14.1	<60	—	—	9.2	—	—	—	—
72275	120	2940	1630	35	60	—	4	3.14	—	—	—	—
High-K KREEP	43	1300	1080	33	20	20	3.6	7.5	40	—	—	—
61156 (VHA)	—	917	780	59	690	6.6	5.0	4.5	1750	370	—	—

	Rb (μg/g)	Sr (μg/g)	Y (μg/g)	Zr (μg/g)	Nb (μg/g)	Ru (ng/g)	Pd (ng/g)	Ag (ng/g)	Cd (ng/g)	In (ng/g)	Sb (ng/g)	Te (ng/g)
15382	15.4	189	—	1068	—	—	<0.6	0.44	87	2.66	0.17	1.0
15386	16.2	187	—	970	—	—	—	—	10	1.8	—	—
15405	34	172	—	1620	—	—	<0.9	2.33	14	23	0.88	5.7
14303	113	230	—	1020	—	—	—	—	—	—	—	—
72275	13	85.6	—	623	—	—	—	—	—	—	—	—
High-K KREEP	22	200	300	1700	80	500	—	—	15	1.2	—	—
61156 (VHA)	2.43	153	62.3	299	16.3	—	59	—	—	—	—	—

TABLE A6.9. (continued)

	Cs (ng/g)	Ba (μg/g)	La (μg/g)	Ce (μg/g)	Nd (μg/g)	Sm (μg/g)	Eu (μg/g)	Gd (μg/g)	Tb (μg/g)	Ho (μg/g)	Yb (μg/g)	Lu (μg/g)
15382	725	702	73.8	215	115	31.4	2.75	42.9	6.2	—	21.6	3.07
15386	800	744	70.8	179	114	33	2.56	45.4	5.3	—	21.3	2.84
15405	1055	1695	217	558	328	87.5	2.65	110	17.3	—	60.4	8.42
14303	2200	2080	57	147	93	22.8	3.30	—	4.7	6.7	18	2.6
72275	450	398	49	130	81.8	22.8	1.61	—	4.7	5.8	13	1.8
High-K KREEP	1200	1200	110	270	180	49	3.0	57	10.0	14	36	5.0
61156 (VHA)	150	207	21.5	53.4	33.1	9.6	1.32	11.9	2.10	3.3	6.65	0.90

	Hf (μg/g)	Ta (μg/g)	W (μg/g)	Re (ng/g)	Os (ng/g)	Ir (ng/g)	Au (ng/g)	Tl (ng/g)	Pb (μg/g)	Bi (ng/g)	Th (μg/g)	U (μg/g)
15382	29.9	3.1	—	0.0089	0.018	0.0132	0.0033	3.2	5.94	290	10.3	3.37
15386	23.6	2.4	—	—	—	0.061	0.22	—	—	—	10.0	2.80
15405	47.9	11.6	—	0.0525	0.007	0.175	0.15	4.8	14	260	56.1	11.0
14303	21	3.1	—	—	—	<2.8	—	—	—	—	17.9	5.6
72275	17.0	1.51	—	—	—	<2.0	—	—	—	—	5.6	1.35
High-K KREEP	37	4.0	2.0	—	—	0.1	0.1	—	—	—	18	5.0
61156 (VHA)	7.3	0.83	0.56	2.6	—	23	22	—	2.1	—	3.24	0.86

* All Fe is reported as FeO, albeit a small proportion may actually be Fe-metal.

References: 15382, 15386 and 15405, literature compilations of *Ryder* (1985); 14303, *Warren et al.* (1983b); 72275, *Stoeser et al.* (1974), *Blanchard et al.* (1975a), *Ryder et al.* (1977), *Salpas et al.* (1987); high-K KREEP, *Warren and Wasson* (1979a), except see *Warren et al.* (1983c) regarding Cs; 61156, numerous references, all cited in *Ryder and Norman* (1980). Note: except for a few REE, if an element is not in this table, no data have been published for that element in these particular samples.

TABLE A6.10. Selected ratios between incompatible elements, which are characteristically enriched, in approximately these proportions, in KREEP.

	K	P	Rb	Zr	Cs	Ba	La	Gd	Tb	Lu	Hf	Ta	U
Be	880	440	2.8	220	0.15	150	14	7.3	1.3	0.64	4.7	0.51	0.64
Li	190	94	0.61	47	0.033	33	3.1	1.6	0.28	0.14	1.0	0.11	0.14
K	1	0.49	0.0032	0.25	0.00017	0.17	0.016	0.0083	0.0014	0.00072	0.0054	0.00058	0.00072
P	2.0	1	0.0065	0.50	0.00035	0.35	0.032	0.017	0.0029	0.0015	0.011	0.0012	0.0015
Rb	310	150	1	77	0.055	55	5.0	2.6	0.45	0.23	1.7	0.18	0.23
Y	23	11	0.073	5.7	0.0040	4.0	0.37	0.19	0.033	0.017	0.12	0.013	0.017
Zr	4.1	2	0.013	1	0.00071	0.71	0.065	0.034	0.0059	0.0029	0.022	0.0024	0.0029
Nb	86	43	0.28	21	0.015	15	1.4	0.71	0.13	0.063	0.46	0.050	0.063
Cs	5800	2800	18	1400	1	1000	92	48	8.3	4.2	31	3.3	4.2
Ba	5.8	2.8	0.018	1.4	0.0010	1	0.092	0.048	0.0083	0.0042	0.031	0.0033	0.0042
La	63	31	0.20	15	0.011	10.9	1	0.52	0.091	0.045	0.34	0.036	0.045
Ce	26	13	0.082	6.3	0.0044	4.4	0.41	0.21	0.037	0.019	0.14	0.015	0.019
Nd	38	19	0.12	9.4	0.0067	6.7	0.61	0.32	0.056	0.028	0.21	0.022	0.028
Sm	140	69	0.45	35	0.024	24	2.2	1.2	0.20	0.102	0.76	0.082	0.102
Gd	120	60	0.39	30	0.021	21	1.9	1	0.18	0.088	0.65	0.070	0.088
Tb	690	340	2.2	170	0.12	120	11	5.7	1	0.50	3.7	0.40	0.50
Ho	490	240	1.6	120	0.086	86	7.9	4.1	0.71	0.36	2.6	0.29	0.36
Yb	190	94	0.61	47	0.033	33	3.1	1.6	0.28	0.14	1.0	0.11	0.14
Lu	1380	680	4.4	340	0.24	240	22	11.4	2.0	1	7.4	0.80	1.00
Hf	190	92	0.59	46	0.032	32	3.0	1.5	0.27	0.14	1	0.11	0.14
Ta	1700	850	5.5	420	0.30	300	28	14	2.5	1.3	9.3	1	1.25
W	3400	1700	11	850	0.60	600	55	29	5.0	2.5	19	2.0	2.5
Th	380	190	1.2	94	0.067	67	6.1	3.2	0.56	0.28	2.1	0.22	0.28
U	1400	680	4.4	340	0.24	240	22	11	2.0	1.0	7.4	0.80	1

To read table, find element for numerator along top row, and denominator element along leftmost column; e.g., the K/Be ratio is 880. Ratios involving Be are based on *Wänke et al.* (1977). All other ratios are based on average high-K KREEP (Table A6.9).

TABLE A6.11. Bulk compositions of some monomict ferroan anorthosites.

	Na_2O (wt.%)	MgO (wt.%)	Al_2O_3 (wt.%)	SiO_2 (wt.%)	CaO (wt.%)	FeO* (wt.%)	Li (μg/g)	C (μg/g)	N (μg/g)	F (μg/g)	P (μg/g)	S (μg/g)	K (μg/g)
15363	0.288	3.85	28.0	45.3	16.8	4.76	—	—	—	—	—	—	107
15415	0.364	0.26	35.6	44.5	20.4	0.21	—	9	—	—	40	<100	122
60015	0.392	0.53	35.0	43.9	19.0	0.33	<6	20	23	18	65	27	54
62236	0.215	3.55	30.1	44.2	17.6	3.67	—	—	—	—	—	—	111
62237	0.205	5.11	29.6	41.9	16.3	5.89	—	—	—	—	—	—	104
65315	0.303	0.25	34.9	44.3	19.1	0.31	—	—	—	14	40	—	58
67455c	0.42	1.31	32.3	44.9	18.1	2.62	3.47	—	—	—	<100	—	235

	Cl (μg/g)	Sc (μg/g)	Ti (μg/g)	V (μg/g)	Cr (μg/g)	Mn (μg/g)	Co (μg/g)	Ni (μg/g)	Cu (μg/g)	Zn (μg/g)	Ga (μg/g)	Ge (ng/g)	As (ng/g)
15363	—	9.3	700	—	650	520	6.0	9	—	6.6	4.5	—	—
15415	150	0.42	120	—	20	45	0.21	9	58	0.26	3.1	1.2	4.1
60015	<8	0.60	100	4.7	38	75	0.8	—	0.5	—	—	—	—
62236	—	5.8	290	—	490	430	7.9	4.0	—	1.7	2.9	10	—
62237	—	4.1	100	—	400	540	12.2	6	—	1.6	2.8	3.3	—
65315	104	0.39	72	—	20	59	0.58	1.4	2.1	93	3.25	—	2
67455c	—	—	780	—	100	300	—	2.5	—	2.7	—	1.8	—

	Se (ng/g)	Br (ng/g)	Rb (μg/g)	Sr (μg/g)	Y (μg/g)	Zr (μg/g)	Nb (μg/g)	Pd (ng/g)	Ag (ng/g)	Cd (ng/g)	In (ng/g)	I (ng/g)	Sb (ng/g)
15363	—	—	<6	140	—	<100	—	—	—	—	—	—	—
15415	0.23	2.3	0.17	188	—	—	—	—	1.73	0.57	0.18	—	0.067
60015	—	<0.09	0.12	173	0.4	0.11	0.2	—	—	—	—	—	—
62236	—	—	—	145	—	—	—	—	—	0.79	1.2	—	—
62237	—	—	—	133	—	—	—	—	—	3.9	<1.1	—	—
65315	—	930	0.17	167	<0.3	15	<0.2	—	—	—	—	47	—
67455c	56	48	0.88	116	—	—	—	<0.31	0.41	1.45	0.73	—	0.11

TABLE A6.11. (continued).

	Te (ng/g)	Cs (ng/g)	Ba (μg/g)	La (μg/g)	Ce (μg/g)	Nd (μg/g)	Sm (μg/g)	Eu (μg/g)	Gd (μg/g)	Tb (μg/g)	Dy (μg/g)	Yb (μg/g)	Lu (μg/g)
15363	—	<200	<60	0.31	0.52	—	0.131	0.88	—	0.042	—	0.28	0.045
15415	2.1	26	6.2	0.15	0.33	0.19	0.053	0.81	0.056	0.0085	0.054	0.034	0.0043
60015	—	—	9	0.13	0.63	0.35	0.07	0.82	0.06	—	—	0.02	0.003
62236	—	—	<60	0.18	0.68	—	0.093	0.61	—	—	—	0.15	0.022
62237	—	—	6	0.19	0.47	0.28	0.078	0.61	—	0.017	—	0.101	0.016
65315	—	15	4.8	0.12	—	—	0.04	0.74	—	—	0.056	0.026	0.004
67455c	<0.24	56	13.6	—	0.92	0.67	0.228	0.80	0.324	—	0.394	0.260	0.030

	Hf (μg/g)	Ta (μg/g)	W (μg/g)	Re (ng/g)	Os (ng/g)	Ir (ng/g)	Au (ng/g)	Tl (ng/g)	Pb (μg/g)	Bi (ng/g)	Th (ng/g)	U (ng/g)
15363	<0.15	<0.12	—	0.057	0.95	1.03	0.061	—	—	—	<100	—
15415	0.014	—	0.026	0.00084	—	<0.010	0.117	0.09	0.23	0.097	4	2
60015	0.011	<0.01	—	—	—	—	—	—	0.19	—	3.7	1.3
62236	—	—	—	0.007	—	0.02	0.006	—	—	—	<10	<40
62237	0.035	—	—	—	—	0.07	0.08	—	—	—	<12	4.3
65315	0.49	—	0.019	—	—	—	—	—	—	—	—	<0.6
67455c	—	—	—	<0.0003	<0.012	0.001	0.0025	0.32	—	0.25	—	5.7

* All Fe is reported as FeO, albeit a small proportion may actually be Fe-metal.

References: 15363, *Warren et al.* (1987); 15415, compilation by *Ryder* (1985); 60015, 62236 and 62237, references listed by *Ryder and Norman* (1980), plus, for 62237, *Haskin et al.* (1981); 65315, *Wänke et al.* (1974); 67455c (clast 67455,32), *Lindstrom et al.* (1977a) and *Hertogen et al.* (1977).

TABLE A6.12. Bulk compositions of some monomict Mg-rich rocks.

	Na_2O (wt.%)	MgO (wt.%)	Al_2O_3 (wt.%)	SiO_2 (wt.%)	CaO (wt.%)	TiO_2 (wt.%)	FeO* (wt.%)	Li (μg/g)	F (μg/g)	P (μg/g)	S (μg/g)
15455c	0.44	6.9	27.0	47.7	14.8	0.10	2.91	7.2	—	220	—
61224,6	0.91	12.8	13.2	50.7	11.6	0.40	9.91	—	—	—	—
67435c	0.14	31.7	18.3	37.5	6.7	0.05	5.55	—	—	—	—
67915c	1.25	3.0	11.8	56.0	9.2	5.1	12.3	—	—	[40]	—
72415	0.13	44.8	1.3	40.3	1.1	0.03	11.7	—	—	200	44
76535	0.23	20.0	19.9	43.0	10.8	0.05	5.0	3.0	9	100	<100
77215	0.40	12.5	15.0	51.1	9.1	0.33	9.9	12.3	—	480	—

	K (μg/g)	Cl (μg/g)	Sc (μg/g)	V (μg/g)	Cr (μg/g)	Mn (μg/g)	Co (μg/g)	Ni (μg/g)	Zn (μg/g)	Ga (μg/g)	Ge (ng/g)
15455c	540	—	5.3	—	1180	376	27.2	21	1.4	—	33
61224,6	140	—	20.8	—	1990	1230	23.6	8.3	4.0	3.0	4.3
67435c	110	—	1.9	101	510	800	57	1230	—	—	—
67915c	4500	—	32	3	200	1240	6.6	—	—	—	—
72415	24	<6	4.3	50	2300	940	55	200	5	—	150
76535	233	<0.8	1.94	—	730	500	27.6	44	1.2	—	1.7
77215	1440	—	15.6	—	2470	1270	28.0	2	3.1	4.4	15.2

	Se (ng/g)	Br (ng/g)	Rb (μg/g)	Sr (μg/g)	Y (μg/g)	Zr (μg/g)	Nb (μg/g)	Ag (ng/g)	Cd (ng/g)	In (ng/g)	I (ng/g)
15455c	8.3	35	1.1	131	—	70	—	1.7	1.0	0.05	—
61224,6	—	—	—	160	—	[170]	—	—	4.1	<0.6	—
67435c	—	—	—	—	—	—	—	—	—	—	—
67915c	—	—	—	260	—	300	—	—	—	—	—
72415	5.0	18	0.036	10	1.1	2.6	0.3	15	0.6	—	0.9
76535	4.1	3.2	0.22	114	—	17	—	0.12	0.60	—	1.1
77215	77	42	4.38	104	—	175	—	0.62	4.9	0.30	—

TABLE A6.12. (continued).

	Sb (ng/g)	Te (ng/g)	Cs (ng/g)	Ba (μg/g)	La (μg/g)	Ce (μg/g)	Nd (μg/g)	Sm (μg/g)	Eu (μg/g)	Gd (μg/g)	Tb (μg/g)	Dy (μg/g)
15455c	0.079	2.6	126	90	4.8	11.2	6.8	1.81	1.21	2.21	0.35	2.59
61224,6	—	—	—	32	1.47	4.3	<9	0.87	1.43	—	0.22	—
67435c	—	—	—	18	1.3	—	—	0.63	0.33	—	0.10	0.6
67915c	—	—	—	340	22.7	54	37	11.0	2.42	—	2.2	15
72415	1.6	0.3	14	4.1	0.15	0.37	—	0.08	0.061	—	0.017	0.11
76535	0.014	0.28	14	33	1.51	3.8	2.3	0.61	0.70	0.73	—	0.80
77215	0.121	1.0	180	176	8.5	24.6	14.2	4.0	1.05	6.6	0.89	7.1

	Yb (μg/g)	Lu (μg/g)	Hf (μg/g)	Ta (μg/g)	Re (ng/g)	Ir (ng/g)	Au (ng/g)	Tl (ng/g)	Pb (μg/g)	Bi (ng/g)	Th (ng/g)	U (ng/g)
15455c	1.43	0.216	0.67	0.14	0.004	0.01	0.016	0.054	0.59	0.14	630	170
61224,6	1.06	0.16	0.55	0.16	0.013	0.148	0.079	—	—	—	190	<600
67435c	0.38	0.053	0.37	[0.02]	—	—	—	—	—	—	—	—
67915c	8.5	1.27	8.6	2.2	—	—	—	—	—	—	3900	1000
72415	0.074	0.012	0.10	—	0.05	1.6	1.4	0.041	—	0.8	<150	5
76535	0.56	0.079	0.41	—	0.0012	0.0054	0.0025	0.012	—	0.037	190	54
77215	4.5	0.68	3.4	0.37	0.008	0.071	0.045	0.61	1.08	0.13	1840	600

* All Fe is reported as FeO, although a small proportion may actually be Fe-metal.

References: 15455c (norite), references compiled by *Ryder* (1985); 61224,6 (gabbro), *Marvin and Warren* (1980); 67435c (spinel troctolite), *Prinz et al.* (1973), *Ma et al.* (1981a); 67915c (sodic ferrogabbro), *Taylor et al.* (1980); 72415 (dunite), references compiled by *Ryder and Norman* (1979) — principally *Laul and Schmitt* (1975b) and *Higuchi and Morgan* (1975); 76535 (troctolite), references compiled by *Ryder and Norman* (1979), plus *Garg and Ehmann* (1976); 77215 (norite), references compiled by *Ryder and Norman* (1979), including those for 77075 and 77077, which are pieces of the same norite as 77215.

TABLE A6.13. Bulk compositions of some monomict "evolved" lithologies.

	Na_2O (wt.%)	MgO (wt.%)	Al_2O_3 (wt.%)	SiO_2 (wt.%)	K_2O (wt.%)	CaO (wt.%)	TiO_2 (wt.%)	FeO* (wt.%)
12033;507	1.9	0.3	12.1	73	5.6	1.6	0.7	3.2
12073c	2.14	0.35	32.3	48.3	0.25	15.8	0.13	1.1
14047c	1.56	2.77	28.1	48.1	0.21	14.8	0.42	4.2
14321c	0.52	0.07	12.5	74.2	8.1	8.8	0.33	5.6
67975c	0.39	9.8	11.3	—	1.1	13.4	3.53	14.5
	Sc (μg/g)	V (μg/g)	Cr (μg/g)	Mn (μg/g)	Co (μg/g)	Ni (μg/g)	Zn (μg/g)	Ga (μg/g)
12033;507	—	—	<600	<500	<8	<21	—	7
12073c	1.97	—	98	140	7.1	71	1.16	17
14047c	9.2	—	274	480	6.7	9.5	3.2	12
14321c	3.0	—	17	175	0.94	4.9	1.9	9.0
67975c	38.8	58	1770	1710	14.8	<80	—	—
	Ge (ng/g)	Br (ng/g)	Rb (μg/g)	Sr (μg/g)	Zr (μg/g)	Cd (ng/g)	Cs (ng/g)	Ba (μg/g)
12033;507	—	—	—	—	—	—	—	8000
12073c	32	<1200	—	750	310	—	—	620
14047c	67	—	—	380	470	9.6	220	600
14321c	87	—	167	64	660	34	5700	2160
67975c	—	—	25	159	—	—	410	1200
	La (μg/g)	Ce (μg/g)	Nd (μg/g)	Sm (μg/g)	Eu (μg/g)	Tb (μg/g)	Dy (μg/g)	Yb (μg/g)
12033;507	—	—	—	—	—	—	—	—
12073c	16.2	35	16	4.6	8.4	0.87	5.8	2.7
14047c	27.7	64	40	10.7	5.9	2.17	11.3	7.2
14321c	44.3	117	59	17.3	1.17	4.3	31.5	32.2
67975c	88	240	—	45	—	—	—	—
	Lu (μg/g)	Hf (μg/g)	Ta (μg/g)	Re (ng/g)	Ir (ng/g)	Au (ng/g)	Th (ng/g)	U (ng/g)
12033;507	—	—	—	—	—	—	—	—
12073c	0.37	1.4	0.18	0.037	0.11	—	1.2	0.4
14047c	1.13	6.8	0.64	0.061	0.76	0.074	2.8	0.71
14321c	5.1	13.9	8.3	<0.018	0.047	0.035	65	23.4
67975c	—	—	—	—	—	—	—	—

* All Fe is reported as FeO, although a small proportion may actually be Fe-metal.

References: 12033,507 (felsite), *Warren et al.* (1987); 12073c (alkali anorthosite), *Reed et al.* (1971b), *Warren et al.* (1981); 14047c (alkali anorthosite), *Warren et al.* (1983a); 14321c (granite), *Warren et al.* (1983b); 67975c (alkali gabbronorite), *James et al.* (1987).

TABLE A6.14. Major element oxides of the bulk average of matrix samples of fragmental breccias (wt.%).

	Bulk Avg.	67015(i)	67015(ii)	67016(i)	67016(ii)	67115	67455(i)	67455(ii)	72275	14063(i)	14063(ii)
SiO_2	45.1	(44.8)	46.0	45.3	44.8	44.8	44.5	45.2	48.3	—	45.0
TiO_2	0.32	0.51	0.50	0.44	0.35	0.24	0.21	0.20	1.0	1.5	1.64
Al_2O_3	30.4	29.0	29.5	30.01	28.2	31.2	30.8	30.6	16.3	22.0	21.6
Cr_2O_3	0.06	0.08	0.06	—	0.08	0.06	0.05	0.05	0.35	0.18	0.19
FeO	3.34	4.26	3.65	3.57	3.94	2.60	3.58	4.37	11.9	7.0	6.9
MnO	0.05	—	0.05	0.05	0.05	0.04	0.05	0.06	0.17	0.08	0.09
MgO	3.14	5.1	3.9	3.5	4.4	3.0	2.83	3.4	10.3	—	10.7
CaO	17.0	15.7	15.4	16.9	16.7	17.8	17.1	18.1	11.0	13.1	12.6
Na_2O	0.48	0.51	0.52	0.48	0.49	0.51	0.44	0.38	0.44	0.84	0.86
K_2O	0.04	—	0.08	0.06	0.04	0.08	0.02	0.03	0.25	0.17	0.17
P_2O_5	—	—	—	0.07	0.02	0.02	0.03	0.01	—	—	0.25
Σ	99.9	(100)	99.7	100.4	99.1	100.4	99.6	102.4	100.0	—	100.0
Mg/(Mg+Fe) atom ratio	0.63	0.68	0.66	0.64	0.67	0.67	0.58	0.58	0.61	—	0.73

Bulk average: *James* (1981); 67015(i): *Marvin et al.* (1987); 67015(ii): *Wänke et al.* (1975); 67016(i): *Duncan et al.* (1973); 67016(ii): *Wänke et al.* (1976); 67115: *Rose et al.* (1973a); 67455(i): *Lindstrom et al.* (1977a); 67455(ii): *Wänke et al.* (1973); 72275: *Blanchard et al.* (1975a); 14063(i): *Laul et al.* (1972a); 14063(ii): average of 3 chips, *Rose et al.* (1972).

TABLE A6.15. Sr, incompatible elements, and transition metals in matrix samples of fragmental breccias (μg/g).

	67015(i)	67015(ii)	67016(i)	67016(ii)	67115	67455(i)	67455(ii)	72275	14063(i)	14063(ii)
Li	—	—		—	4.8	4.0	—	—		23
Rb	—	1.42	1.1	—	1.2	0.38	—	—		5.0
Sr	189	195	191	162	180	174	130	—		208
Zr	—	55	62.5	46	22		17	—		300
Hf	2.18	1.67		1.16			0.40	16.5		
Ba	83	86.2	67	60	50	23.6	40	—	360	315
Th	1.07	0.7		0.53			—	6.1		
U	0.28	0.22		—			0.053	—	1.1	
Ta	0.34	0.21		0.18			0.40	1.7		
La	5.83	4.90		3.76			1.35	50.5	26.5	28
Ce	15.7	11.6		10.1		3.32	3.7	130		
Nd	—	7.9		7.6		2.08				
Sm	2.71	2.14		1.64		0.64	0.60	24.6	10.6	
Eu	1.18	1.16		1.06		0.91	0.84	1.57	2.4	
Gd	—	2.6		—			0.90			
Tb	0.58	0.47		0.33				4.9		
Dy	—	3.1		2.11		1.11	0.92	—		
Ho	—	0.7		—			0.2	—		
Er	—	1.9		—		0.68	0.63	—		
Tm	—	—		—						
Yb	2.19	1.79		1.35	0.6	0.60	0.52	15.0	10	8.2
Lu	0.305	0.24		0.19		0.08	0.085	2.01	1.4	
Sc	6.7	7.5		6.6	23		6.8	44.7	13.6	15.3
Cr	—	483		540	—		420	—		
Co	16.9	9.7		10.4	6.2		10.0	30.4	20	16
Ni	187	110	36.7	100	62		28	75		110
Mn		392					420			

67015(i): *Marvin et al.* (1987); 67015(ii); *Wänke et al.* (1975); 67016(i): *Duncan et al.* (1973); 67016(ii): *Wänke et al.* (1975); 67115: *Rose et al.* (1973a); 67455(i): *Lindstrom et al.* (1977a); 67455(ii): *Wänke et al.* (1973); 72275: *Blanchard et al.* (1975a); 14063(i): *Laul et al.* (1972a); 14063(ii): average of three chips, *Rose et al.* (1972).

TABLE A6.16. Volatile and siderophile elements in matrix samples of fragmental breccias (ng/g).

	67015	67016(i)	67016(ii)	67115	67455(i)	67455(ii)	72275	14064
Zn	3600		9100	4200	5000	8500	2700	3100
Ga	4100	—				3400	406	—
Ge	30	—	11.6	18.7	17.4	—		32.9
Cd	—	—	0.56	2.31	1.37		13	16.7
In	—	—	0.46	0.22	1.09			—
Ir	—	10	2.31	1.59	1.08	4	2.26	1.63
Au	1.1	4.8	0.455	0.164	0.355	1	0.82	0.128

67015: *Wänke et al.* (1975); 67016(i): *Wänke et al.* (1976); 67016(ii): *Hertogen et al.* (1977); 67455(i): *Hertogen et al.* (1977); 67115: *Hertogen et al.* (1977); 67455(ii): *Wänke et al.* (1973); 72275: *Morgan et al.* (1975); 14064: *Gros et al.* (1976).

TABLE A6.17. Major oxides in glassy melt breccias and impact glasses (wt.%).

	60095 sphere	64455 coat	63566 glass with clasts	68815 breccia matrix	15017 shell	15255 coat
SiO_2	44.8	44.8	45.1	45.1	49.9*	46.4
TiO_2	0.48	0.44	0.22	0.49	—	1.80
Al_2O_3	25.9	25.8	29.2	27.2	14.9	14.1
Cr_2O_3	—	0.15	0.09	0.10	0.44	0.44
FeO	5.7	5.6	4.7	4.8	14.3	14.7
MnO	—	0.06	0.06	0.06	0.20	0.22
MgO	7.9	8.1	4.6	5.9	10.7	11.1
CaO	14.6	14.3	16.0	15.5	9.7	10.7
Na_2O	0.32	0.36	0.57	0.42	0.44	0.38
K_2O	0.12	0.13	0.06	0.14	0.21	0.16
P_2O_5	—	—	—	0.18	—	0.11
Σ	99.8	99.7	100.6	99.9	—	100.1
Mg/(Mg+Fe) atom ratio	0.71	0.72	0.64	0.69	0.57	0.57

* This SiO_2 value suspiciously high.

60095, 63566, 64455: *See et al.* (1986); 68815: *LSPET* (1973a); 15017: *Wänke et al.* (1972); 15255: *Nava et al.* (1977).

TABLE A6.18. Incompatible elements and transition metals in glassy melt breccias and impact glasses (μg/g).

	63566	64455 coat	15017 shell	15255 rind	60095
Li	—	—	—	18.0	—
Rb	4.7	3.1	—	7.49	—
Sr	200		135	134	—
Zr	260		437	501	—
Nb	—				—
Hf	6.37	4.3	10.3		4.90
Ba	—		300	383	200
Th	2.72		3.93		2.60
U	0.78		—		0.99
Pb	—		—		—
Ta	0.74				0.68
La	19.2	12.6	28.2	—	14.4
Ce	51.2	32.1	77.7	71.5	41.7
Nd	32.5	21.0	56	53.9	—
Sm	8.5	5.9	12.7	15.0	7.0
Eu	1.19	1.11	1.42	1.67	1.22
Gd	10.5	7.4	—		—
Tb	1.76	1.14	2.79		1.27
Dy	11.0	7.5	16.8	20.0	—
Ho	2.48	1.6	3.7		—
Er	6.6	4.5	—	12.2	—
Tm	0.97	—	—		—
Yb	6.04	3.92	9.49	11.0	4.3
Lu	0.80	0.56	1.32	1.54	0.71
Sc	7.7	7.0	29.9		7.1
Cr	830	1000	3000		780
Co	53.0	48.2	40.6		40
Ni	990	760	260		412
Mn	578		1530		—

63566: *Borchardt et al.* (1986); 64455: *Haskin et al.* (1973); 15017: *Ganapathy et al.* (1973); 15255: *Nava et al.* (1977); 60095: *Morris et al.* (1986).

TABLE A6.19. Volatile and siderophile elements in glassy melt breccias and impact glasses.

	60095	64455 coat	15017 shell
μg/g			
Cs	64	144	273
Zn	1550	2400	5800
ng/g			
Ge	306	500	241
Cd	1.8	5.2	4.2
Ir	25.4	40.6	9.1
Au	7.11	12.7	2.9

64455 coat, 60095: *Ganapathy et al.* (1974); 15017: *Ganapathy et al.* (1973).

TABLE A6.20. Major element oxides in crystalline melt breccias (impact melt breccias) (wt.%).

	14066	14068	15445	60315	60335	62235	66095	67475	73215	72395	77135	76015
SiO_2	49.2	47.2	44.6	46.8	46.3	47.1	44.9	44.4	46.4	46.9	46.2	46.4
TiO_2	1.0	1.39	1.47	1.38	0.57	1.19	0.72	0.36	0.70	1.75	1.53	1.53
Al_2O_3	15.9	13.3	16.7	17.1	25.0	18.9	23.7	30.9	20.6	18.1	17.8	17.8
Cr_2O_3	0.17	—	—	0.24	0.15	—	—	0.03	0.25	0.20	0.21	—
FeO	10.1	10.0	9.8	8.6	4.6	9.5	7.5	2.9	7.3	9.3	9.1	9.1
MnO	0.12	0.13	0.14	0.11	0.08	0.13	0.08	0.04	0.10	0.12	0.13	0.12
MgO	11.4	17.6	16.0	13.4	7.7	10.2	8.9	2.6	11.6	12.0	12.4	12.7
CaO	10.1	8.38	10.0	10.5	14.2	11.6	13.5	17.2	11.9	1.3	11.1	11.1
Na_2O	0.84	0.75	—	0.61	0.62	0.42	0.45	0.60	0.50	0.69	0.69	0.69
K_2O	0.94	0.59	—	0.49	0.27	0.33	0.16	0.04	0.20	0.29	0.27	0.26
P_2O_5	—	0.55	0.21	0.48	0.21	0.39	0.25	<0.02	—	0.33	0.30	0.29
Σ	98.8	99.8	99.0	99.7	99.7	99.8	100.2	99.1	99.6	101.0	99.7	100.0
Mg/ (Mg+Fe) atom ratio	0.67	0.76	0.74	0.74	0.75	0.66	0.68	0.62	0.74	0.70	0.71	0.71

14066: *Wänke et al.* (1972); 14068: *Hubbard et al.* (1972a); 15445: *Ridley et al.* (1973); 60315, 60335: *Rose et al.* (1973a,b); 62235: *Hubbard et al.* (1973); 66095: *Duncan et al.* (1973); 67475: *Lindstrom et al.* (1977a); 73215: *Blanchard et al.* (1976); 72395: *Wänke et al.* (1975); 77135: *Rhodes et al.* (1974); 76015: *Simonds* (1975).

TABLE A6.21. Incompatible and transition metal trace elements in crystalline melt breccias (impact melt breccias) (μg/g).

	14066	14068	15445	60315	60335	62235	66095	67475	73215	72395	77135	76015
Li			14.1					5.33		24.8		21.6
Rb		14.5	3.56	9.80	7.1	9.32	11.0	0.672		6.21	6.2	6.57
Sr		139	160	156		161		216		167	174	177
Zr			315							570	508	507
Hf	30		10.5		7.0		5.0		9.5	13.7		—
Ba		780	237	445		568	150	48.5		386		358
Th							2.2		4.1	6.05		5.56
U		3.47	0.800	2.05		2.53	1.0			2.06		1.96
Ta	3.6						0.44		1.4	1.82		—
La	75	—	22.1	45.5	22.0	60.1	18.5	—	27.0	39.7		33.4
Ce	200	157	57.6	113	58.0	153	50.0	6.66	70	95		84.9
Nd		93.4	35.7	71.3	36.4	94.3		4.22		61		54.0
Sm		28.1	10.1	20.1	10.0	27.1	8.8	1.21	12.5	16.8		15.2
Eu	2.76	2.01	1.85	1.89	1.38	2.03	1.63	1.28	1.43	1.93		1.99
Gd		29.1	11.9	23.8		32.2		1.43		21.1		18.9
Tb	7.8				2.03		1.3		2.6	3.7		—
Dy	39	35.1	13.2	26.3	13.9	35.0	9.4	1.68		23.2		19.9
Ho					2.9		1.3			5.1		—
Er			7.71	15.5		21.2	4.1	1.06		13.9		11.7
Tm							—					—
Yb	25.1	20.0	6.90	14.0	6.88	18.7	4.9	1.01	9.1	12.4		10.8
Lu	3.6		1.02		0.95		0.90	0.140	1.30	1.88		1.30
Sc	20				7.9		6.8	—	14.7	18.7		—
Cr	1190		1750	1477	910	1309	860	200	1700	1400		1188
Co	30				16		44		25.3	31.1		
Ni	—				300		710		65	260	62	135
Mn	920		1085		550		550	300	800	930		950

14066: *Wänke et al.* (1972); 14068: *Hubbard et al.* (1972a); 15445: *Ridley et al.* (1973); 60315, 62235: *Hubbard et al.* (1973); 60335: *Haskin et al.* (1973); 66095: *Brunfelt et al.* (1973a,b); 67475, *Lindstrom et al.* (1977a); 73215: *Blanchard et al.* (1976); 72395: *Wänke et al.* (1977); 77135: *Rhodes et al.* (1974); 76015: *Simonds* (1975).

TABLE A6.22. Volatile, chalcophile, and siderophile elements in crystalline melt breccias (impact melt breccias) (ng/g).

	15445	65015	62295	66095	73215	77135	76315
Cs	177	405	530	160	161	250	250
Zn	2.5	0.48	16.5	50.5	2.0	3.3	3.1
Se	91	245	186	314	72	144	100
Te	4.7	3.25	12.5	20	5.9	8.84	4.04
Ge	630	380	642	2140	175	618	346
Cd	5.3	9.25	4.9	328	18	3.5	5.0
Br	96	22	60	825	26	45	48
Ir	6.21	11.6	3.58	16.6	4.9	10.5	5.42
Re	0.668	1.16	0.336	2.13	0.37	1.06	0.507
Au	6.02	10.2	3.10	17.9	2.7	6.45	3.21

15445: *Gros et al.* (1976); 65015, 62295, 66095: *Krähenbühl et al.* (1973); 73215: *Higuchi and Morgan* (1975); 77135, 76315: *Morgan et al.* (1974).

TABLE A6.23. Major element oxides in clast-poor impact melts (wt.%).

	14276	14310(i)	14310 (ii)	62295	64455	68415(i)	68415(ii)
SiO_2	47.6	47.2	47.8	44.7	48.5	45.4	45.3
TiO_2	1.20	1.24	1.11	0.68	0.65	0.32	0.29
Al_2O_3	21.3	20.1	21.5	20.3	22.4	28.6	28.7
Cr_2O_3	0.26	0.18	0.25		0.16	—	0.14
FeO	7.9	8.4	7.6	6.3	5.5	4.3	4.1
MnO	0.12	0.11	0.10	0.10	0.07	0.06	0.05
MgO	7.1	7.9	7.5	15.1	9.3	4.4	4.4
CaO	13.2	12.3	12.9	11.8	13.4	16.4	16.2
Na_2O	0.72	0.63	0.68	0.43	0.57	0.41	0.50
K_2O	0.48	0.49	0.48	0.08	0.245	0.06	0.09
P_2O_5	0.40	0.34	0.43	0.13	—	0.07	0.06
Σ	100.3	98.9	100.4	99.6	100.8	100.0	99.8
Mg/(Mg + Fe) atom ratio	0.62	0.63	0.64	0.81	0.75	0.65	0.66

14276, 14310(ii): *Rose et al.* (1972); 14310(i): *Hubbard et al.* (1972a); 62295: *Hubbard et al.* (1973); 64455: *Haskin et al.* (1973); 68415(i) *LSPET* (1973a); 68415(ii) *Rose et al.* (1973a,b).

TABLE A6.24. Incompatible and transition metal trace elements in clast-poor impact melts (μg/g).

	14276	14310(i)	14310(ii)	62295	64455	68415(i)	68415(ii)
Li	21		23			5.1	5.1
Rb	13	13	15	4.6	6.0	1.704	1.9
Sr	165	193	175	139		182.4	140
Zr	20	842	610			97.5	72
Hf					7.8	2.4	
Ba	700	617	780	187		76.2	70
Th		11				1.26	
U				0.882		0.32	
La	59	56.4	59	18.6	21.1	6.8	
Ce		144		45.9	56.0	18.3	
Nd		87.0		29.0	34.0	10.9	
Sm		24.0		8.30	9.8	3.09	
Eu		2.15		1.18	1.23	1.11	
Gd		2.81		10.1	—	3.78	
Tb		—		—	1.97	—	
Dy		32.7		10.8	12.2	4.18	
Ho		—		—	2.7	—	
Er		19.7		6.85	6.7	2.57	
Tm		—		—		—	
Yb	16	18.4	16	6.06	6.6	2.29	2.0
Lu				0.879	0.96	0.34	
Sc	20		25		7.8		8.2
Cr				773	1110	599	
Co	9.0		17.0		31.1		11
Ni	113	64	120		540		184

14276, 14310(ii): *Rose et al.* (1972); 14310(i): *Hubbard et al.* (1972a); 62295: *Hubbard et al.* (1973); 64455: *Haskin et al.* (1973); 68415(i) *Hubbard et al.* (1974); 68415(ii): *Rose et al.* (1973a,b).

TABLE A6.25. Volatile, chalcophile, and siderophile elements in clast-poor impact melts (ng/g).

	14310(i)	14310(ii)	62295	64455	68415
Cs	540	—	530	280	80
Zn	2300	1500	1650	2200	1450
Se	120	—	186	190	98
Te	4	—	12.5	2.5	4.7
Ge	130	90	642	62	73
Cd	2.6	8.4	4.9	5.3	0.85
Br	235	—	50	1200	140
Ir	10.6	7.8	3.6	2.25	4.58
Re	1.02	—	0.336	0.284	0.434
Au	4.31	—	3.10	1.56	2.65

14310(i): *Morgan et al.* (1972b); 14310(ii): *Baedecker et al.* (1972); 62295, 68415: *Krähenbühl et al.* (1973); 64455: *Ganapathy et al.* (1974).

TABLE A6.26. Major element oxides in granulitic breccias and granulites (wt.%).

	67955	67415	79215	67215	77017	78155	15418
SiO_2	45.0	44.6	44.8	—	44.1	45.6	44.2
TiO_2	0.27	0.32	0.5	0.33	0.41	0.27	0.27
Al_2O_3	27.7	26.0	27.4	27.4	26.6	25.9	26.6
Cr_2O_3	0.11	0.08	0.11	0.11	0.13	0.14	—
FeO	3.8	4.6	4.9	6.4	6.2	5.8	6.7
MnO	0.05	0.06	0.06	—	0.08	0.10	0.10
MgO	7.7	7.8	7.4	5.3	6.1	6.3	5.1
CaO	15.5	15.1	14.4	16.2	15.4	15.2	16.0
Na_2O	0.40	0.52	0.58	0.30	0.30	0.33	0.27
K_2O	0.05	0.04	0.12	—	0.06	0.08	0.02
P_2O_5	0.03	0.03	—	—	0.03	0.04	0.03
Σ	100.6	99.2	100.3	—	99.4	99.8	99.3
Mg/(Mg+Fe) atom ratio	0.78	0.75	0.73	0.60	0.64	0.66	0.58

67955, 77017, 78155, 15418: *Hubbard et al.* (1974); 67415: *Lindstrom et al.* (1977a); 79215: *Blanchard et al.* (1972); 67215: *Lindstrom and Lindstrom* (1986).

TABLE A6.27. Incompatible and transition metal elements in granulitic breccias and granulites (μg/g).

	67955	67415	79215	67215	77017	78155	15418
Li	5.1	6.06	—	—	4.4	5.2	—
Rb	0.884	0.964	—	—	1.31	2.06	—
Sr	169.1	177	—	150	141.5	146.7	150
Zr	124		—	25	59.1	—	<50
Hf	3.1		1.2	0.80	1.6	—	0.40
Ba	61.9	61.2	—	16	49.0	58.8	15
Th	1.03		0.32	0.96	—	1.013	0.049
U	0.38		—	0.032	0.22	0.284	<0.10
Ta			0.125	—	—		0.031
La	4.45		2.65	1.58	3.48	4.02	0.756
Ce	11.3	9.62	6.8	4.3	8.90	10.2	2.05
Nd	7.09	6.23	—	3.0	5.56	6.29	1.6
Sm	2.02	1.84	1.19	0.855	1.60	1.81	0.499
Eu	0.973	1.11	0.84	0.726	0.79	0.874	0.698
Gd	2.57		—	—	2.01	2.32	—
Tb	—		0.28	0.199	—	—	0.149
Dy	2.81	2.75	—	—	2.35	2.64	—
Ho	—		—	—	—	—	—
Er	1.79	1.77	—	—	1.50	1.69	—
Tm	—		—	—	—	—	—
Yb	1.74	1.75	1.37	0.752	1.50	1.73	0.628
Lu	0.25	0.255	0.24	0.125	—	0.259	0.102
Sc	—	—	8.14	12.8	—	—	13.4
Cr	659	—	740	755	881	1008	870
Co	—	—	18.9	12.0	—	—	13.5
Ni	—	—	126	26	—	—	65
Mn	387	465	496	—	620	—	—

67955, 77017, 78155: *Hubbard et al.* (1974); 67415: *Lindstrom et al.* (1977a); 79215: *Blanchard et al.* (1977); 67215, 15418: *Lindstrom and Lindstrom* (1986).

TABLE A6.28. Volatiles and siderophiles in granulitic breccias and granulites (ng/g).

	67955(i)	67955(ii)	67415	78155	77017	15418
Zn	5000	6700	5800	2300	2500	490
Ga	4100	—	—	—	—	—
Ge	120	59	11.2	27	110	17
Cd	≤10	4.3	1.93	63	9.0	2.4
In	≤1.6	—	1.38	—	—	—
Ir	8	5.56	2.04	3.32	17.0	2.2
Au	2.1	1.60	1.02	0.66	5.65	0.26

67955(i): *Wasson et al.* (1977); 67955(ii) *Ganapathy et al.* (1974); 67415 *Hertogen et al.* (1977); 78155, 77017: *Morgan et al.* (1974); 15418: *Ganapathy et al.* (1973).